Advanced Soil Mechanics

Fourth Edition

BRAJA M. DAS

CRC Press
Taylor & Francis Group
A SPON PRESS BOOK

Advanced Soil Mechanics

Fourth Edition

Advanced Soil Mechanics

Fourth Edition

BRAJA M. DAS


CRC Press
Taylor & Francis Group
Boca Raton London New York

CRC Press is an imprint of the
Taylor & Francis Group, an **informa** business

A SPON PRESS BOOK

CRC Press
Taylor & Francis Group
6000 Broken Sound Parkway NW, Suite 300
Boca Raton, FL 33487-2742

Version Date: 20130930

International Standard Book Number-13: 978-1-4822-3483-1 (eBook - PDF)

In the memory of my mother, and to
Janice, Joe, Valerie, and Elizabeth

Contents

Preface

This textbook is intended for use in an introductory graduate level course that broadens (expands) the fundamental concepts acquired by students in their undergraduate work. The introductory graduate course can be followed by advanced courses dedicated to topics such as mechanical and chemical stabilization of soils, geoenvironmental engineering, finite element application to geotechnical engineering, critical state soil mechanics, geosynthetics, rock mechanics, and others.

The first edition of this book was published jointly by Hemisphere Publishing Corporation and McGraw-Hill Book Company of New York with a 1983 copyright. Taylor & Francis Group published the second and third editions with 1997 and 2008 copyrights, respectively. Compared to the third edition, the text is now divided into 11 chapters. Stresses and displacements in a soil mass are now presented in two chapters with two-dimensional problems in Chapter 3 and three-dimensional problems in Chapter 4. Permeability and seepage are now presented in two separate chapters (Chapters 6 and 7). Similarly, the settlement of shallow foundations is now presented in two chapters—elastic settlement in Chapter 10 and consolidation settlement in Chapter 11. Several new example problems have been added. SI units have been used throughout the text.

Some major changes in this edition include the following:

- In Chapter 1, "Soil aggregate, plasticity, and classification," a more detailed description of the relationships between the maximum and minimum void ratios of granular soils is provided. The American Association of State Highway and Transportation Officials (AASHTO) soil classification system has been added to this chapter. Sections on soil compaction procedures in the laboratory, along with recently developed empirical relationships for maximum dry unit weight and optimum moisture content obtained from Proctor compaction tests, have been summarized.
- Chapter 4, "Stresses and displacements in a soil mass: Three-dimensional problems," has new sections on vertical stress due to a

line load of finite length; vertical stress in Westergaard material due to point load; line load of finite length; circularly loaded area; and rectangularly loaded area.

- The fundamental concepts of compaction of clay soil for the construction of clay liners in waste disposal sites as they relate to permeability are discussed in Chapter 6, "Permeability."
- Several new empirical correlations for overconsolidation ratio and compression index for clay soils have been added to Chapter 8, "Consolidation."
- Chapter 9, "Shear strength of soils," provides additional discussion on the components affecting friction angle of granular soils, drained failure envelopes, and secant residual friction angles of clay and clay shale. Also added to this chapter are some new correlations between field vane shear strength, preconsolidation pressure, and overconsolidation ratio of clay soils.
- Chapter 10, "Elastic settlement of shallow foundations," has been thoroughly revised and expanded.
- Discussion related to precompression with sand drains has been added to Chapter 11, "Consolidation settlement of shallow foundations."
- The parameters required for the calculation of stress at the interface of a three-layered flexible system have been presented in graphical form in the Appendix, which should make interpolation easier.

Acknowledgments

Thanks are due to my wife, Janice, for her help in preparing the revised manuscript. I would also like to thank Tony Moore, senior editor, Taylor & Francis Group, for working with me during the entire publication process of the book.

Chapter 1

Soil aggregate, plasticity, and classification

1.1 INTRODUCTION

Soils are aggregates of mineral particles; and together with air and/or water in the void spaces, they form three-phase systems. A large portion of the earth's surface is covered by soils, and they are widely used as construction and foundation materials. Soil mechanics is the branch of engineering that deals with the engineering properties of soils and their behavior under stress.

This book is divided into 11 chapters: "Soil Aggregate, Plasticity, and Classification," "Stresses and Strains: Elastic Equilibrium," "Stresses and Displacement in a Soil Mass: Two-Dimensional Problems," "Stresses and Displacement in a Soil Mass: Three-Dimensional Problems," "Pore Water Pressure due to Undrained Loading," "Permeability," "Seepage," "Consolidation," "Shear Strength of Soil," "Elastic Settlement of Shallow Foundations," and "Consolidation Settlement of Shallow Foundations." This chapter is a brief overview of some soil properties and their classification. It is assumed that the reader has been previously exposed to a basic soil mechanics course.

1.2 SOIL: SEPARATE SIZE LIMITS

A naturally occurring soil sample may have particles of various sizes. Over the years, various agencies have tried to develop the size limits of gravel, sand, silt, and clay. Some of these size limits are shown in Table 1.1.

Referring to Table 1.1, it is important to note that some agencies classify clay as particles smaller than 0.005 mm in size, and others classify it as particles smaller than 0.002 mm in size. However, it needs to be realized that particles defined as clay on the basis of their size are not necessarily clay minerals. Clay particles possess the tendency to develop plasticity when mixed with water; these are clay minerals. Kaolinite, illite, montmorillonite, vermiculite, and chlorite are examples of some clay minerals.

Table 1.1 Soil: separate size limits

Agency	*Classification*	*Size limits (mm)*
U.S. Department of Agriculture (USDA)	Gravel	>2
	Very coarse sand	2–1
	Coarse sand	1–0.5
	Medium sand	0.5–0.25
	Fine sand	0.25–0.1
	Very fine sand	0.1–0.05
	Silt	0.05–0.002
	Clay	<0.002
International Society of Soil Mechanics and Foundation Engineering (ISSMFE)	Gravel	>2
	Coarse sand	2–0.2
	Fine sand	0.2–0.02
	Silt	0.02–0.002
	Clay	<0.002
Federal Aviation Administration (FAA)	Gravel	>2
	Sand	2–0.075
	Silt	0.075–0.005
	Clay	<0.005
Massachusetts Institute of Technology (MIT)	Gravel	>2
	Coarse sand	2–0.6
	Medium sand	0.6–0.2
	Fine sand	0.2–0.06
	Silt	0.06–0.002
	Clay	<0.002
American Association of State Highway and Transportation Officials (AASHTO)	Gravel	76.2–2
	Coarse sand	2–0.425
	Fine sand	0.425–0.075
	Silt	0.075–0.002
	Clay	<0.002
Unified (U.S. Army Corps of Engineers, U.S. Bureau of Reclamation, and American Society for Testing and Materials)	Gravel	76.2–4.75
	Coarse sand	4.75–2
	Medium sand	2–0.425
	Fine sand	0.425–0.075
	Silt and clay (fines)	<0.075

Fine particles of quartz, feldspar, or mica may be present in a soil in the size range defined for clay, but these will not develop plasticity when mixed with water. It appears that it is more appropriate for soil particles with sizes <2 or 5 μm as defined under various systems to be called *clay-size particles* rather than *clay*. True clay particles are mostly of colloidal size range (<1 μm), and 2 μm is probably the upper limit.

1.3 CLAY MINERALS

Clay minerals are complex silicates of aluminum, magnesium, and iron. Two basic crystalline units form the clay minerals: (1) a silicon–oxygen tetrahedron, and (2) an aluminum or magnesium octahedron. A silicon–oxygen tetrahedron unit, shown in Figure 1.1a, consists of four oxygen atoms surrounding a silicon atom. The tetrahedron units combine to form a *silica sheet* as shown in Figure 1.2a. Note that the three oxygen atoms located at the base of each tetrahedron are shared by neighboring tetrahedra. Each silicon atom with a positive valence of 4 is linked to four oxygen atoms with a total negative valence of 8. However, each oxygen atom at the base of the tetrahedron is linked to two silicon atoms. This leaves one negative valence charge of the top oxygen atom of each tetrahedron to be counterbalanced. Figure 1.1b shows an octahedral unit consisting of six hydroxyl units surrounding an aluminum (or a magnesium) atom. The combination of the aluminum octahedral units forms a *gibbsite sheet* (Figure 1.2b). If the main metallic atoms in the octahedral units are magnesium, these sheets are referred to as *brucite sheets*. When the silica sheets are stacked over the octahedral sheets, the oxygen atoms replace the hydroxyls to satisfy their valence bonds. This is shown in Figure 1.2c.

Some clay minerals consist of repeating layers of two-layer sheets. A two-layer sheet is a combination of a silica sheet with a gibbsite sheet, or a combination of a silica sheet with a brucite sheet. The sheets are about 7.2 Å thick. The repeating layers are held together by hydrogen bonding and secondary valence forces. *Kaolinite* is the most important clay mineral belonging to this type (Figure 1.3). Other common clay minerals that fall into this category are *serpentine* and *halloysite*.

The most common clay minerals with three-layer sheets are *illite* and *montmorillonite* (Figure 1.4). A three-layer sheet consists of an octahedral sheet in the middle with one silica sheet at the top and one at the bottom.

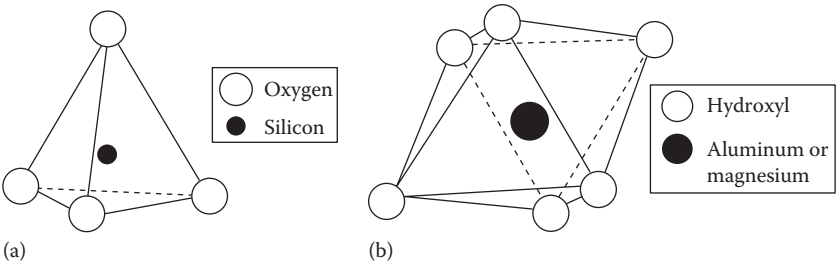

Figure 1.1 (a) Silicon–oxygen tetrahedron unit and (b) aluminum or magnesium octahedral unit.

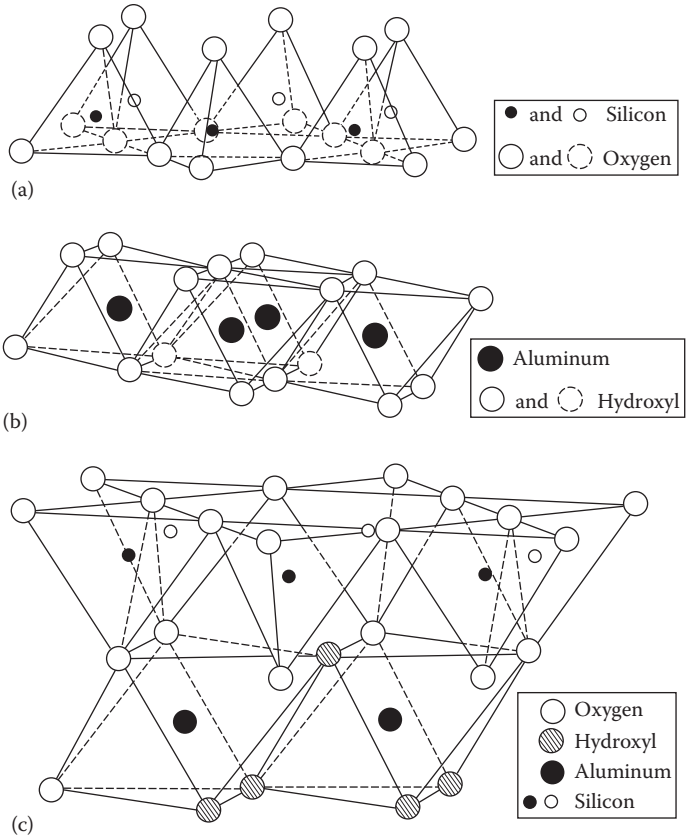

Figure 1.2 (a) Silica sheet, (b) gibbsite sheet, and (c) silica–gibbsite sheet. (After Grim, R.E., *J. Soil Mech. Found. Div., ASCE*, 85(2), 1–17, 1959.)

Repeated layers of these sheets form the clay minerals. *Illite* layers are bonded together by potassium ions. The negative charge to balance the potassium ions comes from the substitution of aluminum for some silicon in the tetrahedral sheets. Substitution of this type by one element for another without changing the crystalline form is known as *isomorphous substitution*. *Montmorillonite* has a similar structure to illite. However, unlike illite, there are no potassium ions present, and a large amount of water is attracted into the space between the three-sheet layers.

The surface area of clay particles per unit mass is generally referred to as *specific surface*. The lateral dimensions of kaolinite platelets are about 1,000–20,000 Å with thicknesses of 100–1,000 Å. Illite particles have lateral dimensions of 1000–5000 Å and thicknesses of 50–500 Å. Similarly, montmorillonite particles have lateral dimensions of 1000–5000 Å with thicknesses of 10–50 Å. If we consider several clay samples all having the same

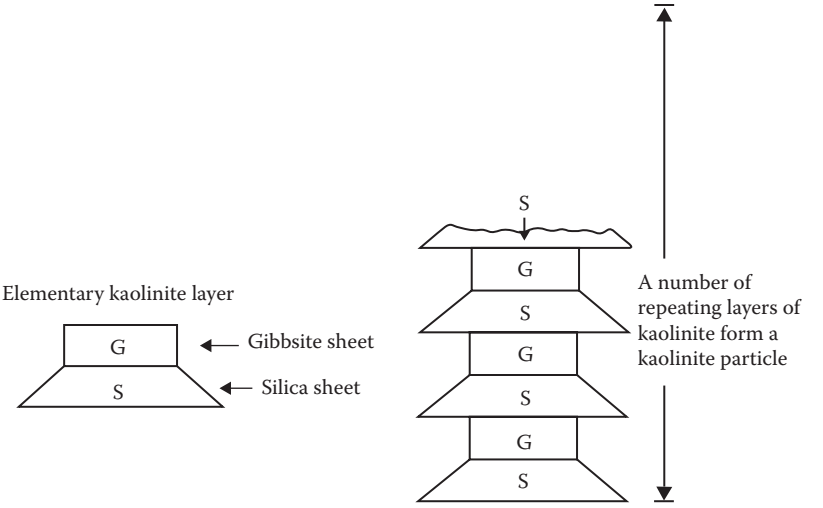

Figure 1.3 Symbolic structure for kaolinite.

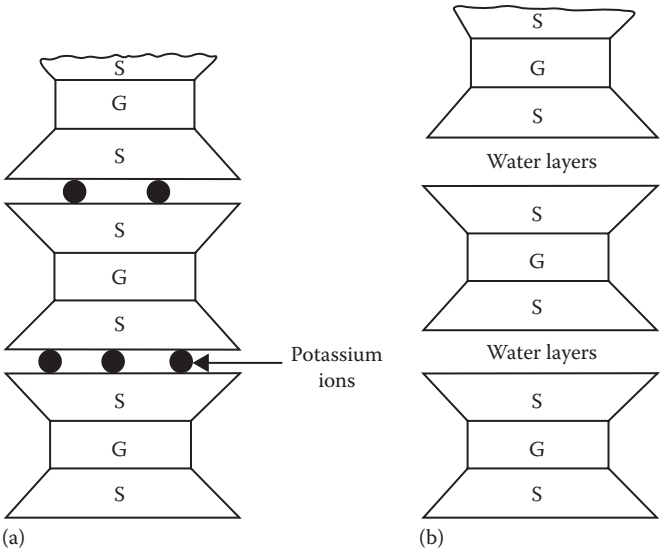

Figure 1.4 Symbolic structure of (a) illite and (b) montmorillonite.

mass, the highest surface area will be in the sample in which the particle sizes are the smallest. So it is easy to realize that the specific surface of kaolinite will be small compared to that of montmorillonite. The specific surfaces of kaolinite, illite, and montmorillonite are about 15, 90, and 800 m^2/g, respectively. Table 1.2 lists the specific surfaces of some clay minerals.

Table 1.2 Specific surface area and cation exchange capacity of some clay minerals

Clay mineral	*Specific surface (m^2/g)*	*Cation exchange capacity (me/100 g)*
Kaolinite	10–20	3
Illite	80–100	25
Montmorillonite	800	100
Chlorite	5–50	20
Vermiculite	5–400	150
Halloysite ($4H_2O$)	40	12
Halloysite ($2H_2O$)	40	12

Clay particles carry a net negative charge. In an ideal crystal, the positive and negative charges would be balanced. However, isomorphous substitution and broken continuity of structures result in a net negative charge at the faces of the clay particles. (There are also some positive charges at the edges of these particles.) To balance the negative charge, the clay particles attract positively charged ions from salts in their pore water. These are referred to as exchangeable ions. Some are more strongly attracted than others, and the cations can be arranged in a series in terms of their affinity for attraction as follows:

$$Al^{3+} > Ca^{2+} > Mg^{2+} > NH_4^+ > K^+ > H^+ > Na^+ > Li^+$$

This series indicates that, for example, Al^{3+} ions can replace Ca^{2+} ions, and Ca^{2+} ions can replace Na^+ ions. The process is called *cation exchange*. For example,

$$Na_{clay} + CaCl_2 \rightleftharpoons Ca_{clay} + NaCl$$

Cation exchange capacity (CEC) of a clay is defined as the amount of exchangeable ions, expressed in milliequivalents, per 100 g of dry clay. Table 1.2 gives the CEC of some clays.

1.4 NATURE OF WATER IN CLAY

The presence of exchangeable cations on the surface of clay particles was discussed in the preceding section. Some salt precipitates (cations in excess of the exchangeable ions and their associated anions) are also present on the surface of dry clay particles. When water is added to clay, these cations and anions float around the clay particles (Figure 1.5).

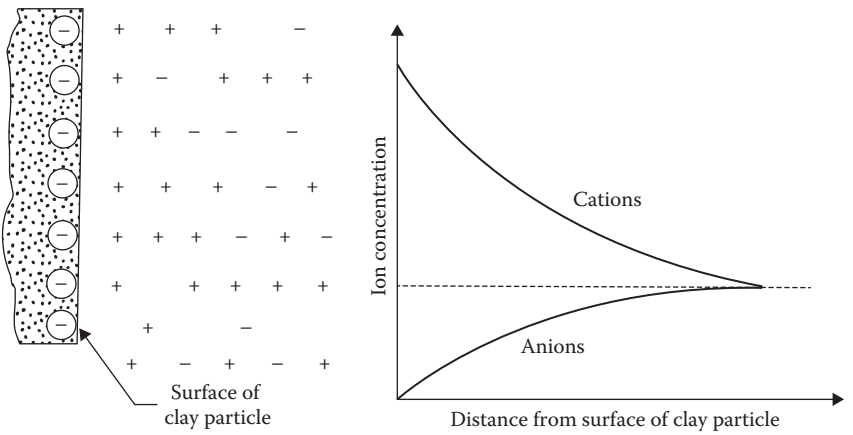

Figure 1.5 Diffuse double layer.

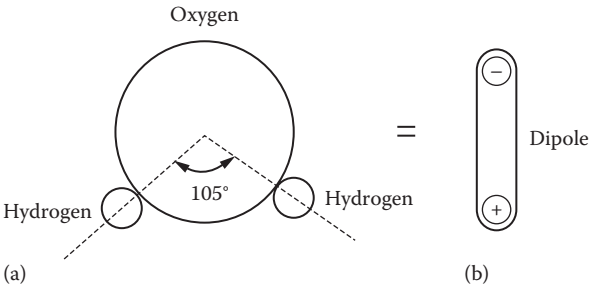

Figure 1.6 Dipolar nature of water: (a) unsymmetrical arrangement of hydrogen atoms; (b) dipole.

At this point, it must be pointed out that water molecules are dipolar, since the hydrogen atoms are not symmetrically arranged around the oxygen atoms (Figure 1.6a). This means that a molecule of water is like a rod with positive and negative charges at opposite ends (Figure 1.6b). There are three general mechanisms by which these dipolar water molecules, or *dipoles*, can be electrically attracted toward the surface of the clay particles (Figure 1.7):

a. Attraction between the negatively charged faces of clay particles and the positive ends of dipoles
b. Attraction between cations in the double layer and the negatively charged ends of dipoles. The cations are in turn attracted by the negatively charged faces of clay particles
c. Sharing of the hydrogen atoms in the water molecules by hydrogen bonding between the oxygen atoms in the clay particles and the oxygen atoms in the water molecules

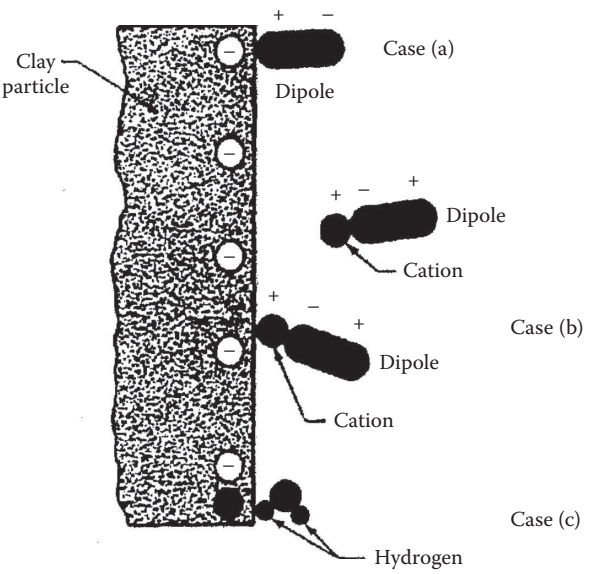

Figure 1.7 Dipolar water molecules in diffuse double layer.

The electrically attracted water that surrounds the clay particles is known as *double-layer water*. The plastic property of clayey soils is due to the existence of double-layer water. Thicknesses of double-layer water for typical kaolinite and montmorillonite crystals are shown in Figure 1.8. Since the innermost layer of double-layer water is very strongly held by a clay particle, it is referred to as *adsorbed water*.

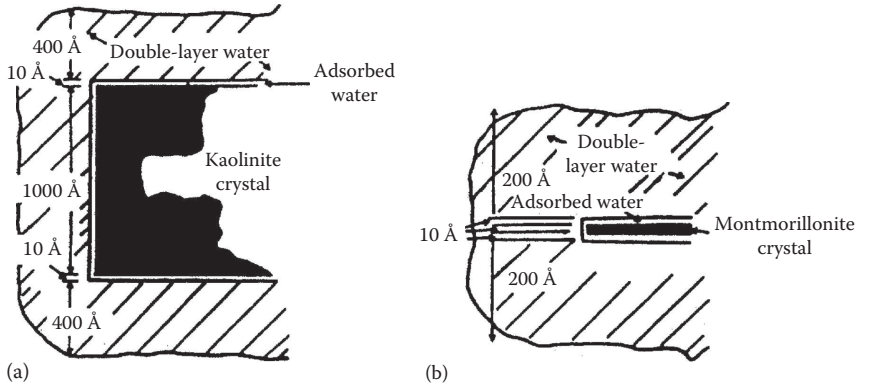

Figure 1.8 Clay water (a) typical kaolinite particle, 10,000 by 1,000 Å and (b) typical montmorillonite particle, 1,000 by 10 Å. (After Lambe, T.W., *Trans. ASCE*, 125, 682, 1960.)

1.5 REPULSIVE POTENTIAL

The nature of the distribution of ions in the diffuse double layer is shown in Figure 1.5. Several theories have been presented in the past to describe the ion distribution close to a charged surface. Of these, the Gouy–Chapman theory has received the most attention. Let us assume that the ions in the double layers can be treated as point charges, and that the surface of the clay particles is large compared to the thickness of the double layer. According to Boltzmann's theorem, we can write that (Figure 1.9)

$$n_+ = n_{+(0)} \exp \frac{-\upsilon_+ e\Phi}{KT} \tag{1.1}$$

$$n_- = n_{-(0)} \exp \frac{-\upsilon_- e\Phi}{KT} \tag{1.2}$$

where

n_+ is the local concentration of positive ions at a distance x
n_- is the local concentration of negative ions at a distance x
$n_{+(0)}$, $n_{-(0)}$ are the concentration of positive and negative ions away from the clay surface in the equilibrium liquid
Φ is the average electric potential at a distance x (Figure 1.10)
υ_+, υ_- are ionic valences
e is the unit electrostatic charge, 4.8×10^{-10} esu
K is the Boltzmann constant, 1.38×10^{-16} erg/K
T is the absolute temperature

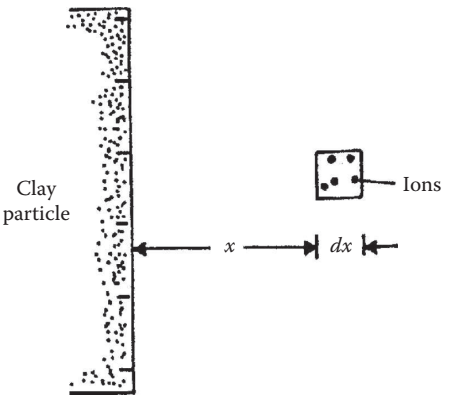

Figure 1.9 Derivation of repulsive potential equation.

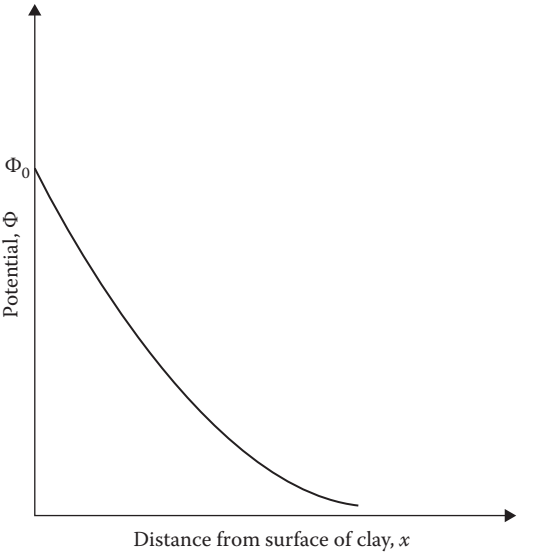

Figure 1.10 Nature of variation of potential Φ with distance from the clay surface.

The charge density ρ at a distance x is given by

$$\rho = \nu_+ e n_+ - \nu_- e n_- \tag{1.3}$$

According to Poisson's equation

$$\frac{d^2\Phi}{dx^2} = \frac{-4\pi\rho}{\lambda} \tag{1.4}$$

where λ is the dielectric constant of the medium.

Assuming $\nu_+ = \nu_-$ and $n_{+(0)} = n_{-(0)} = n_0$, and combining Equations 1.1 through 1.4, we obtain

$$\frac{d^2\Phi}{dx^2} = \frac{8\pi n_0 \nu e}{\lambda} \sinh \frac{\nu e \Phi}{KT} \tag{1.5}$$

It is convenient to rewrite Equation 1.5 in terms of the following nondimensional quantities

$$y = \frac{\nu e \Phi}{KT} \tag{1.6}$$

$$z = \frac{\nu e \Phi_0}{KT} \tag{1.7}$$

and

$$\xi = \kappa x \tag{1.8}$$

where Φ_0 is the potential at the surface of the clay particle and

$$\kappa^2 = \frac{8\pi n_0 e^2 v^2}{\varepsilon KT} (\text{cm}^{-2}) \tag{1.9}$$

Thus, from Equation 1.5

$$\frac{d^2 y}{d\xi^2} = \sinh y \tag{1.10}$$

The boundary conditions for solving Equation 1.10 are

1. At $\xi = \infty$, $y = 0$ and $dy/d\xi = 0$
2. At $\xi = 0$, $y = z$, that is, $\Phi = \Phi_0$

The solution yields the relation

$$e^{y/2} = \frac{(e^{z/2} + 1) + (e^{z/2} - 1)e^{-\xi}}{(e^{z/2} + 1) - (e^{z/2} - 1)e^{-\xi}} \tag{1.11}$$

Equation 1.11 gives an approximately exponential decay of potential. The nature of the variation of the nondimensional potential y with the nondimensional distance is given in Figure 1.11.

For a small surface potential (<25 mV), we can approximate Equation 1.5 as

$$\frac{d^2 \Phi}{dx^2} = \kappa^2 \Phi \tag{1.12}$$

$$\Phi = \Phi_0 e^{-\kappa x} \tag{1.13}$$

Equation 1.13 describes a purely exponential decay of potential. For this condition, the center of gravity of the diffuse charge is located at a distance of $x = 1/\kappa$. The term $1/\kappa$ is generally referred to as the double-layer *thickness*.

There are several factors that will affect the variation of the repulsive potential with distance from the surface of the clay layer. The effect of the cation concentration and ionic valence is shown in Figures 1.12 and 1.13, respectively. For a given value of Φ_0 and x, the repulsive potential Φ decreases with the increase of ion concentration n_0 and ionic valence v.

When clay particles are close and parallel to each other, the nature of variation of the potential will be as shown in Figure 1.14. Note for this case

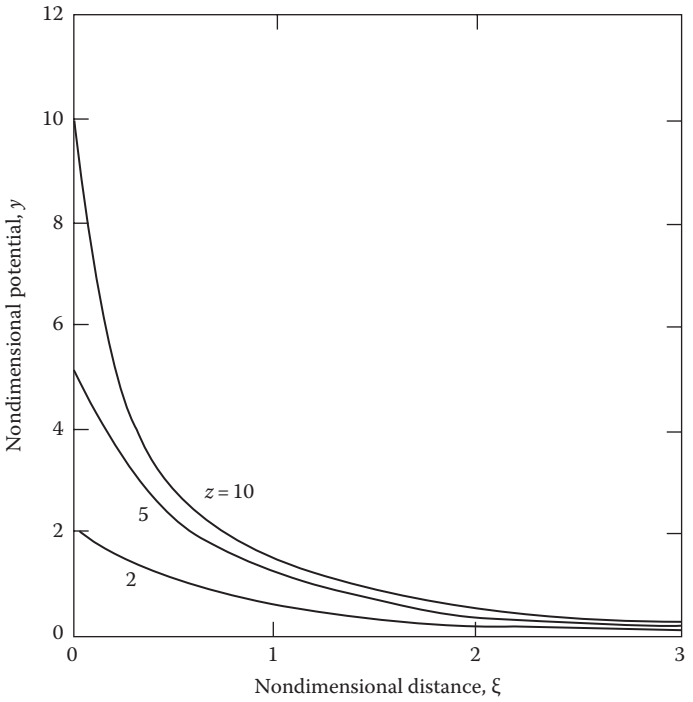

Figure 1.11 Variation of nondimensional potential with nondimensional distance.

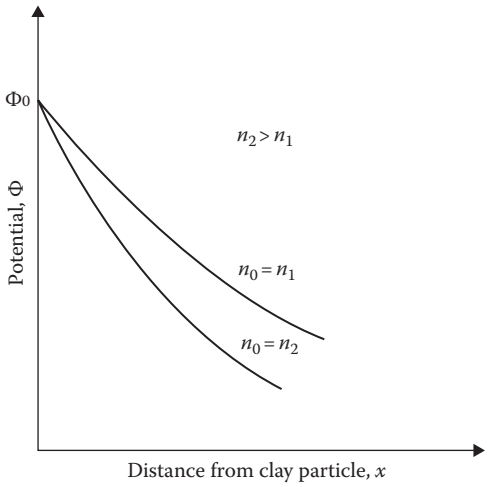

Figure 1.12 Effect of cation concentration on the repulsive potential.

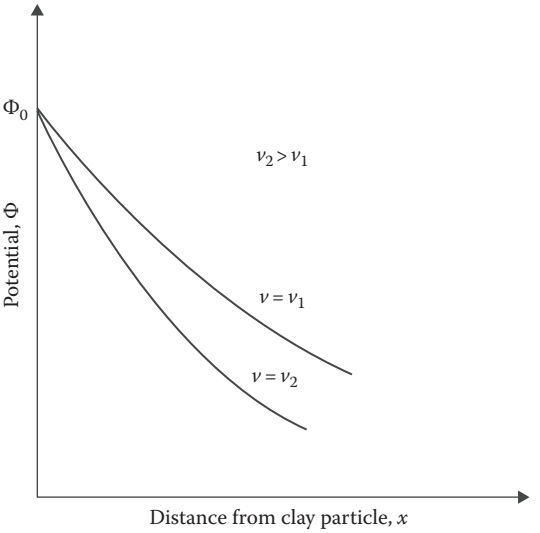

Figure 1.13 Effect of ionic valence on the repulsive potential.

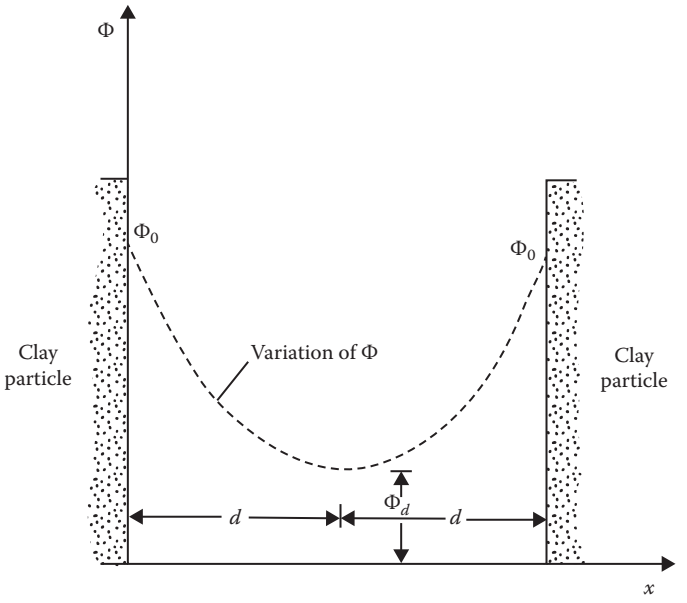

Figure 1.14 Variation of Φ between two parallel clay particles.

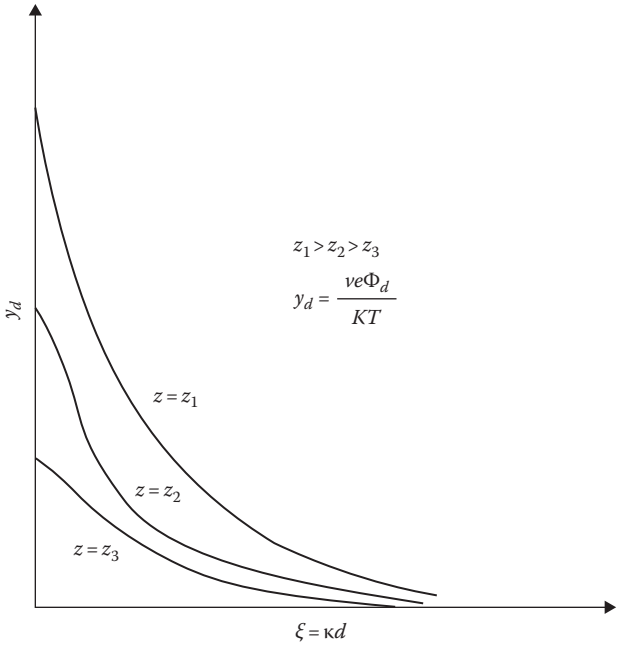

Figure 1.15 Nature of variation of the nondimensional midplane potential for two parallel plates.

that at $x = 0$, $\Phi = \Phi_0$, and at $x = d$ (midway between the plates), $\Phi = \Phi_d$ and $d\Phi/dx = 0$. Numerical solutions for the nondimensional potential $y = y_d$ (i.e., $\Phi = \Phi_d$) for various values of z and $\xi = \kappa d$ (i.e., $x = d$) are given by Verweg and Overbeek (1948) (see also Figure 1.15).

1.6 REPULSIVE PRESSURE

The repulsive pressure midway between two parallel clay plates (Figure 1.16) can be given by the Langmuir equation

$$p = 2n_0 KT\left[\cosh\frac{ve\Phi_d}{KT} - 1\right] \tag{1.14}$$

where p is the repulsive pressure, that is, the difference between the osmotic pressure midway between the plates in relation to that in the equilibrium solution. Figure 1.17, which is based on the results of Bolt (1956), shows the theoretical and experimental variation of p between two clay particles.

Although the Guoy–Chapman theory has been widely used to explain the behavior of clay, there have been several important objections to this theory. A good review of these objections has been given by Bolt (1955).

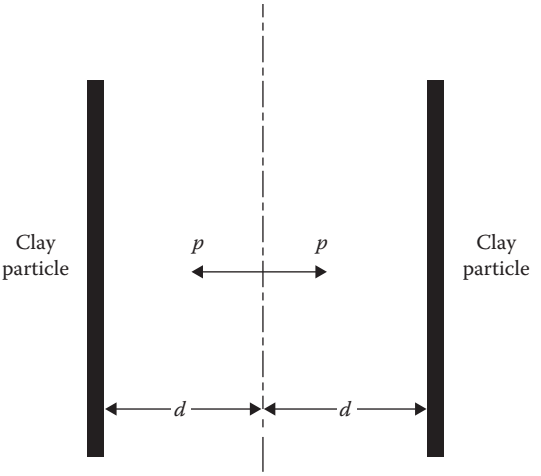

Figure 1.16 Repulsive pressure midway between two parallel clay plates.

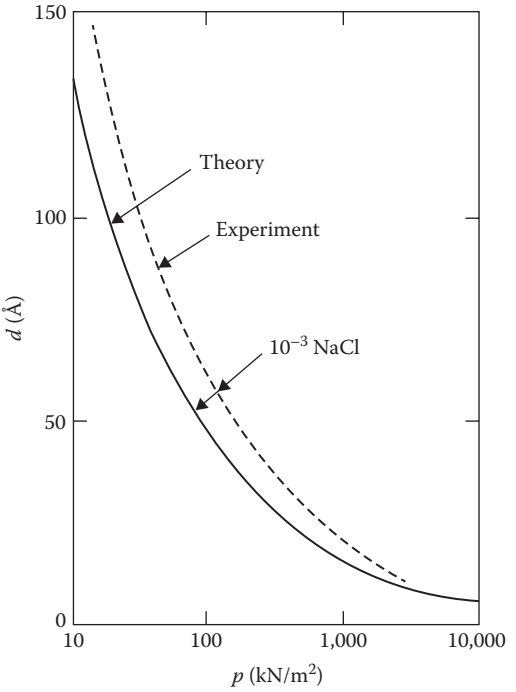

Figure 1.17 Repulsive pressure between sodium montmorillonite clay particles. (After Bolt, G.H., *Geotechnique*, 6, 86, 1956.)

1.7 FLOCCULATION AND DISPERSION OF CLAY PARTICLES

In addition to the repulsive force between the clay particles, there is an attractive force, which is largely attributed to the Van der Waal force. This is a secondary bonding force that acts between all adjacent pieces of matter. The force between two flat parallel surfaces varies inversely as $1/x^3$ to $1/x^4$, where x is the distance between the two surfaces. Van der Waal's force is also dependent on the dielectric constant of the medium separating the surfaces. However, if water is the separating medium, substantial changes in the magnitude of the force will not occur with minor changes in the constitution of water.

The behavior of clay particles in a suspension can be qualitatively visualized from our understanding of the attractive and repulsive forces between the particles and with the aid of Figure 1.18. Consider a dilute suspension of clay particles in water. These colloidal clay particles will undergo Brownian movement and, during this random movement, will come close to each

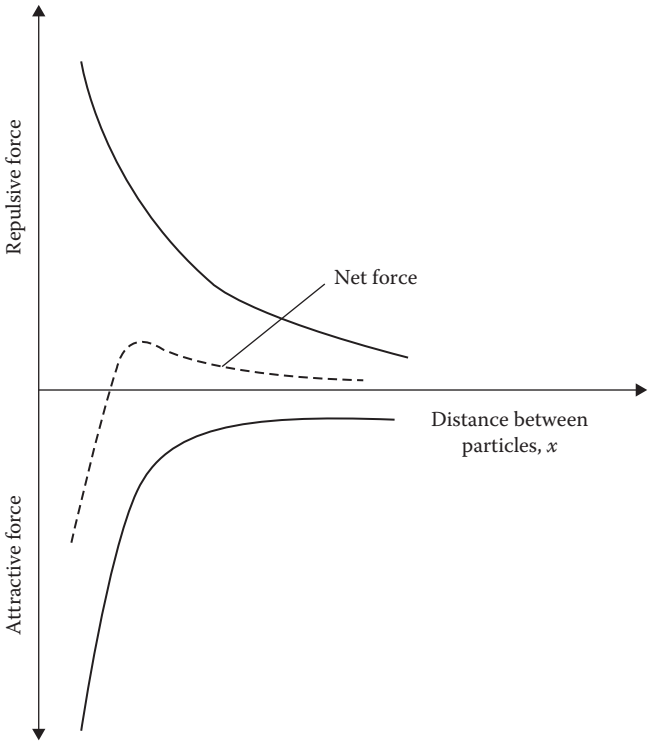

Figure 1.18 Dispersion and flocculation of clay in a suspension.

Figure 1.19 (a) Dispersion and (b) flocculation of clay.

other at distances within the range of interparticle forces. The forces of attraction and repulsion between the clay particles vary at different rates with respect to the distance of separation. The force of repulsion decreases exponentially with distance, whereas the force of attraction decreases as the inverse third or fourth power of distance, as shown in Figure 1.18. Depending on the distance of separation, if the magnitude of the repulsive force is greater than the magnitude of the attractive force, the net result will be repulsion. The clay particles will settle individually and form a dense layer at the bottom; however, they will remain separate from their neighbors (Figure 1.19a). This is referred to as the *dispersed state* of the soil. On the contrary, if the net force between the particles is attraction, flocs will be formed and these flocs will settle to the bottom. This is called *flocculated* clay (Figure 1.19b).

1.7.1 Salt flocculation and nonsalt flocculation

We saw in Figure 1.12 the effect of salt concentration, n_0, on the repulsive potential of clay particles. High salt concentration will depress the double layer of clay particles and hence the force of repulsion. We noted earlier in this section that the Van der Waal force largely contributes to the force of attraction between clay particles in suspension. If the clay particles are suspended in water with a high salt concentration, the flocs of the clay particles formed by dominant attractive forces will give them mostly an orientation approaching parallelism (face-to-face type). This is called a salt-type flocculation (Figure 1.20a).

Another type of force of attraction between the clay particles, which is not taken into account in colloidal theories, is that arising from the electrostatic attraction of the positive charges at the edge of the particles and the negative charges at the face. In a soil–water suspension with low salt concentration, this electrostatic force of attraction may produce a flocculation with an orientation approaching a perpendicular array. This is shown in Figure 1.20b and is referred to as nonsalt flocculation.

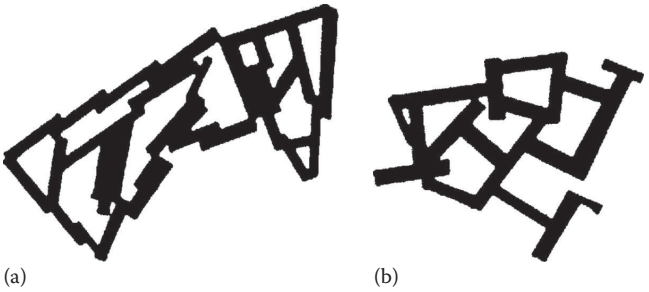

Figure 1.20 (a) Salt and (b) nonsalt flocculation of clay particles.

1.8 CONSISTENCY OF COHESIVE SOILS

The presence of clay minerals in a fine-grained soil will allow it to be remolded in the presence of some moisture without crumbling. If a clay slurry is dried, the moisture content will gradually decrease, and the slurry will pass from a liquid state to a plastic state. With further drying, it will change to a semisolid state and finally to a solid state, as shown in Figure 1.21. In 1911, A. Atterberg, a Swedish scientist, developed a method for describing the limit consistency of fine-grained soils on the basis of moisture content. These limits are the *liquid limit*, the *plastic limit*, and the *shrinkage limit*.

The liquid limit is defined as the moisture content, in percent, at which the soil changes from a liquid state to a plastic state. The moisture contents (in percent) at which the soil changes from a plastic to a semisolid state and from a semisolid to a solid state are defined as the plastic limit and the shrinkage limit, respectively. These limits are generally referred to as the *Atterberg limits*. The Atterberg limits of cohesive soil depend on several factors, such as the amount and type of clay minerals and the type of adsorbed cation.

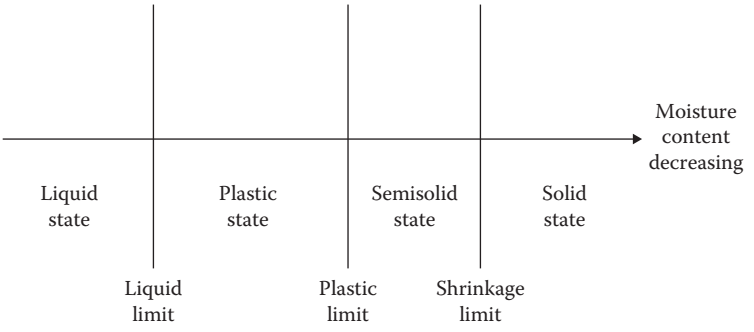

Figure 1.21 Consistency of cohesive soils.

1.8.1 Liquid limit

The liquid limit of a soil is generally determined by the Standard Casagrande device. A schematic diagram (side view) of a liquid limit device is shown in Figure 1.22a. This device consists of a brass cup and a hard rubber base. The brass cup can be dropped onto the base by a cam operated by a crank. To perform the liquid limit test, one must place a soil paste in the cup. A groove is then cut at the center of the soil pat with the standard grooving tool (Figure 1.22b). By using the crank-operated cam, the cup is lifted and dropped from a height of 10 mm. The moisture content, in percent, required to close a distance of 12.7 mm along the bottom of the groove (see Figure 1.22c and d) after 25 blows is defined as the *liquid limit*.

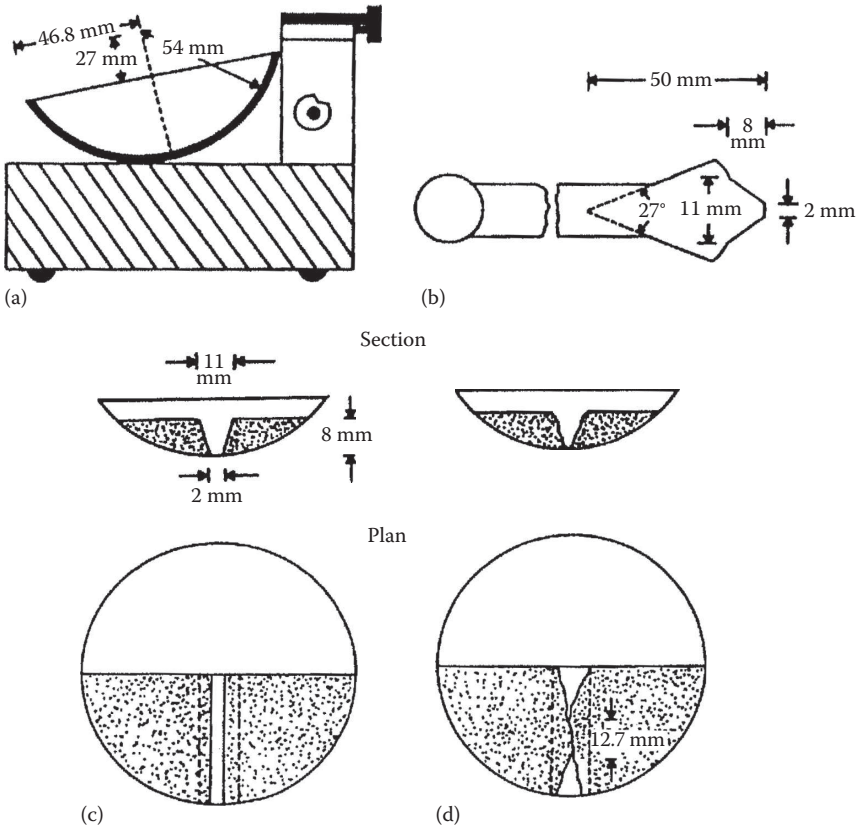

Figure 1.22 Schematic diagram of (a) liquid limit device, (b) grooving tool, (c) soil pat at the beginning of the test, and (d) soil pat at the end of the test.

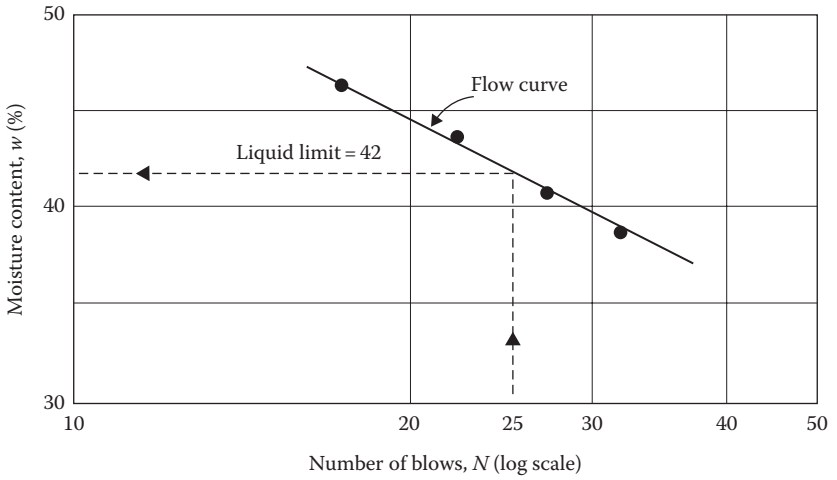

Figure 1.23 Flow curve for the determination of the liquid limit for a silty clay.

It is difficult to adjust the moisture content in the soil to meet the required 12.7 mm closure of the groove in the soil pat at 25 blows. Hence, at least three tests for the same soil are conducted at varying moisture contents, with the number of blows, N, required to achieve closure varying between 15 and 35. The moisture content of the soil, in percent, and the corresponding number of blows are plotted on semilogarithmic graph paper (Figure 1.23). The relationship between moisture content and log N is approximated as a straight line. This line is referred to as the *flow curve*. The moisture content corresponding to $N = 25$, determined from the flow curve, gives the liquid limit of the soil. The slope of the flow line is defined as the *flow index* and may be written as

$$I_F = \frac{w_1 - w_2}{\log(N_2/N_1)} \tag{1.15}$$

where

I_F is the flow index
w_1 is the moisture content of soil, in percent, corresponding to N_1 blows
w_2 is the moisture content corresponding to N_2 blows

Note that w_2 and w_1 are exchanged to yield a positive value even though the slope of the flow line is negative. Thus, the equation of the flow line can be written in a general form as

$$w = -I_F \log N + C \tag{1.16}$$

where C is a constant.

From the analysis of hundreds of liquid limit tests in 1949, the U.S. Army Corps of Engineers, at the Waterways Experiment Station in Vicksburg, Mississippi, proposed an empirical equation of the form

$$LL = w_N \left(\frac{N}{25}\right)^{\tan\beta} \tag{1.17}$$

where

N is the number of blows in the liquid limit device for a 12.7 mm groove closure
w_N is the corresponding moisture content
$\tan\beta = 0.121$ (but note that $\tan\beta$ is not equal to 0.121 for all soils)

Equation 1.17 generally yields good results for the number of blows between 20 and 30. For routine laboratory tests, it may be used to determine the liquid limit when only one test is run for a soil. This procedure is generally referred to as the *one-point method* and was also adopted by ASTM under designation D-4318 (ASTM, 2010). The reason that the one-point method yields fairly good results is that a small range of moisture content is involved when $N = 20–30$.

Another method of determining the liquid limit, which is popular in Europe and Asia, is the *fall cone method* (British Standard—BS 1377). In this test, the liquid limit is defined as the moisture content at which a standard cone of apex angle 30° and weight of 0.78 N (80 gf) will penetrate a distance $d = 20$ mm in 5 s when allowed to drop from a position of point contact with the soil surface (Figure 1.24a). Due to the difficulty in achieving the liquid limit from a single test, four or more tests can be conducted at various moisture contents to determine the fall cone penetration, d, in 5 s. A semilogarithmic graph can then be plotted with moisture content w versus cone penetration d. The plot results in a straight line. The moisture content corresponding to $d = 20$ mm is the liquid limit (Figure 1.24b). From Figure 1.24b, the *flow index* can be defined as

$$I_{FC} = \frac{w_2(\%) - w_1(\%)}{\log d_2 - \log d_1} \tag{1.18}$$

where w_1, w_2 are the moisture contents at cone penetrations of d_1 and d_2, respectively.

1.8.2 Plastic limit

The *plastic limit* is defined as the moist content, in percent, at which the soil crumbles when rolled into threads of 3.2 mm diameter. The plastic limit is the lower limit of the plastic stage of soil. The plastic limit test is simple

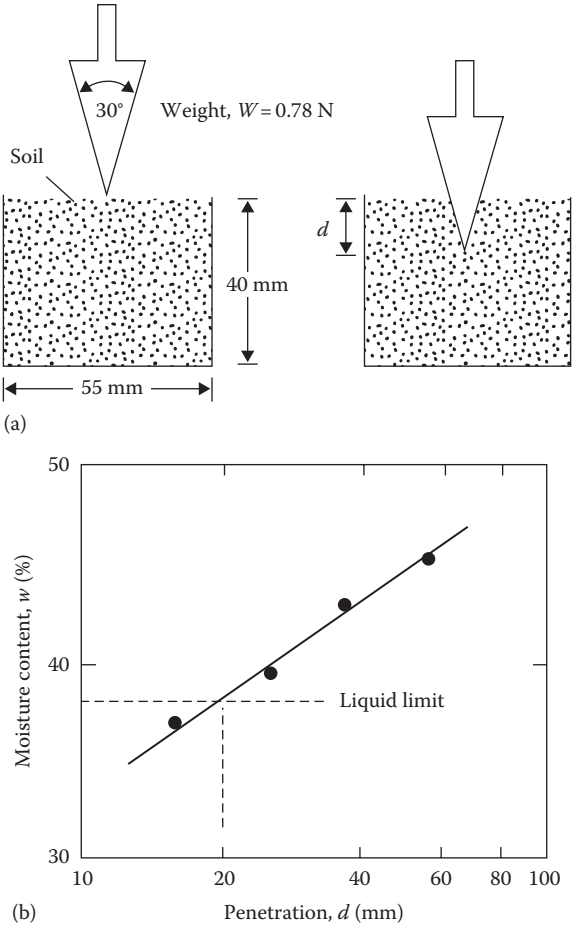

Figure 1.24 (a) Fall cone test and (b) plot of moisture content versus cone penetration for determination of liquid limit.

and is performed by repeated rolling of an ellipsoidal size soil mass by hand on a ground glass plate. The procedure for the plastic limit test is given by ASTM Test Designation D-4318 (ASTM, 2010).

As in the case of liquid limit determination, the fall cone method can be used to obtain the plastic limit. This can be achieved by using a cone of similar geometry, but with a mass of 2.35 N (240 gf). Three to four tests at varying moist contents of soil are conducted, and the corresponding cone penetrations d are determined. The moisture content corresponding to a cone penetration of d = 20 mm is the plastic limit. Figure 1.25 shows the liquid and plastic limit determined by the fall cone test for Cambridge Gault clay reported by Wroth and Wood (1978).

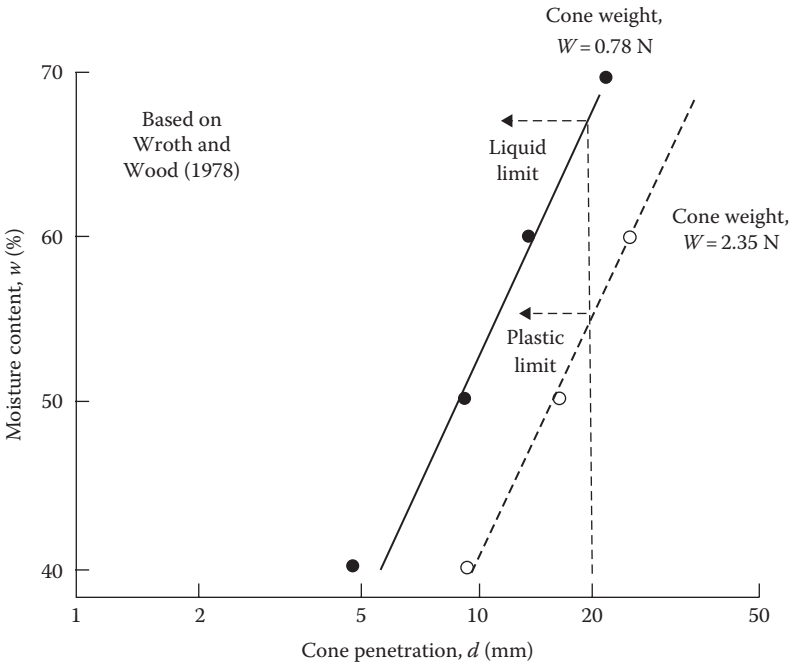

Figure 1.25 Liquid and plastic limits for Cambridge Gault clay determined by the fall cone test.

The difference between the liquid limit and the plastic limit of a soil is defined as the plasticity index, PI

$$\mathrm{PI} = \mathrm{LL} - \mathrm{PL} \tag{1.19}$$

where
LL is the liquid limit
PL is the plastic limit

Sridharan et al. (1999) showed that the plasticity index can be correlated to the flow index as obtained from the liquid limit tests. According to their study

$$\mathrm{PI}(\%) = 4.12 I_{\mathrm{F}}(\%) \tag{1.20}$$

and

$$\mathrm{PI}(\%) = 0.74 I_{\mathrm{FC}}(\%) \tag{1.21}$$

1.9 LIQUIDITY INDEX

The relative consistency of a cohesive soil can be defined by a ratio called the *liquidity index* LI. It is defined as

$$\text{LI} = \frac{w_N - \text{PL}}{\text{LL} - \text{PL}} = \frac{w_N - \text{PL}}{\text{PI}} \tag{1.22}$$

where w_N is the natural moisture content. It can be seen from Equation 1.22 that, if w_N = LL, then the liquidity index is equal to 1. Again, if w_N = PL, the liquidity index is equal to 0. Thus, for a natural soil deposit which is in a plastic state (i.e., LL $\geq w_N \geq$ PL), the value of the liquidity index varies between 1 and 0. A natural deposit with $w_N \geq$ LL will have a liquidity index greater than 1. In an undisturbed state, these soils may be stable; however, a sudden shock may transform them into a liquid state. Such soils are called *sensitive clays*.

1.10 ACTIVITY

Since the plastic property of soil is due to the adsorbed water that surrounds the clay particles, we can expect that the type of clay minerals and their proportional amounts in a soil will affect the liquid and plastic limits. Skempton (1953) observed that the plasticity index of a soil linearly increases with the percent of clay-size fraction (percent finer than 2μ by weight) present in it. This relationship is shown in Figure 1.26.

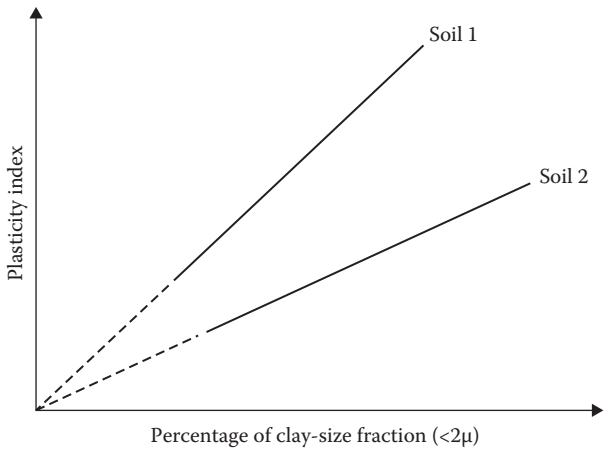

Figure 1.26 Relationship between plasticity index and percentage of clay-size fraction by weight.

Table 1.3 Activities of clay minerals

Mineral	*Activity (A)*
Smectites	1–7
Illite	0.5–1
Kaolinite	0.5
Halloysite ($4H_2O$)	0.5
Halloysite ($2H_2O$)	0.1
Attapulgite	0.5–1.2
Allophane	0.5–1.2

The average lines for all the soils pass through the origin. The correlations of PI with the clay-size fractions for different clays plot separate lines. This is due to the type of clay minerals in each soil. On the basis of these results, Skempton defined a quantity called activity, which is the slope of the line correlating PI and percent finer than 2μ. This activity A may be expressed as

$$A = \frac{\text{PI}}{(\text{percentage of clay-size fraction by weight})} \tag{1.23}$$

Activity is used as an index for identifying the swelling potential of clay soils. Typical values of activities for various clay minerals are given in Table 1.3.

Seed et al. (1964a) studied the plastic property of several artificially prepared mixtures of sand and clay. They concluded that, although the relationship of the plasticity index to the percent of clay-size fraction is linear (as observed by Skempton), it may not always pass through the origin. This is shown in Figure 1.27. Thus, the activity can be redefined as

$$A = \frac{\text{PI}}{\text{percent of clay-size fraction} - C'} \tag{1.24}$$

where C' is a constant for a given soil. For the experimental results shown in Figure 1.27, $C' = 9$.

Further works of Seed et al. (1964b) have shown that the relationship of the plasticity index to the percentage of clay-size fractions present in a soil can be represented by two straight lines. This is shown qualitatively in Figure 1.28. For clay-size fractions greater than 40%, the straight line passes through the origin when it is projected back.

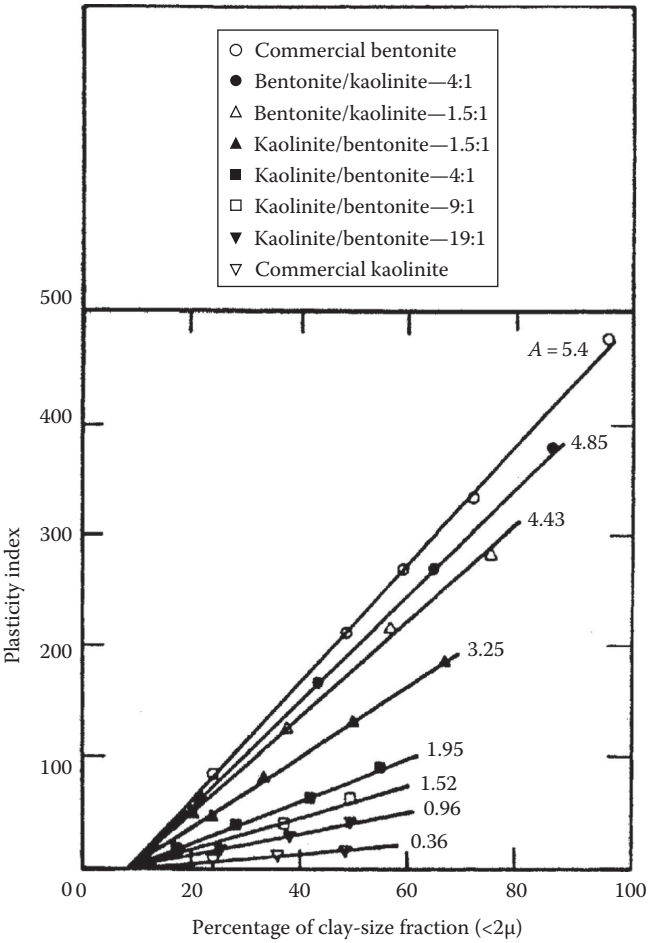

Figure 1.27 Relationship between plasticity index and clay-size fraction by weight for kaolinite/bentonite clay mixtures. (After Seed, H.B. et al., *J. Soil Mech. Found. Eng. Div., Am. Soc. Civ. Eng.*, 90(SM4), 107, 1964.)

1.11 GRAIN-SIZE DISTRIBUTION OF SOIL

For a basic understanding of the nature of soil, the distribution of the grain size present in a given soil mass must be known. The grain-size distribution of coarse-grained soils (gravelly and/or sandy) is determined by sieve analysis. Table 1.4 gives the opening size of some U.S. sieves.

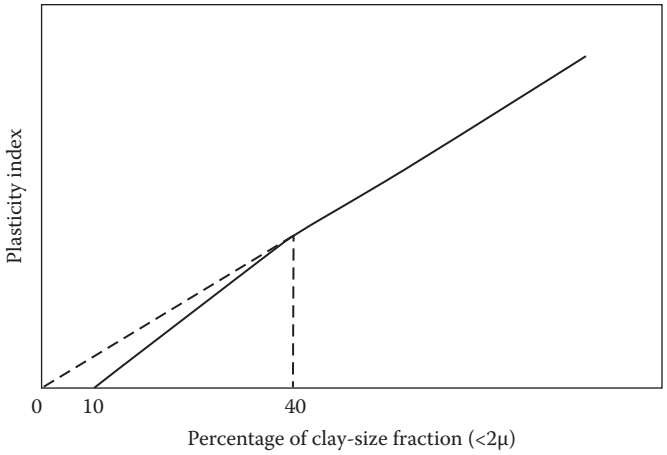

Figure 1.28 Simplified relationship between plasticity index and percentage of clay-size fraction by weight. (After Seed, H.B. et al., *J. Soil Mech. Found. Eng. Div., Am. Soc. Civ. Eng.*, 90(SM6), 75, 1964.)

Table 1.4 U.S. standard sieves

Sieve no.	*Opening size (mm)*
3	6.35
4	4.75
6	3.36
8	2.38
10	2.00
16	1.19
20	0.84
30	0.59
40	0.425
50	0.297
60	0.25
70	0.21
100	0.149
140	0.105
200	0.075
270	0.053

The cumulative percent by weight of a soil passing a given sieve is referred to as the *percent finer*. Figure 1.29 shows the results of a sieve analysis for a sandy soil. The grain-size distribution can be used to determine some of the basic soil parameters, such as the effective size, the uniformity coefficient, and the coefficient of gradation.

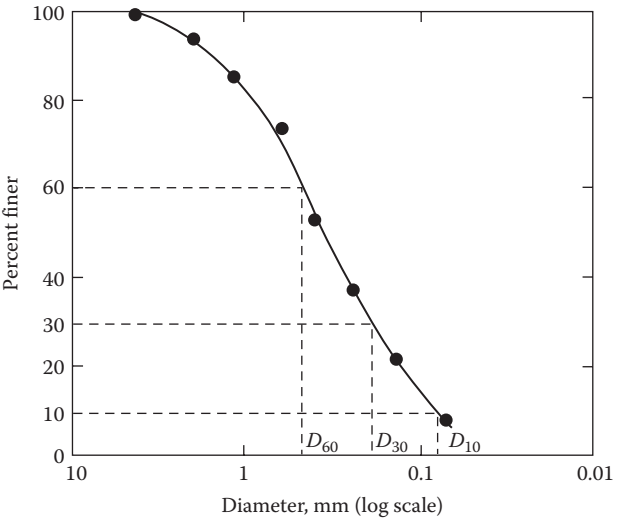

Figure 1.29 Grain-size distribution of a sandy soil.

The *effective size* of a soil is the diameter through which 10% of the total soil mass is passing and is referred to as D_{10}. The *uniformity coefficient* C_u is defined as

$$C_u = \frac{D_{60}}{D_{10}} \tag{1.25}$$

where D_{60} is the diameter through which 60% of the total soil mass is passing.

The *coefficient of gradation* C_c is defined as

$$C_c = \frac{(D_{30})^2}{(D_{60})(D_{10})} \tag{1.26}$$

where D_{30} is the diameter through which 30% of the total soil mass is passing.

A soil is called a *well-graded* soil if the distribution of the grain sizes extends over a rather large range. In that case, the value of the uniformity coefficient is large. Generally, a soil is referred to as well graded if C_u is larger than about 4–6 and C_c is between 1 and 3. When most of the grains in a soil mass are of approximately the same size—that is, C_u is close to 1—the soil is called *poorly graded*. A soil might have a combination of two or more well-graded soil fractions, and this type of soil is referred to as a *gap-graded* soil.

The sieve analysis technique described earlier is applicable for soil grains larger than No. 200 (0.075 mm) sieve size. For fine-grained soils, the procedure used for determination of the grain-size distribution is hydrometer analysis. This is based on the principle of sedimentation of soil grains.

1.12 WEIGHT–VOLUME RELATIONSHIPS

Figure 1.30a shows a soil mass that has a total volume V and a total weight W. To develop the weight–volume relationships, the three phases of the soil mass, that is, soil solids, air, and water, have been separated in Figure 1.30b. Note that

$$W = W_s + W_w \tag{1.27}$$

and, also

$$V = V_s + V_w + V_a \tag{1.28}$$

$$V_v = V_w + V_a \tag{1.29}$$

where

W_s is the weight of soil solids
W_w is the weight of water
V_s is the volume of the soil solids
V_w is the volume of water
V_a is the volume of air

The weight of air is assumed to be zero. The volume relations commonly used in soil mechanics are void ratio, porosity, and degree of saturation.

Void ratio e is defined as the ratio of the volume of voids to the volume of solids:

$$e = \frac{V_u}{V_s} \tag{1.30}$$

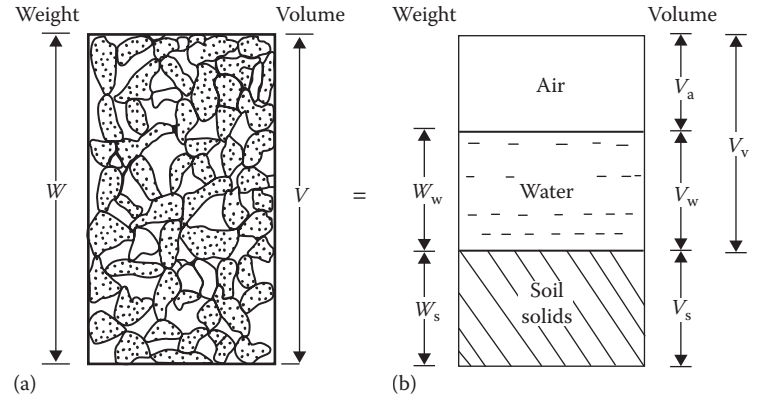

Figure 1.30 Weight–volume relationships for soil aggregate: (a) soil mass of volume V; (b) three phases of the soil mass.

Porosity n is defined as the ratio of the volume of voids to the total volume:

$$n = \frac{V_u}{V} \tag{1.31}$$

Also, $V = V_s + V_v$
and so

$$n = \frac{V_u}{V_s + V_u} = \frac{V_u/V_s}{(V_s/V_s) + (V_u/V_s)} = \frac{e}{1+e} \tag{1.32}$$

Degree of saturation S_r is the ratio of the volume of water to the volume of voids and is generally expressed as a percentage:

$$S_r(\%) = \frac{V_w}{V_u} \times 100 \tag{1.33}$$

The weight relations used are moisture content and unit weight. *Moisture content w* is defined as the ratio of the weight of water to the weight of soil solids, generally expressed as a percentage:

$$w(\%) = \frac{W_w}{W_s} \times 100 \tag{1.34}$$

Unit weight γ is the ratio of the total weight to the total volume of the soil aggregate:

$$\gamma = \frac{W}{V} \tag{1.35}$$

This is sometimes referred to as moist unit weight since it includes the weight of water and the soil solids. If the entire void space is filled with water (i.e., $V_a = 0$), it is a saturated soil; Equation 1.35 will then give us the saturated unit weight γ_{sat}.

The dry unit weight γ_d is defined as the ratio of the weight of soil solids to the total volume:

$$\gamma_d = \frac{W_s}{V} \tag{1.36}$$

Useful weight–volume relations can be developed by considering a soil mass in which the volume of soil solids is unity, as shown in Figure 1.31. Since $V_s = 1$, from the definition of void ratio given in Equation 1.30, the

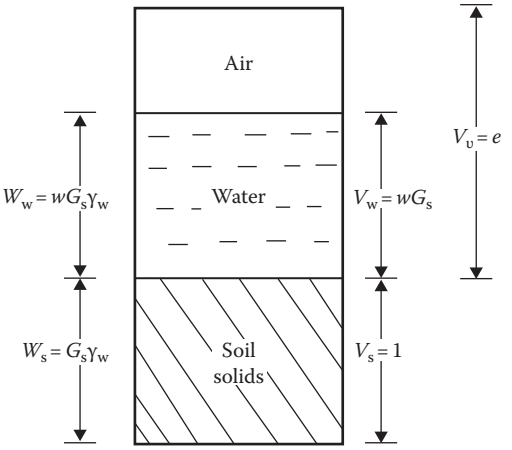

Figure 1.31 Weight–volume relationship for $V_s = 1$.

volume of voids is equal to the void ratio e. The weight of soil solids can be given by

$$W_s = G_s \gamma_w V_s = G_s \gamma_w \quad (\text{since } V_s = 1)$$

where

G_s is the specific gravity of soil solids
γ_w is the unit weight of water (9.81 kN/m^3)

From Equation 1.34, the weight of water is $W_w = wW_s = wG_s\gamma_w$. So the moist unit weight is

$$\gamma = \frac{W}{V} = \frac{W_s + W_w}{V_s + V_u} = \frac{G_s\gamma_w + wG_s\gamma_w}{1+e} = \frac{G_s\gamma_w(1+w)}{1+e} \tag{1.37}$$

The dry unit weight can also be determined from Figure 1.31 as

$$\gamma_d = \frac{W_s}{V} = \frac{G_s\gamma_w}{1+e} \tag{1.38}$$

The degree of saturation can be given by

$$S_r = \frac{V_w}{V_u} = \frac{W_w/\gamma_w}{V_u} = \frac{wG_s\gamma_w/\gamma_w}{e} = \frac{wG_s}{e} \tag{1.39}$$

For saturated soils, $S_r = 1$. So, from Equation 1.39,

$$e = wG_s \tag{1.40}$$

By referring to Figure 1.32, the relation for the unit weight of a saturated soil can be obtained as

$$\gamma_{sat} = \frac{W}{V} = \frac{W_s + W_w}{V} = \frac{G_s\gamma_w + e\gamma_w}{1+e} \tag{1.41}$$

Basic relations for unit weight such as Equations 1.37, 1.38, and 1.41 in terms of porosity n can also be derived by considering a soil mass that has a total volume of unity as shown in Figure 1.33. In this case (for $V = 1$), from Equation 1.31, $V_v = n$. So, $V_s = V - V_v = 1 - n$.

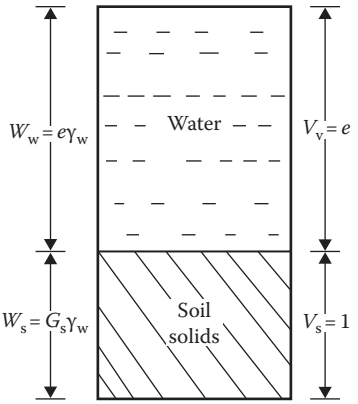

Figure 1.32 Weight–volume relation for saturated soil with $V_s = 1$.

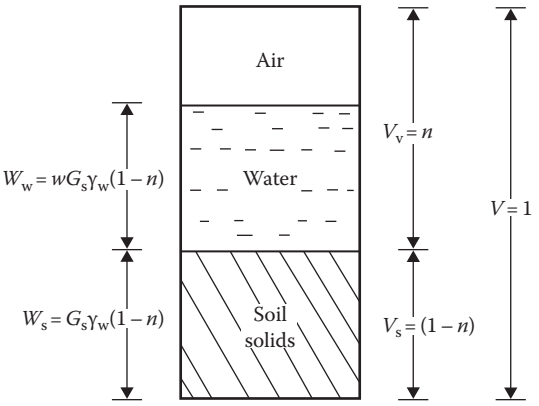

Figure 1.33 Weight–volume relationship for $V = 1$.

The weight of soil solids is equal to $(1 - n)G_s\gamma_w$, and the weight of water $W_w = wW_s = w(1 - n)G_s\gamma_w$. Thus, the moist unit weight is

$$\gamma = \frac{W}{V} = \frac{W_s + W_w}{V} = \frac{(1-n)G_s\gamma_w + w(1-n)G_s\gamma_w}{1}$$

$$= G_s\gamma_w(1-n)(1+w) \tag{1.42}$$

The dry unit weight is

$$\gamma_d = \frac{W_s}{V} = (1-n)G_s\gamma_w \tag{1.43}$$

If the soil is saturated (Figure 1.34),

$$\gamma_{sat} = \frac{W_s + W_w}{V} = (1-n)G_s\gamma_w + n\gamma_w = [G_s - n(G_s - 1)]\gamma_w \tag{1.44}$$

Table 1.5 gives some typical values of void ratios and dry unit weights encountered in granular soils.

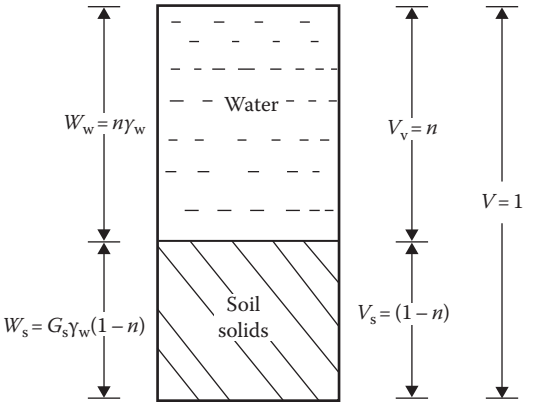

Figure 1.34 Weight–volume relationship for saturated soil with $V = 1$.

Table 1.5 Typical values of void ratios and dry unit weights for granular soils

	Void ratio, e		*Dry unit weight, γ_d*	
Soil type	*Maximum*	*Minimum*	*Minimum (kN/m³)*	*Maximum (kN/m³)*
Gravel	0.6	0.3	16	20
Coarse sand	0.75	0.35	15	19
Fine sand	0.85	0.4	14	19
Standard Ottawa sand	0.8	0.5	14	17
Gravelly sand	0.7	0.2	15	22
Silty sand	1	0.4	13	19
Silty sand and gravel	0.85	0.15	14	23

Example 1.1

For a soil in natural state, given $e = 0.8$, $w = 24\%$, and $G_s = 2.68$.

a. Determine the moist unit weight, dry unit weight, and degree of saturation.
b. If the soil is completely saturated by adding water, what would its moisture content be at that time? Also, find the saturated unit weight.

Solution

Part a:

From Equation 1.37, the moist unit weight is

$$\gamma = \frac{G_s \gamma_w (1 + w)}{1 + e}$$

Since $\gamma_w = 9.81\ \text{kN/m}^3$,

$$\gamma = \frac{(2.68)(9.81)(1 + 0.24)}{1 + 0.8} = 18.11\ \text{kN/m}^3$$

From Equation 1.38, the dry unit weight is

$$\gamma_d = \frac{G_s \gamma_w}{1 + e} = \frac{(2.68)(9.81)}{1 + 0.8} = 14.61\ \text{kN/m}^3$$

From Equation 1.39, the degree of saturation is

$$S_r(\%) = \frac{wG_s}{e} \times 100 = \frac{(0.24)(2.68)}{0.8} \times 100 = 80.4\%$$

Part b:

From Equation 1.40, for saturated soils, $e = wG_s$, or

$$w(\%) = \frac{e}{G_s} \times 100 = \frac{0.8}{2.68} \times 100 = 29.85\%$$

From Equation 1.41, the saturated unit weight is

$$\gamma_{sat} = \frac{G_s \gamma_w + e\gamma_w}{1 + e} = \frac{9.81(2.68 + 0.8)}{1 + 0.8} = 18.97\ \text{kN/m}^3$$

1.13 RELATIVE DENSITY AND RELATIVE COMPACTION

Relative density is a term generally used to describe the degree of compaction of coarse-grained soils. Relative density D_r is defined as

$$D_r = \frac{e_{max} - e}{e_{max} - e_{min}} \tag{1.45}$$

where

e_{max} is the maximum possible void ratio
e_{min} is the minimum possible void ratio
e is the void ratio in natural state of soil

Equation 1.45 can also be expressed in terms of dry unit weight of the soil:

$$\gamma_d(\max) = \frac{G_s \gamma_w}{1 + e_{min}} \quad \text{or} \quad e_{min} = \frac{G_s \gamma_w}{\gamma_d(\max)} - 1 \tag{1.46}$$

Similarly,

$$e_{max} = \frac{G_s \gamma_w}{\gamma_d(\min)} - 1 \tag{1.47}$$

and

$$e = \frac{G_s \gamma_w}{\gamma_d} - 1 \tag{1.48}$$

where $\gamma_d(\max)$, $\gamma_d(\min)$, and γ_d are the maximum, minimum, and natural-state dry unit weights of the soil. Substitution of Equations 1.46 through 1.48 into Equation 1.45 yields

$$D_r = \left[\frac{\gamma_d(\max)}{\gamma_d}\right] \cdot \left[\frac{\gamma_d - \gamma_d(\min)}{\gamma_d(\max) - \gamma_d(\min)}\right] \tag{1.49}$$

Relative density is generally expressed as a percentage. It has been used by several investigators to correlate the angle of friction of soil, the soil liquefaction potential, etc.

Another term occasionally used in regard to the degree of compaction of coarse-grained soils is *relative compaction*, R_c, which is defined as

$$R_c = \frac{\gamma_d}{\gamma_d(\max)} \tag{1.50a}$$

Comparing Equations 1.49 and 1.50a,

$$R_c = \frac{R_o}{1 - D_r(1 - R_o)} \tag{1.50b}$$

where $R_o = \gamma_d(\min)/\gamma_d(\max)$.

Lee and Singh (1971) reviewed 47 different soils and gave the approximate relation between relative compaction and relative density as

$$R_c = 80 + 0.2D_r \tag{1.50c}$$

where D_r is in percent.

1.14 RELATIONSHIP BETWEEN e_{max} AND e_{min}

The maximum and minimum void ratios for granular soils described in Section 1.13 depend on several factors such as

- Grain size
- Grain shape
- Nature of grain-size distribution
- Fine content F_c (i.e., fraction smaller than 0.075 mm)

Following are some of the correlations now available in the literature related to e_{max} and e_{min} of granular soils.

- Clean sand (F_c = 0%–5%)

Miura et al. (1997) conducted an extensive study of the physical characteristics of about 200 samples of granular material, which included mostly clean sand, some glass beads, and lightweight aggregates (LWA). Figure 1.35 shows a plot of e_{max} versus e_{min} obtained from that study, which shows that

$$e_{max} \cong 1.62e_{min} \tag{1.51}$$

Cubrinovski and Ishihara (2002) analyzed a large number of clean sand samples based on which it was suggested that

$$e_{max} = 0.072 + 1.53e_{min} \tag{1.52}$$

The data points upon which Equation 1.52 is based and an additional 55 data points for clean sand given by Patra et al. (2010) are shown in Figure 1.36. From this figure, it appears that Equation 1.51 may be taken as a good average approximation. The difference in the angularity or roundness of the particles of different soils is another major factor causing the scatter.

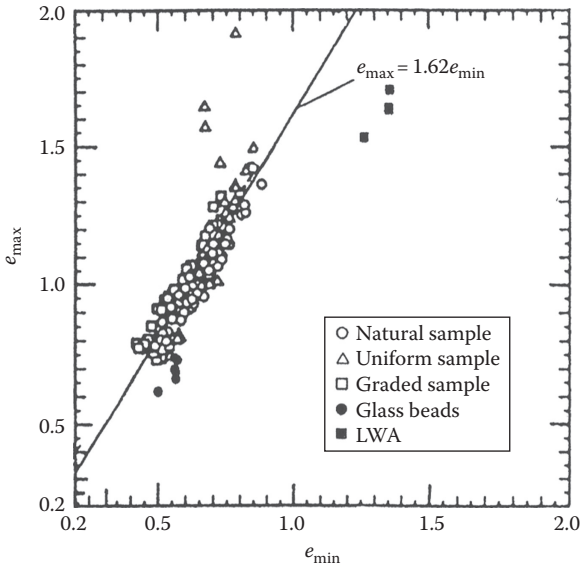

Figure 1.35 Plot of e_{max} versus e_{min} based on the results of Miura et al. (1997).

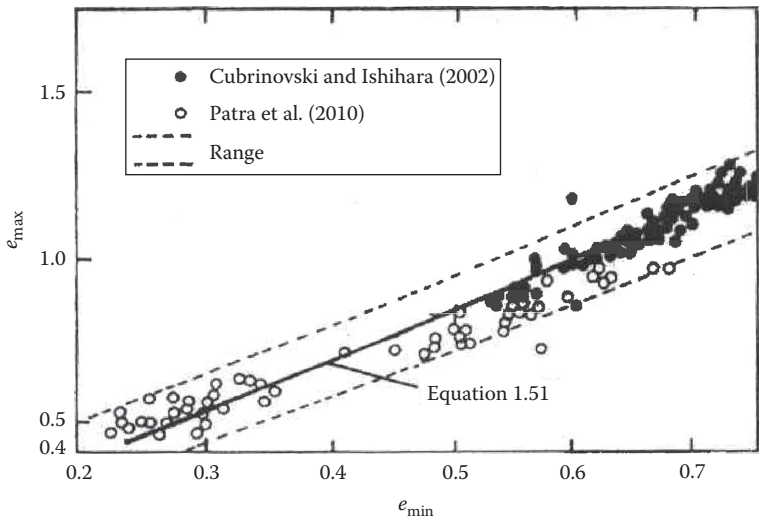

Figure 1.36 Plot of e_{max} versus e_{min} for clean sand.

Based on best-fit linear regression lines, Cubrinovski and Ishihara (2002) also provided the following relationships for other soils:

- Sand with fines ($5\% < F_c \leq 15\%$)

$$e_{max} = 0.25 + 1.37e_{min} \tag{1.53}$$

- Sand with fines and clay ($15\% < F_c \leq 30\%$; $P_c = 5\%–20\%$)

$$e_{max} = 0.44 + 1.21e_{min} \tag{1.54}$$

- Silty soils ($30\% < F_c \leq 70\%$; $P_c = 5\%–20\%$)

$$e_{max} = 0.44 + 1.32e_{min} \tag{1.55}$$

where
F_c is the fine fraction for which grain size is smaller than 0.075 mm
P_c is the clay-size fraction (<0.005 mm)

Based on a very large database, Cubrinovski and Ishihara (1999, 2002) developed a unique relationship between $e_{max} - e_{min}$ and median grain size D_{50}. The database included results from clean sand, sand with fines, and sand with clay, silty soil, gravelly sand, and gravel. This relationship is shown in Figure 1.37. In spite of some scatter, the average line can be given by the relation

$$e_{max} - e_{min} = 0.23 + \frac{0.06}{D_{50}(\text{mm})} \tag{1.56}$$

It appears that the upper and lower limits of $e_{max} - e_{min}$ versus D_{50} as shown in Figure 1.37 can be approximated as

- Lower limit

$$e_{max} - e_{min} = 0.16 + \frac{0.045}{D_{50}(\text{mm})} \tag{1.57}$$

- Upper limit

$$e_{max} - e_{min} = 0.29 + \frac{0.079}{D_{50}(\text{mm})} \tag{1.58}$$

1.15 SOIL CLASSIFICATION SYSTEMS

Soil classification is the arrangement of soils into various groups or subgroups to provide a common language to express briefly the general usage characteristics without detailed descriptions. At the present time, two major soil classification

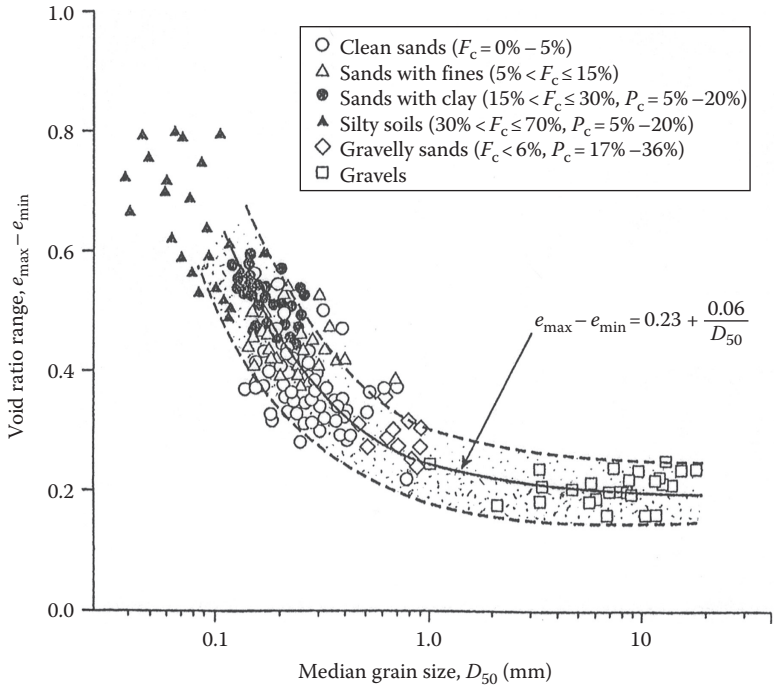

Figure 1.37 Plot of $e_{max} - e_{min}$ versus median grain size (D_{50}). (Redrawn after Cubrinovski and Ishihara, *Soils Found.*, 42(6), 65–78, 2002.)

systems are available for general engineering use. They are the unified system and the American Association of State Highway and Transportation Officials (AASHTO) system. Both systems use simple index properties such as grain-size distribution, liquid limit, and plasticity index of soil.

1.15.1 Unified system

The unified system of soil classification was originally proposed by A. Casagrande in 1948 and was then revised in 1952 by the Corps of Engineers and the U.S. Bureau of Reclamation. In its present form [also see ASTM D-2487, ASTM (2010)], the system is widely used by various organizations, geotechnical engineers in private consulting business, and building codes.

Initially, there are two major divisions in this system. A soil is classified as a coarse-grained soil (gravelly and sandy) if more than 50% is retained on a No. 200 sieve and as a fine-grained soil (silty and clayey) if 50% or more is passing through a No. 200 sieve. The soil is then further classified by a number of subdivisions, as shown in Table 1.6.

Table 1.6 Unified soil classification system

Major divisions	*Group symbols*	*Typical names*	*Criteria or classification*[a]
Coarse-grained soils (<50% passing No. 200 sieve)[a]			
Gravels (<50% of coarse fraction passing No. 4 sieve)			
Gravels with few or no fines	GW	Well-graded gravels; gravel–sand mixtures (few or no fines)	$C_u = \frac{D_{60}}{D_{10}} > 4; \quad C_c = \frac{(D_{30})^2}{(D_{10})(D_{60})}$ Between 1 and 3
	GP	Poorly graded gravels; gravel–sand mixtures (few or no fines)	Not meeting the two criteria for GW
Gravels with fines	GM	Silty gravels; gravel–sand–silt mixtures	Atterberg limits below *A*-line *or* plasticity index less than 4[b] (see Figure 1.38)
	GC	Clayey gravels; gravel–sand–clay mixtures	Atterberg limits above *A*-line *with* plasticity index greater than 7[b] (see Figure 1.38)
Sands (≥50% of coarse fraction passing No. 4 sieve)			
Clean sands (few or no fines)	SW	Well-graded sands; gravelly sands (few or no fines)	$C_u = \frac{D_{60}}{D_{10}} > 6; \quad C_c = \frac{(D_{30})^2}{(D_{10})(D_{60})}$ Between 1 and 3
	SP	Poorly graded sands; gravelly sands (few or no fines)	Not meeting the two criteria for SW

Sands with fines (appreciable amount of fines)	SM	Silty sands; sand–silt mixtures	Atterberg limits below *A*-line *or* plasticity index less than 4[b] (see Figure 1.38)
	SC	Clayey sands; sand–clay mixtures	Atterberg limits above *A*-line *with* plasticity index greater than 7[b] (see Figure 1.38)
Fine-grained soils (≥50% passing No. 200 sieve)			
Silts and clay (liquid limit less than 50)	ML	Inorganic silts; very fine sands; rock flour; silty or clayey fine sands	See Figure 1.38
	CL	Inorganic clays (low to medium plasticity); gravelly clays; sandy clays; silty clays; lean clays	See Figure 1.38
	OL	Organic silts; organic silty clays (low plasticity)	See Figure 1.38
Silts and clay (liquid limit greater than 50)	MH	Inorganic silts; micaceous or diatomaceous fine sandy or silty soils; elastic silt	See Figure 1.38
	CH	Inorganic clays (high plasticity); fat clays	See Figure 1.38
	OH	Organic clays (medium to high plasticity); organic silts	See Figure 1.38
Highly organic silts	Pt	Peat; mulch; and other highly organic soils	

Group symbols are G, gravel; W, well-graded; S, sand; P, poorly graded; C, clay; H, high plasticity; M, silt; L, low plasticity; O, organic silt or clay; Pt, peat and highly organic soil.

[a] Classification based on percentage of fines: <5% passing No. 200: GW. GP. SW. SP: >12% passing No. 200: GM. GC. SM. SC: 5%–12% passing No. 200: borderline—dual symbols required such as GW–GM. GW–GC. GP–GM. GP–SC. SW–SM. SW–SC. SP–SM. SP–SC.

[b] Atterberg limits above *A*-line and plasticity index between 4 and 7 are borderline cases. It needs dual symbols (see Figure 1.38).

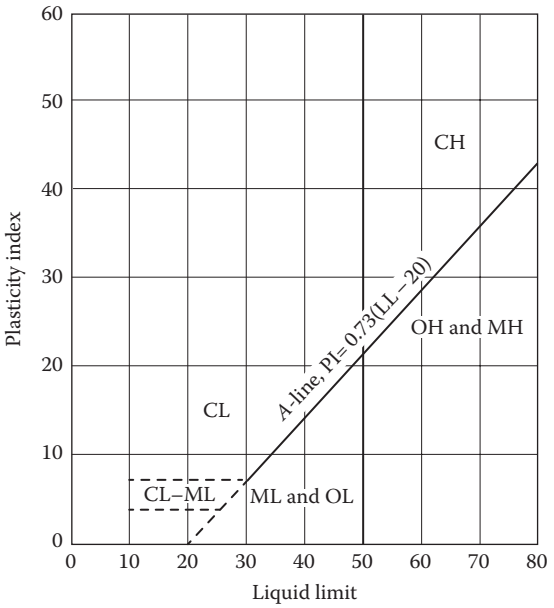

Figure 1.38 Plasticity chart.

Example 1.2

For a soil specimen, given the following,

Passing No. 4 sieve = 92%	Passing No. 40 sieve = 78%
Passing No. 10 sieve = 81%	Passing No. 200 sieve = 65%
Liquid limit = 48	Plasticity index = 32

classify the soil by the unified classification system.

Solution

Since more than 50% is passing through a No. 200 sieve, it is a fine-grained soil, that is, it could be ML, CL, OL, MH, CH, or OH. Now, if we plot LL = 48 and PI = 32 on the plasticity chart given in Figure 1.38, it falls in the zone CL. So the soil is classified as CL.

1.15.2 AASHTO classification system

This system of soil classification was developed in 1929 as the Public Road Administration Classification System. It has undergone several revisions, with the present version proposed by the Committee on Classification of Materials for Subgrades and Granular Type Roads of the Highway Research Board in 1945 [ASTM (2010) Test Designation D-3282].

The AASHTO classification system in present use is given in Table 1.7. According to this system, soil is classified into seven major

Table 1.7 Classification of highway subgrade materials

General classification	*Granular materials (35% or less of total sample passing No. 200 sieve)*						
	A-1			*A-2*			
Group classification	A-1-a	A-1-b	A-3	A-2-4	A-2-5	A-2-6	A-2-7
Sieve analysis (percent passing)							
No. 10	50 max.						
No. 40	30 max.	50 max.	50 min.				
No. 200	15 max.	25 max.	10 max.	35 max.	35 max.	35 max.	35 max.
Characteristics of fraction passing							
No. 40							
Liquid limit				40 max.	41 min.	40 max.	41 min.
Plasticity index	6 max.		NP	10 max.	10 max.	11 min.	11 min.
Usual types of significant constituent materials	Stone fragments, gravel, and sand		Fine sand	Silty or clayey gravel and sand			
General subgrade rating	Excellent to good						
General classification	Silt–clay materials (more than 35% or total sample passing No. 200 sieve)						
							A-7
							A-7-5[a]
Group classification	A-4		A-5		A-6		A-7-6[b]
Sieve analysis (percent passing)							
No. 10							
No. 40							
No. 200	36 min.		36 min.		36 min.		36 min.
Characteristics of fraction passing							
No. 40							
Liquid limit	40 max.		41 min.		40 max.		41 min.
Plasticity index	10 max.		10 max.		11 min.		11 min.
Usual types of significant constituent materials	Silty soils				Clayey soils		
General subgrade rating	Fair to poor						

[a] For A-7-5, PI $\leq$ LL $-$ 30.
[b] For A-7-6, PI $>$ LL $-$ 30.

groups: A-1 through A-7. Soils classified into Groups A-1, A-2, and A-3 are granular materials, where 35% or less of the particles pass through the No. 200 sieve. Soils where more than 35% pass through the No. 200 sieve are classified into groups A-4, A-5, A-6, and A-7. These are mostly silt and clay-type materials. The classification system is based on the following criteria:

1. Grain size
   Gravel: Fraction passing the 75 mm sieve and retained on No. 10 (2 mm) U.S. sieve
   Sand: Fraction passing the No. 10 (2 mm) U.S. sieve and retained on the No. 200 (0.075 mm) U.S. sieve
   Silt and clay: Fraction passing the No. 200 U.S. sieve
2. Plasticity: The term *silty* is applied when the fine fractions of the soil have a plasticity index of 10 or less. The term *clayey* is applied when the fine fractions have a plasticity index of 11 or more.
3. If cobbles and *boulders* (size larger than 75 mm) are encountered, they are excluded from the portion of the soil sample on which classification is made. However, the percentage of such material is recorded.

To classify a soil according to Table 1.7, the test data are applied from left to right. By the process of elimination, the first group from the left into which the test data will fit is the correct classification.

For the evaluation of the quality of a soil as a highway subgrade material, a number called the *group index* (GI) is also incorporated with the groups and subgroups of the soil. The number is written in parentheses after the group or subgroup designation. The group index is given by the equation

$$\text{GI} = (F - 35)[0.2 + 0.005(\text{LL} - 40)] + 0.01(F - 15)(\text{PI} - 10) \tag{1.59}$$

where

F is the percent passing the No. 200 sieve
LL is the liquid limit
PI is the plasticity index

The first term of Equation 1.59—that is, $(F - 35)[0.2 + 0.005(\text{LL} - 40)]$—is the partial group index determined from the liquid limit. The second term—that is, $0.01(F - 15)(\text{PI} - 10)$—is the partial group index determined from the plasticity index. Following are the rules for determining the group index:

1. If Equation 1.59 yields a negative value for GI, it is taken as 0.
2. The group index calculated from Equation 1.59 is rounded off to the nearest whole number (e.g., GI = 3.4 is rounded off to 3; GI = 3.5 is rounded off to 4).

3. There is no upper limit for the group index.
4. The group index of soils belonging to groups A-1-a, A-1-b, A-2-4, A-2-5, and A-3 is always 0.
5. When calculating the group index for soils that belong to groups A-2-6 and A-2-7, use the partial group index for PI, or

$$GI = 0.01(F - 15)(PI - 10) \tag{1.60}$$

In general, the quality of performance of a soil as a subgrade material is inversely proportional to the group index.

Example 1.3

Classify the following soil by the AASHTO classification system.

Passing No. 10 sieve: 100%
Passing No. 40 sieve: 92%
Passing No. 200 sieve: 86%
Liquid limit (LL): 70
Plasticity index (PI): 32

Solution

Percent passing the No. 200 sieve is 86%. So, it is a silty clay material (i.e., A-4, A-5, A-6, or A-7) as shown in Table 1.7. Proceeding from left to right, we see that it falls under A-7. For this case, PI = 32 < LL – 30. So, this is A-7-5. From Equation 1.59

$$GI = (F - 35)[0.2 + 0.005(LL - 40)] + 0.01(F - 15)(PI - 10)$$

Now, $F = 86$; LL = 70; PI = 32; so

$$GI = (86 - 35)[0.2 + 0.005(70 - 40)] + 0.01(86 - 15)(32 - 10)$$
$$= 33.47 \triangleq 33$$

Thus, the soil is A-7-5(33).

1.16 COMPACTION

Compaction of loose fills is a simple way of increasing the stability and load-bearing capacity of soils, and this is generally achieved by using smooth-wheel rollers, sheepsfoot rollers, rubber-tired rollers, and vibratory rollers. In order to write the specifications for field compaction, Proctor

compaction tests are generally conducted in the laboratory. A brief description of the Proctor compaction test procedure is as follows:

1.16.1 Standard Proctor compaction test

A standard laboratory soil compaction test was first developed by Proctor (1933), and this is usually referred to as the *standard Proctor test* (ASTM designation D-698). The test is conducted by compaction of three layers of soil in a mold that is 944 cm^3 in volume. Each layer of soil is subjected to 25 blows by a hammer weighing 24.6 N with a 304.8 mm drop. From the known volume of the mold, weight of moist compacted soil in the mold, and moisture content of the compacted soil, the dry unit weight of compaction can be determined as

$$\gamma_{moist} = \frac{\text{Weight of moist soil in the mold}}{\text{Volume of the mold}}$$

$$\gamma_d = \frac{\gamma_{moist}}{1 + w}$$

where

γ_{moist} is the moist unit weight of compacted soil
γ_d is the dry unit weight of compacted soil
w is the moisture content of soil

The test can be repeated several times at various moist contents of soil. By plotting a graph of γ_d against the corresponding moisture content, the optimum moisture content w_{opt} and the maximum dry unit weight $\gamma_{d(max)}$ can be obtained (Figure 1.39). Also plotted in Figure 1.39 is the variation of

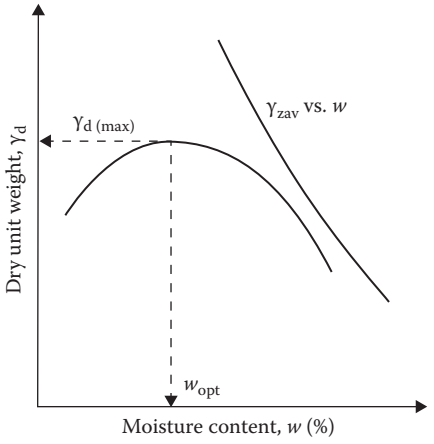

Figure 1.39 Nature of variation of γ_d versus w.

the dry unit weights, assuming the degree of saturation to be 100%. These are the *theoretical maximum* dry unit weights that can be attained for a given moisture content when there will be no air in the void spaces. With the degree of saturation as 100%

$$e = wG_s \tag{1.61}$$

The maximum dry unit weight at a given moisture content with zero air voids can be given by (Equation 1.38)

$$\gamma_{zav} = \frac{G_s\gamma_w}{1+e} = \frac{G_s\gamma_w}{1+wG_s} = \frac{\gamma_w}{(1/G_s)+w} \tag{1.62}$$

where γ_{zav} is the zero-air-void unit weight (dry).

For standard Proctor compaction test, the compaction energy E can be expressed as

$$E = \frac{(24.5\,\text{N/blow})(3\,\text{layers})(25\,\text{blows/layer})(0.3048\,\text{m})}{(944/10^6)\text{m}^3}$$

$$= 593{,}294\,\text{N-m/m}^3 \triangleq 593\,\text{kN-m/m}^3$$

1.16.2 Modified Proctor compaction test

With the development of heavier compaction equipment, the standard Proctor test has been modified for better representation of field conditions. In the *modified Proctor test* (ASTM designation D-1577), the same mold as in the standard Proctor test is used. However, the soil is compacted in 5 layers, with a 44.5 N hammer giving 25 blows to each layer. The height of drop of the hammer is 457.2 mm. Hence, the compactive effort in the modified Proctor test is equal to

$$E = \frac{(25\,\text{blows/layer})(5\,\text{layers})(44.5\,\text{N/blow})(0.4572\,\text{m})}{(944/10^6)\,\text{m}^3}$$

$$= 2{,}694{,}041\,\text{N-m/m}^3 \triangleq 2604\,\text{kN-m/m}^3$$

The maximum dry unit weight obtained from the modified Proctor test will be higher than that obtained from the standard Proctor test due to the application of higher compaction energy. It will also be accompanied by a lower optimum moisture content compared to that obtained from the standard Proctor compaction test.

1.17 EMPIRICAL RELATIONSHIPS FOR PROCTOR COMPACTION TESTS

Omar et al. (2003) presented the results of modified Proctor compaction tests on 311 soil samples. Of these samples, 45 were gravelly soil (GP, GP–GM, GW, GW–GM, and GM), 264 were sandy soil (SP, SP–SM, SW–SM, SW, SC–SM, SC, and SM), and two were clay with low plasticity (CL). Based on the tests, the following correlations were developed:

$$\gamma_{d(max)} = [4,804,574G_s - 195.55(\mathrm{LL})^2 + 156,971(R\#4)^{0.5} - 9,527,830]^{0.5} \tag{1.63}$$

$$\ln(w_{opt}) = 1.195 \times 10^{-4}(\mathrm{LL})^2 - 1.964G_s - 6.617 \times 10^{-5}(R\#4) + 7.651 \tag{1.64}$$

where

$\rho_{d(max)}$ is the maximum dry density
w_{opt} is the optimum moisture content (%)
G_s is the specific gravity of soil solids
LL is the liquid limit, in percent
R#4 is the percent retained on No. 4 sieve

For granular soils with less than 12% fines (i.e., finer than No. 200 sieve), relative density may be a better indicator for end product compaction specification in the field. Based on laboratory compaction tests on 55 clean sands (less than 5% finer than No. 200 sieve), Patra et al. (2010) provided the following relationships:

$$D_r = AD_{50}^{-B} \tag{1.65}$$

$$A = 0.216\ln E - 0.850 \tag{1.66}$$

$$B = -0.03\ln E + 0.306 \tag{1.67}$$

where

D_r is the maximum relative density of compaction achieved with compaction energy E, kN-m/m^3
D_{50} is the median grain size, mm

Gurtug and Sridharan (2004) proposed correlations for optimum moisture content and maximum dry unit weight with the plastic limit PL of cohesive soils. These correlations can be expressed as

$$w_{opt}(\%) = [1.95 - 0.38(\log E)](\text{PL}) \tag{1.68}$$

$$\gamma_{d(max)}(\text{kN/m}^3) = 22.68e^{0.0183w_{opt}(\%)} \tag{1.69}$$

where

PL is the plastic limit, %
E is the compaction energy, kN-m/m^3

For modified Proctor test, $E \approx 2700$ kN/m^3. Hence,

$$w_{opt}(\%) \cong 0.65(\text{PL})$$

$$\gamma_{d(max)}(\text{kN/m}^3) \cong 22.68e^{-0.012(\text{PL})}$$

Osman et al. (2008) analyzed a number of laboratory compaction test results on fine-grained (cohesive) soil, including those provided by Gurtug and Sridharan (2004). Based on this study, the following correlations were developed:

$$w_{opt}(\%) \cong (1.99 - 0.165\ln E)(\text{PI}) \tag{1.70}$$

$$\gamma_{d(max)}(\text{kN/m}^3) \cong L - Mw_{opt}(\%) \tag{1.71}$$

where

$$L = 14.34 + 1.195\ln E \tag{1.72}$$

$$M = -0.19 + 0.073\ln E \tag{1.73}$$

w_{opt} is the optimum moisture content, %
PI is the plasticity index, %
$\gamma_{d(max)}$ is the maximum dry unit weight, kN/m^3
E is the compaction energy, kN-m/m^3

DiMatteo et al. (2009) analyzed the results of 71 fine-grained soils and provided the following correlations for optimum moisture content w_{opt} and maximum dry unit weight $\gamma_{d(max)}$ for modified Proctor tests (E = 2700 kN-m/m^3)

$$w_{opt}(\%) = -0.86(\text{LL}) + 3.04\left(\frac{\text{LL}}{G}\right) + 2.2 \tag{1.74}$$

$$\gamma_{d(max)}(\text{kN/m}^3) = 40.316\left(w_{opt}^{-0.295}\right)(\text{PI}^{0.32}) - 2.4 \tag{1.75}$$

where

LL is the liquid limit, %
PI is the plasticity index, %
G_s is the specific gravity of soil solids

Example 1.4

For a sand with 4% finer than No. 200 sieve, estimate the maximum relative density of compaction that may be obtained from a modified Proctor test. Given D_{50} = 1.4 mm.

Solution

For the modified Proctor test, E = 2696 kN-m/m^3.
From Equation 1.66

$$A = 0.216\ln E - 0.850 = (0.216)(\ln 2696) - 0.850 = 0.856$$

From Equation 1.67

$$B = -0.03\ln E + 0.306 = -(0.03)(\ln 2696) + 0.306 = 0.069$$

From Equation 1.65

$$D_r = AD_{50}^{-B} = (0.856)(1.4)^{-0.069} = 0.836 = 83.6\%$$

Example 1.5

For a silty clay soil given LL = 43 and PL = 18. Estimate the maximum dry unit weight of compaction that can be achieved by conducting modified Proctor test. Use Equation 1.71.

Solution

For the modified Proctor test, E = 2696 kN-m/m^3.
From Equations 1.72 and 1.73

$$L = 14.34 + 1.195\ln E = 14.34 + 1.195\ln(2696) = 23.78$$

$$M = -0.19 + 0.073\ln E = -0.19 + 0.073\ln(2696) = 0.387$$

From Equation 1.70

$$w_{opt}\,(\%) = (1.99 - 0.165 \ln E)(\text{PI})$$
$$= [1.99 - 0.165 \ln (2696)](43 - 18)$$
$$= 17.16\%$$

From Equation 1.71

$$\gamma_{d(max)} = L - Mw_{opt} = 23.78 - (0.387)(17.16) = 17.14 \text{ kN/m}^3$$

REFERENCES

American Society for Testing and Materials, *Annual Book of ASTM Standards*, sec. 4, vol. 04.08, ASTM, West Conshohocken, PA, 2010.

Atterberg, A., Uber die Physikalische Bodenuntersuschung und Uber die Plastizitat der Tone, *Int. Mitt. Bodenkunde*, 1, 5, 1911.

Bolt, G. H., Analysis of validity of Gouy-Chapman theory of the electric double layer, *J. Colloid Sci.*, 10, 206, 1955.

Bolt, G. H., Physical chemical analysis of compressibility of pure clay, *Geotechnique*, 6, 86, 1956.

Casagrande, A., Classification and identification of soils, *Trans. ASCE*, 113, 901–930, 1948.

Cubrinovski, M. and K. Ishihara, Empirical correlation between SPT N-value and relative density for sandy soils, *Soils Found.*, 39(5), 61–71, 1999.

Cubrinovski, M. and K. Ishihara, Maximum and minimum void ratio characteristics of sands, *Soils Found.*, 42(6), 65–78, 2002.

DiMatteo, L. D., F. Bigotti, and R. Rico, Best-fit model to estimate proctor properties of compacted soil, *J. Geotech. Geoenviron. Eng., Am. Soc. Civ. Eng.*, 135(7), 992–996, 2009.

Grim, R.E., Physico-Chemical Properties of Soils, *J. Soil Mech. Found. Div., ASCE*, 85(SM2), 1–17, 1959.

Gurtug, Y. and A. Sridharan, Compaction behaviour and prediction of its characteristics of fine grained soils with particular reference to compaction energy, *Soils Found.*, 44(5), 27–36, 2004.

Lambe, T. W., Compacted clay: Structure, *Trans. ASCE*, 125, 682–717, 1960.

Lee, K. L. and A. Singh, Relative density and relative compaction, *J. Soil Mech. Found. Div., Am. Soc. Civ. Eng.*, 97(SM7), 1049–1052, 1971.

Miura, K., K. Maeda, M. Furukama, and S. Toki, Physical characteristics of sands with different primary properties, *Soils Found.*, 37(3), 53–64, 1997.

Omar, M., S. Abdallah, A. Basma, and S. Barakat, Compaction characteristics of granular soils in United Arab Emirates, *Geotech. Geol. Eng.*, 21(3), 283–295, 2003.

Osman, S., E. Togrol, and C. Kayadelen, Estimating compaction behavior of fine-grained soils based on compaction energy, *Can. Geotech. J.*, 45(6), 877–887, 2008.

Patra, C. R., N. Sivakugan, B. M. Das, and S. K. Rout, Correlation of relative density of clean sand with median grain size and compaction energy, *Int. J. Geotech. Eng.*, 4(2), 196–203, 2010.

Proctor, R. R., Design and construction of rolled earth dams, *Eng. News Record*, 3, 245–248, 286–289, 348–351, 372–376, 1933.

Seed, H. B., R. J. Woodward, and R. Lundgren, Clay mineralogical aspects of the Atterberg limits, *J. Soil Mech. Found. Eng. Div., Am. Soc. Civ. Eng.*, 90(SM4), 107–131, 1964a.

Seed, H. B., R. J. Woodward, and R. Lundgren, Fundamental aspects of Atterberg limits, *J. Soil Mech. Found. Eng. Div., Am. Soc. Civ. Eng.*, 90(SM6), 75–105, 1964b.

Skempton, A. W., The colloidal activity of clay, *Proc. 3rd Int. Conf. Soil Mech. Found. Eng.*, Zurich, Switzerland, Vol. 1, pp. 57–61, 1953.

Sridharan, A., H. B. Nagaraj, and K. Prakash, Determination of the plasticity index from flow index, *Geotech. Testing J.*, ASTM, 22(2), 175–181, 1999.

Verweg, E. J. W. and J. Th. G. Overbeek, *Theory of Stability of Lyophobic Colloids*, Elsevier-North Holland, Amsterdam, the Netherlands, 1948.

Wroth, C. P. and D. M. Wood, The correlation of index properties with some basic engineering properties of soils, *Can. Geotech. J.*, 15(2), 137–145, 1978.

Chapter 2

Stresses and strains

Elastic equilibrium

2.1 INTRODUCTION

An important function in the study of soil mechanics is to predict the stresses and strains imposed at a given point in a soil mass due to certain loading conditions. This is necessary to estimate settlement and to conduct stability analysis of earth and earth-retaining structures, as well as to determine stress conditions on underground and earth-retaining structures.

An idealized stress–strain diagram for a material is shown in Figure 2.1. At low stress levels, the strain increases linearly with stress (branch *ab*), which is the elastic range of the material. Beyond a certain stress level, the material reaches a plastic state, and the strain increases with no further increase in stress (branch *bc*). The theories of stresses and strains presented in this chapter are for the elastic range only. In determining stress and strain in a soil medium, one generally resorts to the principles of the theory of elasticity, although soil in nature is not fully homogeneous, elastic, or isotropic. However, the results derived from the elastic theories can be judiciously applied to the problem of soil mechanics.

2.2 BASIC DEFINITION AND SIGN CONVENTIONS FOR STRESSES

An elemental soil mass with sides measuring dx, dy, and dz is shown in Figure 2.2. Parameters σ_x, σ_y, and σ_z are the normal stresses acting on the planes normal to the x, y, and z axes, respectively. The normal stresses are considered positive when they are directed onto the surface. Parameters τ_{xy}, τ_{yx}, τ_{yz}, τ_{zy}, τ_{zx}, and τ_{xz} are shear stresses. The notations for the shear stresses follow.

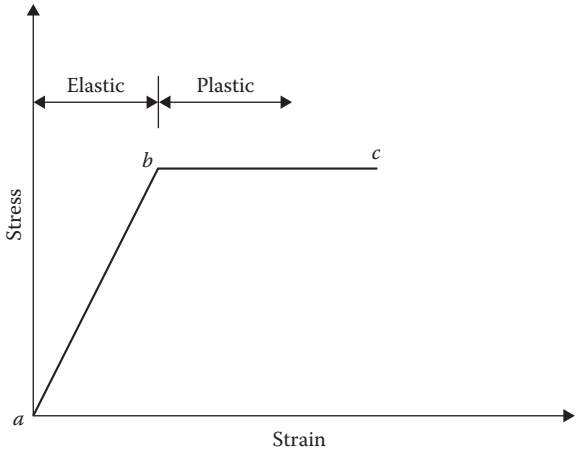

Figure 2.1 Idealized stress–strain diagram.

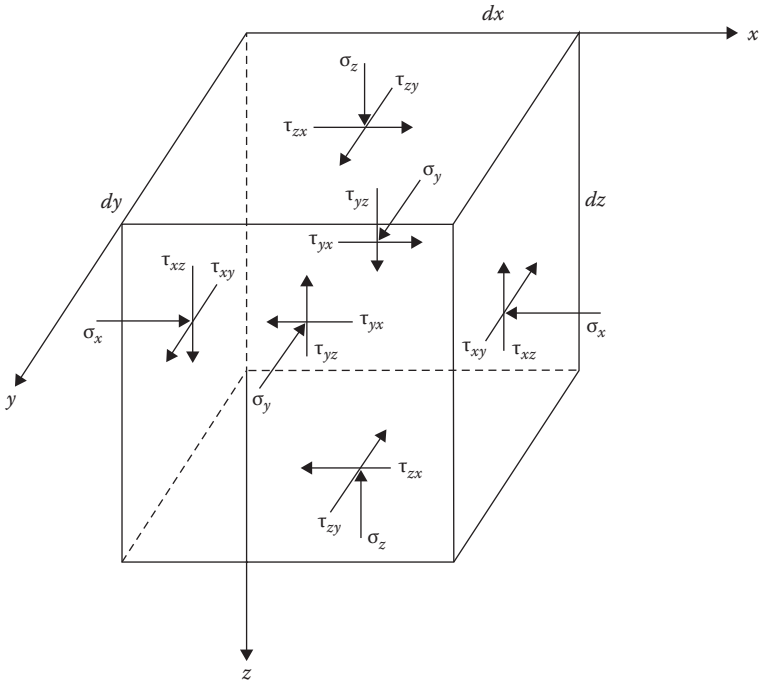

Figure 2.2 Notations for normal and shear stresses in a Cartesian coordinate system.

If τ_{ij} is a shear stress, it means the stress is acting on a plane normal to the i axis, and its direction is parallel to the j axis. A shear stress τ_{ij} is considered positive if it is directed in the negative j direction while acting on a plane whose outward normal is the positive i direction. For example, all shear stresses are positive in Figure 2.2. For equilibrium

$$t_{xy} = t_{yx} \tag{2.1}$$

$$t_{xz} = t_{zz} \tag{2.2}$$

$$t_{yz} = t_{zy} \tag{2.3}$$

Figure 2.3 shows the notations for the normal and shear stresses in a polar coordinate system (two-dimensional case). For this case, σ_r and σ_θ are the normal stresses, and $\tau_{r\theta}$ and $\tau_{\theta r}$ are the shear stresses. For equilibrium, $\tau_{r\theta} = \tau_{\theta r}$. Similarly, the notations for stresses in a cylindrical coordinate system are shown in Figure 2.4. Parameters σ_r, σ_θ, and σ_z are the normal stresses, and the shear stresses are $\tau_{r\theta} = \sigma_{\theta r}$, $\sigma_{\theta z} = \sigma_{z\theta}$, and $\tau_{rz} = \tau_{zr}$.

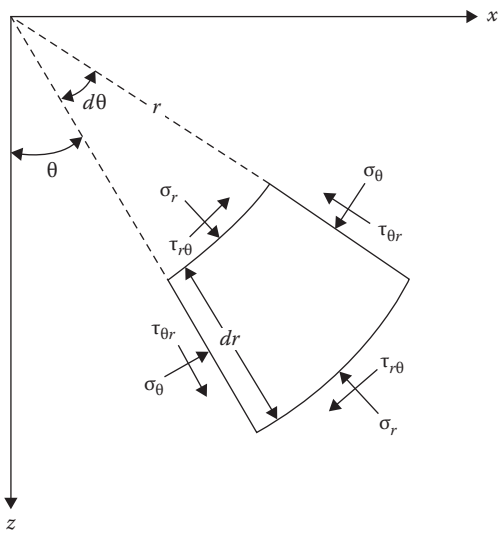

Figure 2.3 Notations for normal and shear stresses in a polar coordinate system.

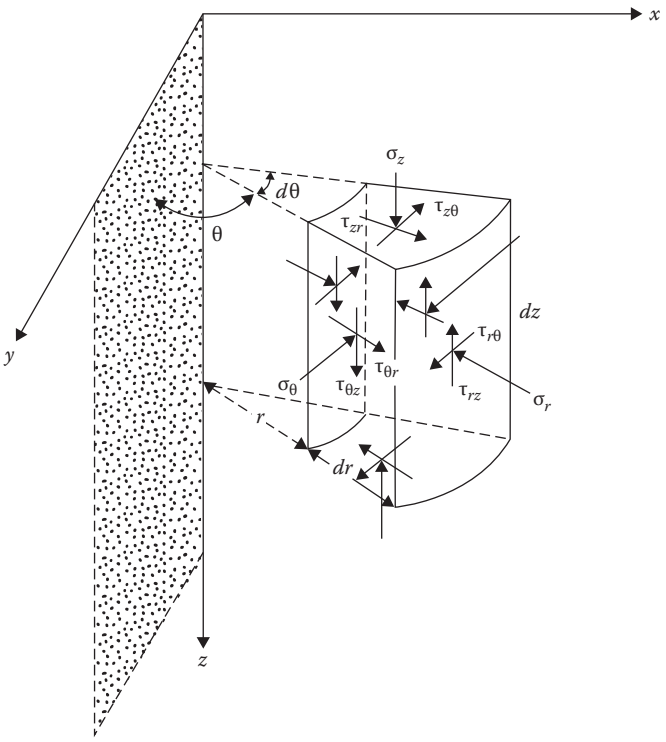

Figure 2.4 Notations for normal and shear stresses in cylindrical coordinates.

2.3 EQUATIONS OF STATIC EQUILIBRIUM

Figure 2.5 shows the stresses acting on an elemental soil mass with sides measuring *dx*, *dy*, and *dz*. Let γ be the unit weight of the soil. For equilibrium, summing the forces in the *x* direction

$$\sum F_x = \left(\sigma_x - \left(\sigma_x + \frac{\partial \sigma_x}{\partial x} dx\right)\right) dy\, dz + \left(\tau_{zx} - \left(\tau_{zx} + \frac{\partial \tau_{zx}}{\partial z} dz\right)\right) dx\, dy$$

$$+ \left(\tau_{yx} - \left(\tau_{yx} + \frac{\partial \tau_{yx}}{\partial y} dy\right)\right) dx\, dz = 0$$

or

$$\frac{\partial \sigma_x}{\partial x} + \frac{\partial \tau_{yx}}{\partial y} + \frac{\partial \tau_{zx}}{\partial z} = 0 \tag{2.4}$$

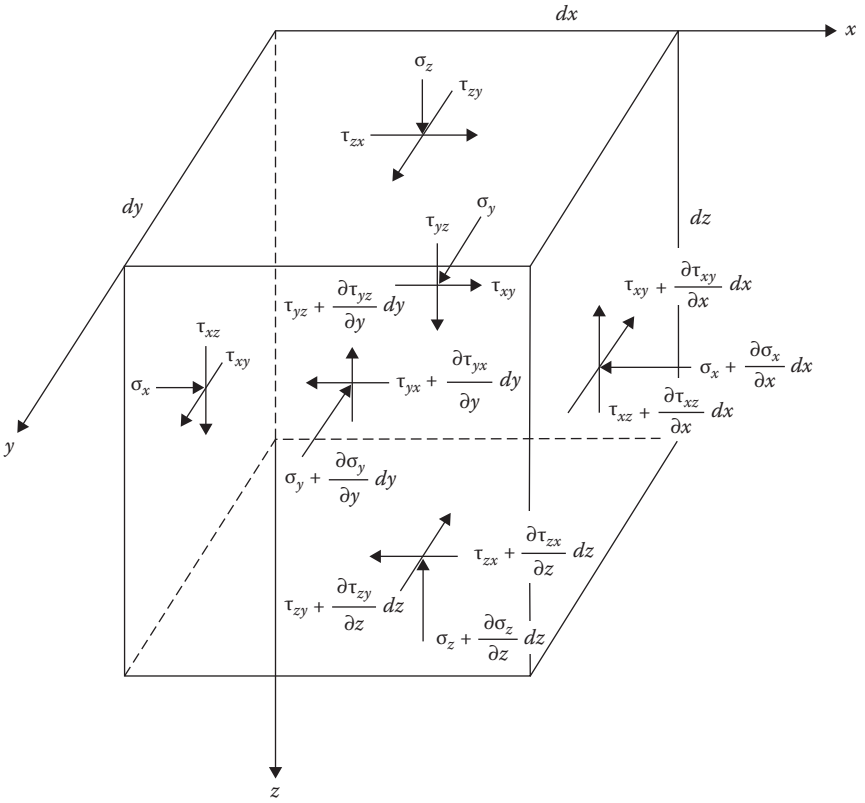

Figure 2.5 Derivation of equations of equilibrium.

Similarly, along the y direction, $\Sigma F_y = 0$, or

$$\frac{\partial \sigma_y}{\partial y} + \frac{\partial \tau_{xy}}{\partial x} + \frac{\partial \tau_{zy}}{\partial z} = 0 \tag{2.5}$$

Along the z direction

$$\sum F_z = \left(\sigma_z - \left(\sigma_z + \frac{\partial \sigma_z}{\partial z} dz\right)\right) dx\, dy + \left(\tau_{xz} - \left(\tau_{xz} + \frac{\partial \tau_{xz}}{\partial x} dx\right)\right) dy\, dz$$

$$+ \left(\tau_{yz} - \left(\tau_{yz} + \frac{\partial \tau_{yz}}{\partial y} dy\right)\right) dx\, dz + \gamma (dx\, dy\, dz) = 0$$

The last term of the preceding equation is the self-weight of the soil mass.

Thus

$$\frac{\partial \sigma_z}{\partial z} + \frac{\partial \tau_{xz}}{\partial x} + \frac{\partial \tau_{yz}}{\partial y} - \gamma = 0 \tag{2.6}$$

Equations 2.4 through 2.6 are the static equilibrium equations in the Cartesian coordinate system. These equations are written in terms of *total stresses*.

They may, however, be written in terms of *effective stresses* as

$$\sigma_x = \sigma'_x + u = \sigma'_x + \gamma_w h \tag{2.7}$$

where

σ'_x is the effective stress
u is the pore water pressure
γ_w is the unit weight of water
h is the pressure head

Thus

$$\frac{\partial \sigma_x}{\partial x} = \frac{\partial \sigma'_x}{\partial x} + \gamma_w \frac{\partial h}{\partial x} \tag{2.8}$$

Similarly

$$\frac{\partial \sigma_y}{\partial y} = \frac{\partial \sigma'_y}{\partial y} + \gamma_w \frac{\partial h}{\partial y} \tag{2.9}$$

and

$$\frac{\partial \sigma_z}{\partial z} = \frac{\partial \sigma'_z}{\partial z} + \gamma_w \frac{\partial h}{\partial z} \tag{2.10}$$

Substitution of the proper terms in Equations 2.4 through 2.6 results in

$$\frac{\partial \sigma'_x}{\partial x} + \frac{\partial \tau_{yx}}{\partial y} + \frac{\partial \tau_{zx}}{\partial z} + \gamma_w \frac{\partial h}{\partial x} = 0 \tag{2.11}$$

$$\frac{\partial \sigma'_y}{\partial y} + \frac{\partial \tau_{xy}}{\partial x} + \frac{\partial \tau_{zy}}{\partial z} + \gamma_w \frac{\partial h}{\partial y} = 0 \tag{2.12}$$

$$\frac{\partial \sigma'_z}{\partial z} + \frac{\partial \tau_{xz}}{\partial x} + \frac{\partial \tau_{yz}}{\partial y} + \gamma_w \frac{\partial h}{\partial z} - \gamma' = 0 \tag{2.13}$$

where γ' is the effective unit weight of soil. Note that the shear stresses will not be affected by the pore water pressure.

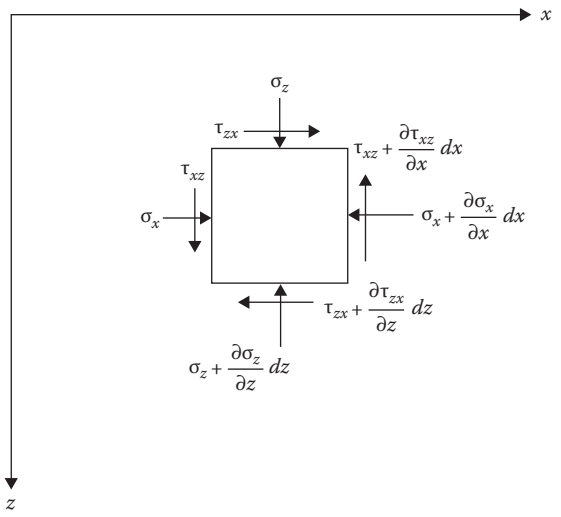

Figure 2.6 Derivation of static equilibrium equation for a two-dimensional problem in Cartesian coordinates.

In soil mechanics, a number of problems can be solved by two-dimensional stress analysis. Figure 2.6 shows the cross-section of an elemental soil prism of unit length with the stresses acting on its faces. The static equilibrium equations for this condition can be obtained from Equations 2.4 through 2.6 by substituting $\tau_{xy} = \tau_{yx} = 0$, $\tau_{yz} = \tau_{zy} = 0$, and $\partial\sigma_y/\partial y = 0$. Note that $\tau_{xz} = \tau_{zx}$. Thus

$$\frac{\partial \sigma_x}{\partial x} + \frac{\partial \tau_{xz}}{\partial z} = 0 \tag{2.14}$$

$$\frac{\partial \sigma_z}{\partial z} + \frac{\partial \tau_{xz}}{\partial x} - \gamma = 0 \tag{2.15}$$

Figure 2.7 shows an elemental soil mass in polar coordinates. Parameters σ_r and σ_θ are the normal components of stress in the radial and tangential directions, and $\tau_{\theta r}$ and $\tau_{r\theta}$ are the shear stresses. In order to obtain the static equations of equilibrium, the forces in the radial and tangential directions need to be considered. Thus

$$\begin{aligned}\sum F_r = {} & \left(\sigma_r r\, d\theta - \left(\sigma_r + \frac{\partial \sigma_r}{\partial r} dr\right)(r + dr)\, d\theta\right) \\ & + \left(\tau_{\theta r}\, dr \sin d\theta/2 + \left(\sigma_\theta + \frac{\partial \sigma_\theta}{\partial \theta} d\theta\right) dr \sin d\theta/2\right) \\ & + \left(\tau_{r\theta}\, dr \cos d\theta/2 - \left(\tau_{r\theta} + \frac{\partial \tau_{r\theta}}{\partial \theta} d\theta\right) dr \cos d\theta/2\right) + \gamma(r\, d\theta\, dr)\cos\theta = 0\end{aligned}$$

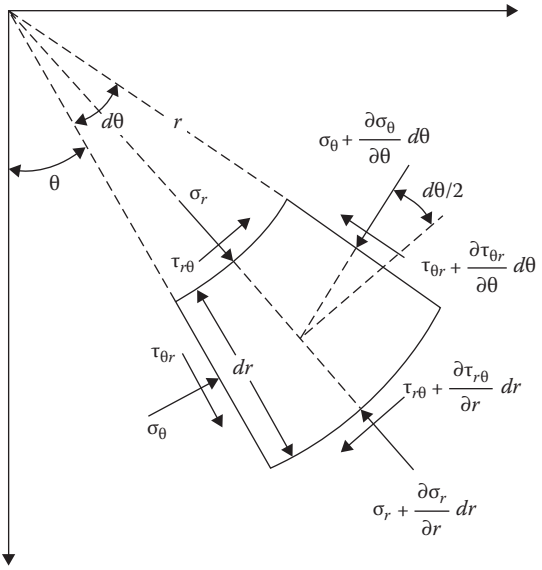

Figure 2.7 Derivation of static equilibrium equation for a two-dimensional problem in polar coordinates.

Taking sin $d\theta/2 \approx d\theta/2$ and cos $d\theta/2 \approx 1$, neglecting infinitesimally small quantities of higher order, and noting that $\partial(\sigma_r r)/\partial r = r(\partial\sigma_r/\partial r) + \sigma_r$ and $\tau_{\theta r} = \tau_{r\theta}$, the previous equation yields

$$\frac{\partial \sigma_r}{\partial r} + \frac{1}{r}\frac{\partial \tau_{r\theta}}{\partial \theta} + \frac{\sigma_r - \sigma_\theta}{r} - \gamma \cos\theta = 0 \tag{2.16}$$

Similarly, the static equation of equilibrium obtained by adding the components of forces in the tangential direction is

$$\frac{1}{r}\frac{\partial \sigma_\theta}{\partial \theta} + \frac{\partial \tau_{r\theta}}{\partial r} + \frac{2\tau_{r\theta}}{r} + \gamma \sin\theta = 0 \tag{2.17}$$

The stresses in the cylindrical coordinate system on a soil element are shown in Figure 2.8. Summing the forces in the radial, tangential, and vertical directions, the following relations are obtained:

$$\frac{\partial \sigma_r}{\partial r} + \frac{1}{r}\frac{\partial \tau_{r\theta}}{\partial \theta} + \frac{\partial \tau_{zr}}{\partial z} + \frac{\sigma_r - \sigma_\theta}{r} = 0 \tag{2.18}$$

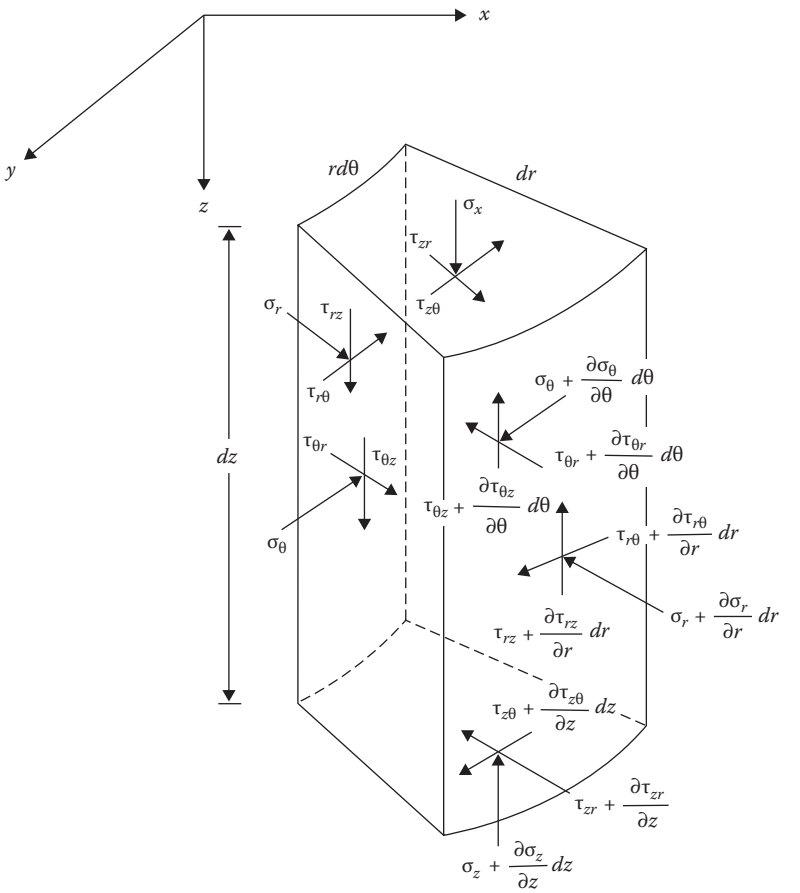

Figure 2.8 Equilibrium equations in cylindrical coordinates.

$$\frac{\partial \tau_{rq}}{\partial r} + \frac{1}{r}\frac{\partial \sigma_q}{\partial q} + \frac{\partial \tau_{qz}}{\partial z} + \frac{2\tau_{rq}}{r} = 0 \tag{2.19}$$

$$\frac{\partial \tau_{zr}}{\partial r} + \frac{1}{r}\frac{\partial \tau_{qz}}{\partial q} + \frac{\partial \sigma_z}{\partial z} + \frac{\tau_{zr}}{r} - g = 0 \tag{2.20}$$

2.4 CONCEPT OF STRAIN

Consider an elemental volume of soil as shown in Figure 2.9a. Owing to the application of stresses, point *A* undergoes a displacement such that its components in the *x*, *y*, and *z* directions are *u*, *v*, and *w*, respectively. The adjacent point *B* undergoes displacements of $u + (\partial u/\partial x)dx$, $v + (\partial v/\partial x)dx$,

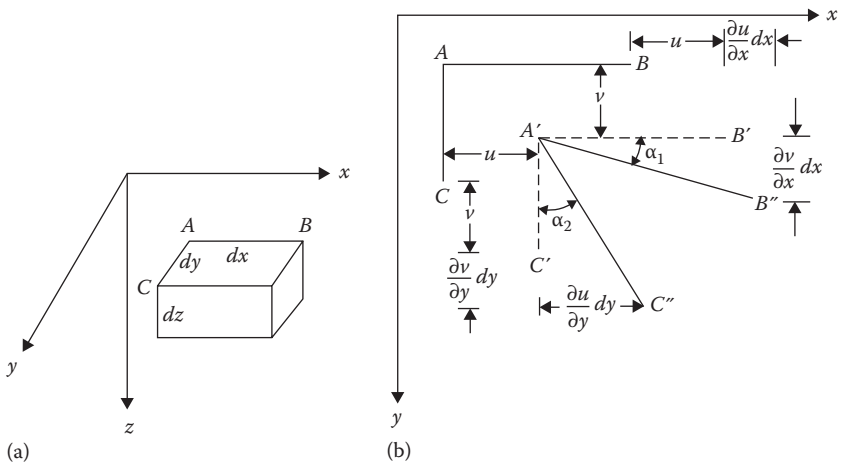

Figure 2.9 Concept of strain: (a) elemental volume of soil measuring *dx dy dz*; (b) rotation of sides *AB* and *AC* of the elemental volume.

and $w + (\partial w/\partial x)dx$ in the x, y, and z directions, respectively. So, the change in the length AB in the x direction is $u + (\partial u/\partial x)dx - u = (\partial u/\partial x)dx$. Hence, the strain in the x direction, $\mathbb{E}_x$, can be given as

$$\mathbb{E}_x = \frac{1}{dx}\left(\frac{\partial u}{\partial x}dx\right) = \frac{\partial u}{\partial x} \tag{2.21}$$

Similarly, the strains in the y and z directions can be written as

$$\mathbb{E}_y = \frac{\partial v}{\partial y} \tag{2.22}$$

$$\mathbb{E}_z = \frac{\partial w}{\partial z} \tag{2.23}$$

where $\in_y$ and $\in_z$ are the strains in the y and z directions, respectively.

Owing to stress application, sides AB and AC of the element shown in Figure 2.9a undergo a rotation as shown in Figure 2.9b (see $A'B''$ and $A'C''$). The small change in angle for side AB is α_1, the magnitude of which may be given as $[(\partial v/\partial x)dx](1/dx) = \partial v/\partial x$, and the magnitude of the change in angle α_2 for side AC is $[(\partial u/\partial y)dy](1/dy) = \partial u/\partial y$. The shear strain γ_{xy} is equal to the sum of the change in angles α_1 and α_2. Therefore

$$\mathbb{g}_{xy} = \frac{\partial u}{\partial y} + \frac{\partial v}{\partial x} \tag{2.24}$$

Similarly, the shear strains γ_{xz} and γ_{yz} can be derived as

$$\gamma_{xz} = \frac{\partial u}{\partial z} + \frac{\partial w}{\partial x} \tag{2.25}$$

and

$$\gamma_{yz} = \frac{\partial v}{\partial z} + \frac{\partial w}{\partial y} \tag{2.26}$$

Generally, in soil mechanics, the compressive normal strains are considered positive. For shear strain, if there is an increase in the right angle *BAC* (Figure 2.9b), it is considered positive. As shown in Figure 2.9b, the shear strains are all negative.

2.5 HOOKE'S LAW

The axial strains for an ideal, elastic, isotropic material in terms of the stress components are given by Hooke's law as

$$\varepsilon_x = \frac{\partial u}{\partial x} = \frac{1}{E}[\sigma_x - \nu(\sigma_y + \sigma_z)] \tag{2.27}$$

$$\varepsilon_y = \frac{\partial v}{\partial y} = \frac{1}{E}[\sigma_y - \nu(\sigma_x + \sigma_z)] \tag{2.28}$$

and

$$\varepsilon_z = \frac{\partial w}{\partial z} = \frac{1}{E}[\sigma_z - \nu(\sigma_x + \sigma_y)] \tag{2.29}$$

where

E is the Young's modulus
ν is the Poisson's ratio

Form the relation given by Equations 2.27 through 2.29, the stress components can be expressed as

$$\sigma_x = \frac{\nu E}{(1+\nu)(1-2\nu)}(\varepsilon_x + \varepsilon_y + \varepsilon_z) + \frac{E}{1+\nu}\varepsilon_x \tag{2.30}$$

$$\sigma_y = \frac{\nu E}{(1+\nu)(1-2\nu)}(\varepsilon_x + \varepsilon_y + \varepsilon_z) + \frac{E}{1+\nu}\varepsilon_y \tag{2.31}$$

$$\sigma_z = \frac{\nu E}{(1+\nu)(1-2\nu)}(\varepsilon_x + \varepsilon_y + \varepsilon_z) + \frac{E}{1+\nu}\varepsilon_z \tag{2.32}$$

The shear strains in terms of the stress components are

$$\gamma_{xy} = \frac{\tau_{xy}}{G} \tag{2.33}$$

$$\gamma_{xz} = \frac{\tau_{xz}}{G} \tag{2.34}$$

and

$$\gamma_{yz} = \frac{\tau_{yz}}{G} \tag{2.35}$$

where shear modulus

$$G = \frac{E}{2(1+\nu)} \tag{2.36}$$

2.6 PLANE STRAIN PROBLEMS

A state of stress generally encountered in many problems in soil mechanics is the plane strain condition. Long retaining walls and strip foundations are examples where plane strain conditions are encountered. Referring to Figure 2.10, for the strip foundation, the strain in the y direction is zero (i.e., $\in_y = 0$). The stresses at all sections in the xz plane are the same, and the shear stresses on these sections are zero (i.e., $\tau_{yx} = \tau_{xy} = 0$ and $\tau_{yz} = \tau_{zy} = 0$). Thus, from Equation 2.28

$$\varepsilon_y = 0 = \frac{1}{E}[\sigma_y - \nu(\sigma_x + \sigma_z)]$$

$$\sigma_y = \nu(\sigma_x + \sigma_z) \tag{2.37}$$

Substituting Equation 2.37 into Equations 2.27 and 2.29

$$\varepsilon_x = \frac{1-\nu^2}{E}\left[\sigma_x - \frac{\nu}{1-\nu}\sigma_z\right] \tag{2.38}$$

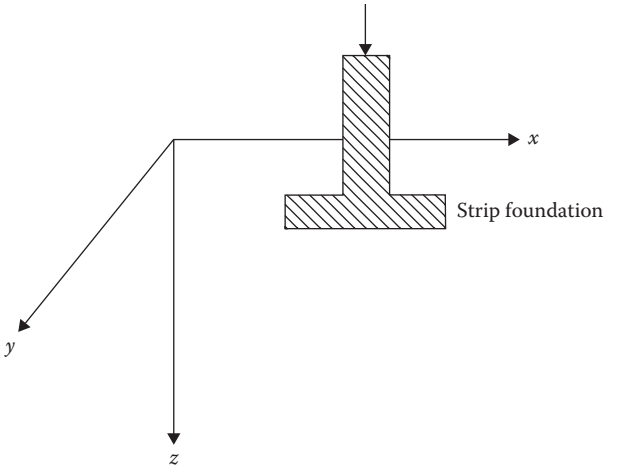

Figure 2.10 Strip foundation: plane strain problem.

and

$$\varepsilon_z = \frac{1-\nu^2}{E}\left[\sigma_z - \frac{\nu}{1-\nu}\sigma_x\right] \tag{2.39}$$

Since $\tau_{xy} = 0$ and $\tau_{yz} = 0$

$$\gamma_{xy} = 0 \qquad \gamma_{yz} = 0 \tag{2.40}$$

and

$$\gamma_{xz} = \frac{\tau_{xz}}{G} \tag{2.41}$$

2.6.1 Compatibility equation

The three strain components given by Equations 2.38, 2.39, and 2.41 are functions of the displacements u and w and are not independent of each other. Hence, a relation should exist such that the strain components give single-valued continuous solutions. It can be obtained as follows. From Equation 2.21, $\in_x = \partial u/\partial x$. Differentiating twice with respect to z

$$\frac{\partial^2 \varepsilon_x}{\partial z^2} = \frac{\partial^3 u}{\partial x\, \partial z^2} \tag{2.42}$$

From Equation 2.23, $\in_z = \partial w/\partial z$. Differentiating twice with respect to x

$$\frac{\partial^2 \in_z}{\partial x^2} = \frac{\partial^3 w}{\partial z\, \partial x^2} \tag{2.43}$$

Similarly, differentiating γ_{xz} (Equation 2.25) with respect to x and z

$$\frac{\partial^2 \gamma_{xz}}{\partial x\, \partial z} = \frac{\partial^3 u}{\partial x\, \partial z^2} + \frac{\partial^3 w}{\partial x^2\, \partial z} \tag{2.44}$$

Combining Equations 2.42 through 2.44, we obtain

$$\frac{\partial^2 \in_x}{\partial z^2} + \frac{\partial^2 \in_z}{\partial x^2} = \frac{\partial^2 \gamma_{xz}}{\partial x\, \partial z} \tag{2.45}$$

Equation 2.45 is the compatibility equation in terms of strain components. Compatibility equations in terms of the stress components can also be derived. Let $E' = E/(1 - \nu^2)$ and $\nu' = \nu/(1 - \nu)$. So, from Equation 2.38, $\in_x = 1/E'(\sigma_x - \nu'\sigma_z)$. Hence

$$\frac{\partial^2 \in_x}{\partial z^2} = \frac{1}{E'}\left[\frac{\partial^2 \sigma_x}{\partial z^2} - \nu'\frac{\partial^2 \sigma_z}{\partial z^2}\right] \tag{2.46}$$

Similarly, from Equation 2.39, $\in_x = (1/E')(\sigma_z - \nu'\sigma_x)$. Thus

$$\frac{\partial^2 \in_z}{\partial x^2} = \frac{1}{E'}\left[\frac{\partial^2 \sigma_z}{\partial x^2} - \nu'\frac{\partial^2 \sigma_x}{\partial x^2}\right] \tag{2.47}$$

Again, from Equation 2.41

$$\gamma_{xz} = \frac{\tau_{xz}}{G} = \frac{2(1+\nu)}{E}\tau_{xz} = \frac{2(1+\nu')}{E'}\tau_{xz} \tag{2.48}$$

$$\frac{\partial^2 \gamma_{xz}}{\partial x\, \partial z} = \frac{2(1+\nu')}{E'}\frac{\partial^2 \tau_{xz}}{\partial x\, \partial z}$$

Substitution of Equations 2.46 through 2.48 into Equation 2.45 yields

$$\frac{\partial^2 \sigma_x}{\partial z^2} + \frac{\partial^2 \sigma_z}{\partial x^2} - \nu'\left[\frac{\partial^2 \sigma_z}{\partial z^2} + \frac{\partial^2 \sigma_x}{\partial x^2}\right] = 2(1+\nu')\frac{\partial^2 \tau_{xz}}{\partial x\, \partial z} \tag{2.49}$$

From Equations 2.14 and 2.15

$$\frac{\partial}{\partial x}\left(\frac{\partial \sigma_x}{\partial x}\right) + \frac{\partial \tau_{xz}}{\partial z}\hat{k} + \frac{\partial}{\partial z}\left(\frac{\partial \sigma_z}{\partial z}\right) + \frac{\partial \tau_{xz}}{\partial x} - \gamma\hat{k} = 0$$

or

$$2\frac{\partial^2 \tau_{xz}}{\partial x\,\partial z} = -\left(\frac{\partial^2 \sigma_x}{\partial x^2}\right) + \frac{\partial^2 \sigma_z}{\partial z^2}\hat{k} + \frac{\partial}{\partial z}(\gamma) \tag{2.50}$$

Combining Equations 2.49 and 2.50

$$\left(\frac{\partial^2}{\partial x^2}\right) + \frac{\partial^2}{\partial z^2}\hat{k}(\sigma_x + \sigma_z) = (1+\nu)\frac{\partial}{\partial z}(\gamma)$$

For weightless materials, or for a constant unit weight γ, the previous equation becomes

$$\left(\frac{\partial^2}{\partial x^2}\right) + \frac{\partial^2}{\partial z^2}\hat{k}(\sigma_x + \sigma_z) = 0 \tag{2.51}$$

Equation 2.51 is the *compatibility equation* in terms of stress.

2.6.2 Stress function

For the plane strain condition, in order to determine the stress at a given point due to a given load, the problem reduces to solving the equations of equilibrium together with the compatibility equation (Equation 2.51) and the boundary conditions. For a weight-less medium (i.e., γ = 0), the equations of equilibrium are

$$\frac{\partial \sigma_x}{\partial x} + \frac{\partial \tau_{xz}}{\partial z} = 0 \tag{2.14}$$

$$\frac{\partial \sigma_z}{\partial z} + \frac{\partial \tau_{xz}}{\partial x} = 0 \tag{2.15}$$

The usual method of solving these problems is to introduce a stress function referred to as *Airy's stress function*. The stress function ϕ in terms of x and z should be such that

$$\sigma_x = \frac{\partial^2 \phi}{\partial z^2} \tag{2.52}$$

$$\sigma_z = \frac{\partial^2 \phi}{\partial x^2} \tag{2.53}$$

$$\tau_{xz} = -\frac{\partial^2 \phi}{\partial x \, \partial z} \tag{2.54}$$

The aforementioned equations will satisfy the equilibrium equations. When Equations 2.52 through 2.54 are substituted into Equation 2.51, we get

$$\frac{\partial^4 \phi}{\partial x^4} + 2\frac{\partial^4 \phi}{\partial x^2 \, \partial z^2} + \frac{\partial^4 \phi}{\partial z^4} = 0 \tag{2.55}$$

So, the problem reduces to finding a function ϕ in terms of x and z such that it will satisfy Equation 2.55 and the boundary conditions.

2.6.3 Compatibility equation in polar coordinates

For solving plane strain problems in polar coordinates, assuming the soil to be weightless (i.e., $\gamma = 0$), the equations of equilibrium are (from Equations 2.16 and 2.17)

$$\frac{\partial \sigma_r}{\partial r} + \frac{1}{r}\frac{\partial \tau_{r\theta}}{\partial \theta} + \frac{\sigma_r - \sigma_\theta}{r} = 0$$

$$\frac{1}{r}\frac{\partial \sigma_\theta}{\partial \theta} + \frac{\partial \tau_{r\theta}}{\partial r} + \frac{2\tau_{r\theta}}{r} = 0$$

The compatibility equation in terms of stresses can be given by

$$\left(\frac{\partial^2}{\partial r^2} + \frac{1}{r}\frac{\partial}{\partial r} + \frac{1}{r^2}\frac{\partial^2}{\partial \theta^2}\right)(\sigma_r + \sigma_\theta) = 0 \tag{2.56}$$

The Airy stress function ϕ should be such that

$$\sigma_r = \frac{1}{r}\frac{\partial \phi}{\partial r} + \frac{1}{r^2}\frac{\partial^2 \phi}{\partial \theta^2} \tag{2.57}$$

$$\sigma_\theta = \frac{\partial^2 \phi}{\partial r^2} \tag{2.58}$$

$$\tau_{rq} = \frac{1}{r^2}\frac{\partial f}{\partial q} - \frac{1}{r}\frac{\partial^2 f}{\partial r\,\partial q} = -\frac{\partial}{\partial r}\left(\frac{1}{r}\frac{\partial f}{\partial q}\right) \tag{2.59}$$

The previous equations satisfy the equilibrium equations. The compatibility equation in terms of stress function is

$$\left(\frac{\partial^2}{\partial r^2} + \frac{1}{r}\frac{\partial}{\partial r} + \frac{1}{r^2}\frac{\partial^2}{\partial q^2}\right)\left(\frac{\partial^2 f}{\partial r^2} + \frac{1}{r}\frac{\partial f}{\partial r} + \frac{1}{r^2}\frac{\partial^2 f}{\partial q^2}\right) = 0 \tag{2.60}$$

Similar to Equation 2.37, for the plane strain condition

$$\sigma_y = \nu(\sigma_r + \sigma_\theta)$$

Example 2.1

The stress at any point inside a semi-infinite medium due to a line load of intensity q per unit length (Figure 2.11) can be given by a stress function

$$f = Ax\tan^{-1}\left(\frac{z}{x}\right)$$

where A is a constant. This equation satisfies the compatibility equation (Equation 2.55). (a) Find σ_x, σ_z, σ_y, and τ_{xz}. (b) Applying proper boundary conditions, find A.

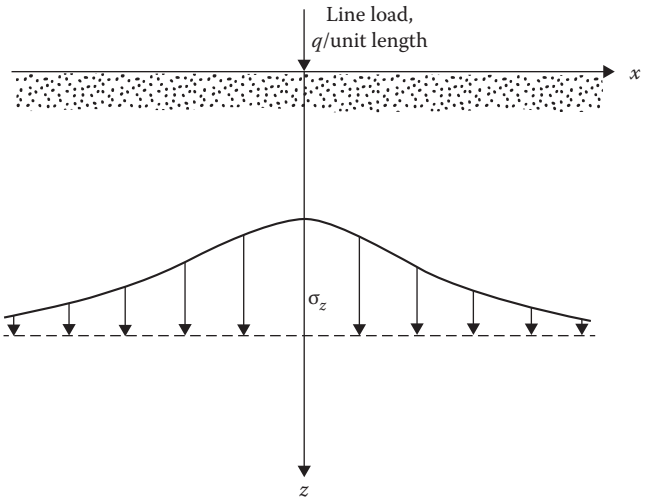

Figure 2.11 Stress at a point due to a line load.

Solution

Part a:

$$\phi = Ax \tan^{-1}\left(\frac{z}{x}\right)$$

The relations for σ_x, σ_z, σ_y, and τ_{xz} are given in Equations 2.52 through 2.54.

$$\sigma_x = \frac{\partial^2 \phi}{\partial z^2}$$

$$\frac{\partial \phi}{\partial z} = Ax \frac{1}{1 + (z/x)^2} \frac{1}{x} = \frac{A}{1 + (z/x)^2}$$

$$\sigma_x = \frac{\partial^2 \phi}{\partial z^2} = -\frac{2Azx^2}{(x^2 + z^2)^2}$$

$$\sigma_x = \frac{\partial^2 \phi}{\partial x^2}$$

$$\frac{\partial \phi}{\partial x} = A \tan^{-1}\frac{z}{x} - \frac{Az}{[1 + (z/x)^2]x} = A \tan^{-1}\frac{z}{x} - \frac{Axz}{(x^2 + z^2)}$$

$$\sigma_z = \frac{\partial^2 \phi}{\partial x^2} = -\frac{A}{1 + (z/x)^2}\frac{z}{x^2} - \frac{Az}{x^2 + z^2} + \frac{2Ax^2 z}{(x^2 + z^2)^2}$$

$$= -\frac{Az}{x^2 + z^2} - \frac{Az}{x^2 + z^2} + \frac{2Ax^2 z}{(x^2 + z^2)^2} = -\frac{2Az^3}{(x^2 + z^2)^2}$$

$$\tau_{xz} = -\frac{\partial^2 \phi}{\partial x \, \partial z}$$

$$\frac{\partial \phi}{\partial x} = A \tan^{-1}\frac{z}{x} - \frac{Axz}{(x^2 + z^2)}$$

$$\frac{\partial^2 \phi}{\partial x \, \partial z} = \frac{A}{1 + (z/x)^2}\frac{1}{x} - \frac{Ax}{x^2 + z^2} + \frac{2Axz^2}{(x^2 + z^2)^2}$$

or

$$\frac{\partial^2 \phi}{\partial x \, \partial z} = \frac{2Axz^2}{(x^2 + z^2)^2}$$

$$\tau_{xz} = -\frac{\partial^2 f}{\partial x\,\partial z} = -\frac{2Axz^2}{(x^2+z^2)^2}$$

$$\sigma_y = \nu(\sigma_x + \sigma_z) = \nu\left[-\frac{2Azx^2}{(x^2+z^2)^2} - \frac{2Az^3}{(x^2+z^2)^2}\right]$$

$$= -\frac{2Az\nu}{(x^2+z^2)^2}(x^2+z^2) = -\frac{2Az\nu}{(x^2+z^2)}$$

Part b: Consider a unit length along the y direction. We can write

$$q = \int_{-\infty}^{+\infty} \sigma_z)(1)(dx) = \int_{-\infty}^{+\infty} \frac{2Az^3}{(x^2+z^2)^2}\,dx$$

$$= -\frac{2Az^3}{2z^2}\left[\frac{x}{x^2+z^2}\right]_{-\infty}^{+\infty} + \int_{-\infty}^{+\infty} \frac{dx}{x^2+z^2}$$

$$= -Az\left[\frac{x}{x^2+z^2}\right]_{-\infty}^{+\infty} + \frac{1}{z}\tan^{-1}\frac{x}{z}\Big]_{-\infty}^{+\infty} = -A(\pi/2 + \pi/2) = -A\pi$$

$$A = -\frac{q}{\pi}$$

So

$$\sigma_x = \frac{2qx^2z}{\pi(x^2+z^2)^2} \qquad \sigma_z = \frac{2qz^3}{\pi(x^2+z^2)^2} \qquad \tau_{xz} = \frac{2qxz^2}{\pi(x^2+z^2)^2}$$

We can see that at $z = 0$ (i.e., at the surface) and for any value of $x \neq 0$, σ_x, σ_z, and τ_{xz} are equal to zero.

2.7 EQUATIONS OF COMPATIBILITY FOR THREE-DIMENSIONAL PROBLEMS

For three-dimensional problems in the Cartesian coordinate system as shown in Figure 2.2, the *compatibility equations in terms of stresses* are (assuming the body force to be zero or constant)

$$-\nabla^2\sigma_x + \frac{1}{1+\nu}\frac{\partial^2\Theta}{\partial x^2} = 0 \tag{2.61}$$

$$\nabla^2\sigma_y + \frac{1}{1+\nu}\frac{\partial^2\Theta}{\partial y^2} = 0 \tag{2.62}$$

$$\nabla^2\sigma_z + \frac{1}{1+\nu}\frac{\partial^2\Theta}{\partial z^2} = 0 \tag{2.63}$$

$$\nabla^2\tau_{xy} + \frac{1}{1+\nu}\frac{\partial^2\Theta}{\partial x\partial y} = 0 \tag{2.64}$$

$$\nabla^2\tau_{yz} + \frac{1}{1+\nu}\frac{\partial^2\Theta}{\partial y\partial z} = 0 \tag{2.65}$$

$$\nabla^2\tau_{xz} + \frac{1}{1+\nu}\frac{\partial^2\Theta}{\partial x\partial z} = 0 \tag{2.66}$$

where

$$\nabla^2 = \frac{\partial^2}{\partial x^2} + \frac{\partial^2}{\partial y^2} + \frac{\partial^2}{\partial z^2}$$

and

$$\Theta = \sigma_x + \sigma_y + \sigma_z$$

The compatibility equations in terms of stresses for the cylindrical coordinate system (Figure 2.4) are as follows (for constant or zero body force):

$$\nabla^2\sigma_z + \frac{1}{1+\nu}\frac{\partial^2\Theta}{\partial z^2} = 0 \tag{2.67}$$

$$\nabla^2\sigma_r + \frac{1}{1+\nu}\frac{\partial^2\Theta}{\partial r^2} - \frac{4}{r^2}\frac{\partial\tau_{r\theta}}{\partial\theta} + \frac{2}{r^2}(\sigma_\theta + \sigma_r) = 0 \tag{2.68}$$

$$\nabla^2\sigma_\theta + \frac{1}{1+\nu}\left(\frac{1}{r}\frac{\partial\Theta}{\partial r} + \frac{1}{r^2}\frac{\partial^2\Theta}{\partial\theta^2}\right) + \frac{4}{r^2}\frac{\partial\tau_{r\theta}}{\partial\theta} - \frac{2}{r^2}(\sigma_\theta + \sigma_r) = 0 \tag{2.69}$$

$$\nabla^2\tau_{rz} + \frac{1}{1+\nu}\frac{\partial^2\Theta}{\partial r\partial z} - \frac{\tau_{rz}}{r^2} - \frac{2}{r^2}\frac{\partial\tau_{\theta z}}{\partial\theta} = 0 \tag{2.70}$$

$$-\nabla^2\tau_{r\theta} + \frac{1}{1+\nu}\frac{\partial}{\partial r}\left(\frac{1}{r}\frac{\partial Q}{\partial \theta}\right) - \frac{4}{r^2}\tau_{r\theta} - \frac{2}{r^2}\frac{\partial}{\partial \theta}(\sigma_\theta - \sigma_r) = 0 \tag{2.71}$$

$$-\nabla^2\tau_{z\theta} + \frac{1}{1+\nu}\frac{1}{r}\frac{\partial^2 Q}{\partial \theta \partial z} + \frac{2}{r}\frac{\partial \tau_{rz}}{\partial \theta} - \frac{\tau_{z\theta}}{r^2} = 0 \tag{2.72}$$

2.8 STRESSES ON AN INCLINED PLANE AND PRINCIPAL STRESSES FOR PLANE STRAIN PROBLEMS

The fundamentals of plane strain problems are explained in Section 2.5. For these problems, the strain in the y direction is zero (i.e., $\tau_{yx} = \tau_{xy} = 0$; $\tau_{yz} = \tau_{zy} = 0$) and σ_y is constant for all sections in the plane.

If the stresses at a point in a soil mass (i.e., σ_x, σ_y, σ_z, $\tau_{xz}(= \tau_{zx})$) are known (as shown in Figure 2.12a), the normal stress σ and the shear stress τ on an inclined plane BC can be determined by considering a soil prism of unit length in the direction of the y axis. Summing the components of all forces in the n direction (Figure 2.12b) gives

$$\sum F_n = 0$$

$$\sigma\, dA = (\sigma_x \cos\theta)(dA\cos\theta) + (\sigma_z \sin\theta)(dA \sin\theta) + (\tau_{xz}\sin\theta)(dA\cos\theta) + (\tau_{xz}\cos\theta)(dA\sin\theta)$$

where dA is the area of the inclined face of the prism. Thus

$$\sigma = \sigma_x \cos^2\theta + \sigma_z \sin^2\theta + 2\tau_{xz}\sin\theta\cos\theta$$

$$= \frac{\sigma_x + \sigma_z}{2} + \frac{\sigma_x - \sigma_z}{2}\cos 2\theta + \tau_{xz}\sin 2\theta \tag{2.73}$$

Similarly, summing the forces in the s direction gives

$$\sum F_s = 0$$

$$\tau\, dA = -(\sigma_x \sin\theta)(dA\cos\theta) + (\sigma_z\cos\theta)(dA\sin\theta) + (\tau_{xz}\cos\theta)(dA\cos\theta) - (\tau_{xz}\sin\theta)(dA\sin\theta)$$

$$\tau = -\sigma_x \sin\theta\cos\theta + \sigma_z \sin\theta\cos\theta + \tau_{xz}(\cos^2\theta - \sin^2\theta)$$

$$= \tau_{xz}\cos 2\theta - \frac{\sigma_x - \sigma_z}{2}\sin 2\theta \tag{2.74}$$

Note that σ_y has no contribution to σ or τ.

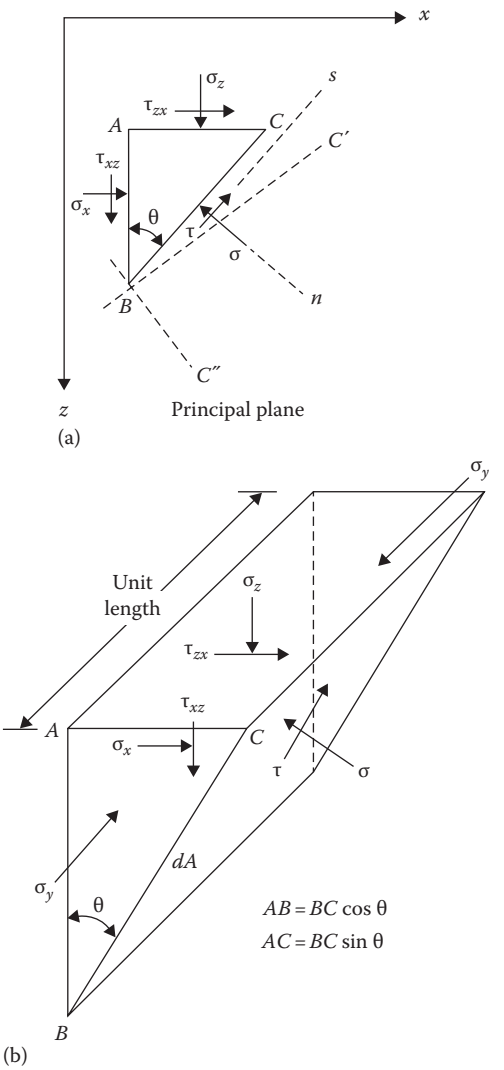

Figure 2.12 (a) Stresses on an inclined plane for the plane strain case; (b) soil prism of unit length in the direction of *y*-axis.

2.8.1 Transformation of stress components from polar to Cartesian coordinate system

In some instances, it is helpful to know the relations for transformation of stress components in a polar coordinate system to a Cartesian coordinate system. This can be done by a principle similar to that demonstrated earlier for finding the stresses on an inclined plane. Comparing Figures 2.12 and 2.13,

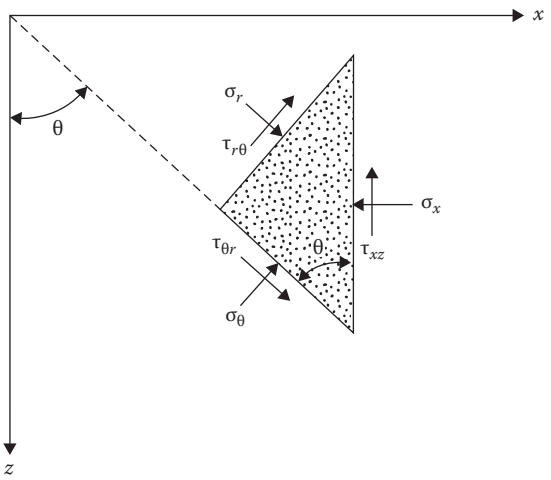

Figure 2.13 Transformation of stress components from polar to Cartesian coordinate system.

it is obvious that we can substitute σ_r for σ_z, σ_θ for σ_x, and $\tau_{r\theta}$ for τ_{xz} in Equations 2.73 and 2.74 to obtain σ_x and τ_{xz} as shown in Figure 2.13. So

$$\sigma_x = \sigma_r \sin^2\theta + \sigma_\theta \cos^2\theta + 2\tau_{r\theta}\sin\theta\cos\theta \tag{2.75}$$

$$\tau_{xz} = -\sigma_\theta \sin\theta\cos\theta + \sigma_r \sin\theta\cos\theta + \tau_{r\theta}(\cos^2\theta - \sin^2\theta) \tag{2.76}$$

Similarly, it can be shown that

$$\sigma_z = \sigma_r \cos^2\theta + \sigma_\theta \sin^2\theta - 2\tau_{r\theta}\sin\theta\cos\theta \tag{2.77}$$

2.8.2 Principal stress

A plane is defined as a *principal plane* if the shear stress acting on it is zero. This means that the only stress acting on it is a normal stress. The normal stress on a principal plane is referred to as the *principal stress*. In a plane strain case, σ_y is a *principal stress*, and the *xz* plane is a principal plane. The orientation of the other two principal planes can be determined by considering Equation 2.74. On an inclined plane, if the shear stress is zero, it follows that

$$\tau_{xz}\cos 2\theta = \left(\frac{\sigma_x - \sigma_z}{2}\right)\sin 2\theta$$

$$\tan 2\theta = \frac{2\tau_{xz}}{\sigma_x - \sigma_z} \tag{2.78}$$

From Equation 2.78, it can be seen that there are two values of θ at right angles to each other that will satisfy the relation. These are the directions of the two principal planes BC' and BC'' as shown in Figure 2.12. Note that there are now three principal planes that are at right angles to each other. Besides σ_y, the expressions for the two other principal stresses can be obtained by substituting Equation 2.78 into Equation 2.73, which gives

$$\sigma_{p(1)} = \frac{\sigma_x + \sigma_z}{2} + \sqrt{\left(\frac{\sigma_x - \sigma_z}{2}\right)^2 + \tau_{xz}^2} \tag{2.79}$$

$$\sigma_{p(3)} = \frac{\sigma_x + \sigma_z}{2} - \sqrt{\left(\frac{\sigma_x - \sigma_z}{2}\right)^2 + \tau_{xz}^2} \tag{2.80}$$

where $\sigma_{p(1)}$ and $\sigma_{p(3)}$ are the principal stresses. Also

$$\sigma_{p(1)} + \sigma_{p(3)} = \sigma_x + \sigma_z \tag{2.81}$$

Comparing the magnitude of the principal stresses, $\sigma_{p(1)} > \sigma_y = \sigma_{p(2)} > \sigma_{p(3)}$. Thus $\sigma_{p(1)}$, $\sigma_{p(2)}$, and $\sigma_{p(3)}$ are referred to as the major, intermediate, and minor principal stresses. From Equations 2.37 and 2.81, it follows that

$$\sigma_y = \nu[\sigma_{p(1)} + \sigma_{p(3)}] \tag{2.82}$$

2.8.3 Mohr's circle for stresses

The shear and normal stresses on an inclined plane (Figure 2.12) can also be determined graphically by using Mohr's circle. The procedure to construct Mohr's circle is explained later.

The sign convention for normal stress is positive for compression and negative for tension. The shear stress on a given plane is positive if it tends to produce a clockwise rotation about a point outside the soil element, and it is negative if it tends to produce a counterclockwise rotation about a point outside the element (Figure 2.14). Referring to plane AB in Figure 2.12a, the normal stress is $+\sigma_x$ and the shear stress is $+\tau_{xz}$. Similarly, on plane AC, the stresses are $+\sigma_z$ and $-\tau_{xz}$. The stresses on planes AB and AC can be plotted on a graph with normal stresses along the abscissa and shear stresses along the ordinate. Points B and C in Figure 2.15 refer to the stress conditions on planes AB and AC, respectively. Now, if points B and C are

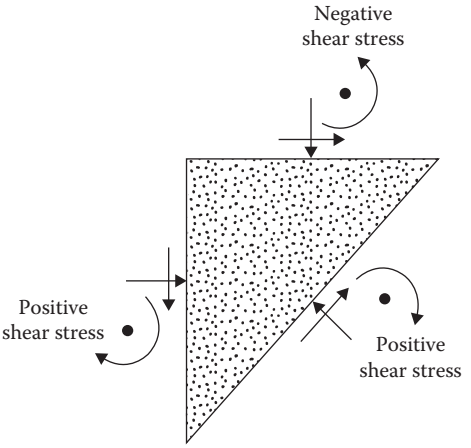

Figure 2.14 Sign convention for shear stress used for the construction of Mohr's circle.

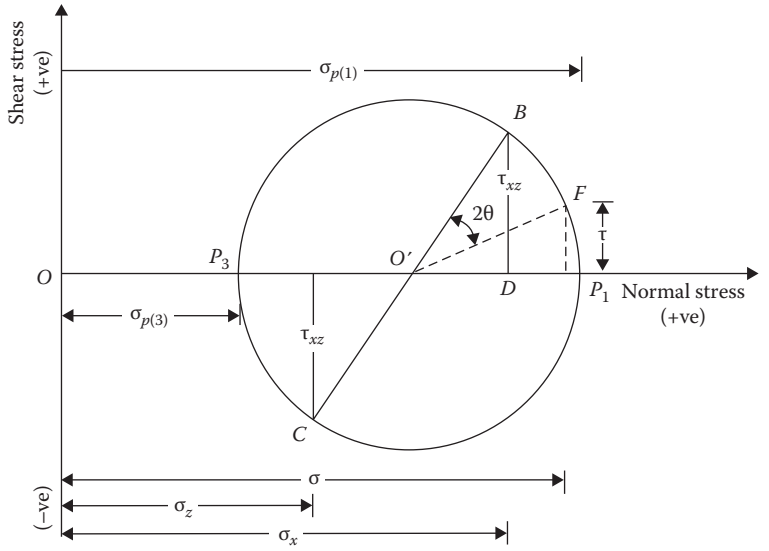

Figure 2.15 Mohr's circle.

joined by a straight line, it will intersect the normal stress axis at O'. With O' as the center and $O'B$ as the radius, if a circle $BP_1\,CP_3$ is drawn, it will be Mohr's circle. The radius of Mohr's circle is

$$O'B = \sqrt{O'D^2 + BD^2} = \sqrt{\left(\frac{\sigma_x - \sigma_z}{2}\right)^2 + \tau_{xz}^2} \tag{2.83}$$

Any radial line in Mohr's circle represents a given plane, and the coordinates of the points of intersection of the radial line and the circumference of Mohr's circle give the stress condition on that plane. For example, let us find the stresses on plane BC. If we start from plane AB and move an angle θ in the clockwise direction in Figure 2.12, we reach plane BC. In Mohr's circle in Figure 2.15, the radial line $O'B$ represents the plane AB. We move an angle 2θ in the clockwise direction to reach point F. Now the radial line $O'F$ in Figure 2.15 represents plane BC in Figure 2.12. The coordinates of point F will give us the stresses on the plane BC.

Note that the ordinates of points P_1 and P_3 are zero, which means that $O'P_1$ and $O'P_3$ represent the major and minor principal planes, and $OP_1 = \sigma_{p(1)}$ and $OP_3 = \sigma_{p(3)}$:

$$\sigma_{p(1)} = OP_1 = OO' + O'P_1 = \frac{\sigma_x + \sigma_z}{2} + \sqrt{\left(\frac{\sigma_x - \sigma_z}{2}\right)^2 + \tau_{xz}^2}$$

$$\sigma_{p(3)} = OP_3 = OO' - O'P_3 = \frac{\sigma_x + \sigma_z}{2} - \sqrt{\left(\frac{\sigma_x - \sigma_z}{2}\right)^2 + \tau_{xz}^2}$$

The previous two relations are the same as Equations 2.79 and 2.80. Also note that the principal plane $O'P_1$ in Mohr's circle can be reached by moving clockwise from $O'B$ through angle $BO'P_1 = \tan^{-1}[2\tau_{xz}/(\sigma_x - \sigma_z)]$. The other principal plane $O'P_3$ can be reached by moving through angle $180° + \tan^{-1}[2\tau_{xz}/(\sigma_x - \sigma_z)]$ in the clockwise direction from $O'B$. So, in Figure 2.12, if we move from plane AB through angle $(1/2)\tan^{-1}[2\tau_{xz}/(\sigma_x - \sigma_z)]$, we will reach plane BC', on which the principal stress $\sigma_{p(1)}$ acts. Similarly, moving clockwise from plane AB through angle $1/2\{180° + \tan^{-1}[2\tau_{xz}/(\sigma_x - \sigma_z)]\} = 90° + (1/2)\tan^{-1}[2\tau_{xz}/(\sigma_x - \sigma_z)]$ in Figure 2.12, we reach plane BC'', on which the principal stress $\sigma_{p(3)}$ acts. These are the same conclusions as derived from Equation 2.78.

2.8.4 Pole method for finding stresses on an inclined plane

A pole is a unique point located on the circumference of Mohr's circle. If a line is drawn through the pole parallel to a given plane, the point of intersection of this line and Mohr's circle will give the stresses on the plane. The procedure for finding the pole is shown in Figure 2.16.

Figure 2.16a shows the same stress element as Figure 2.12. The corresponding Mohr's circle is given in Figure 2.16b. Point B on Mohr's circle represents the stress conditions on plane AB (Figure 2.16a). If a line is drawn through B parallel to AB, it will intersect Mohr's circle at P. Point P is the

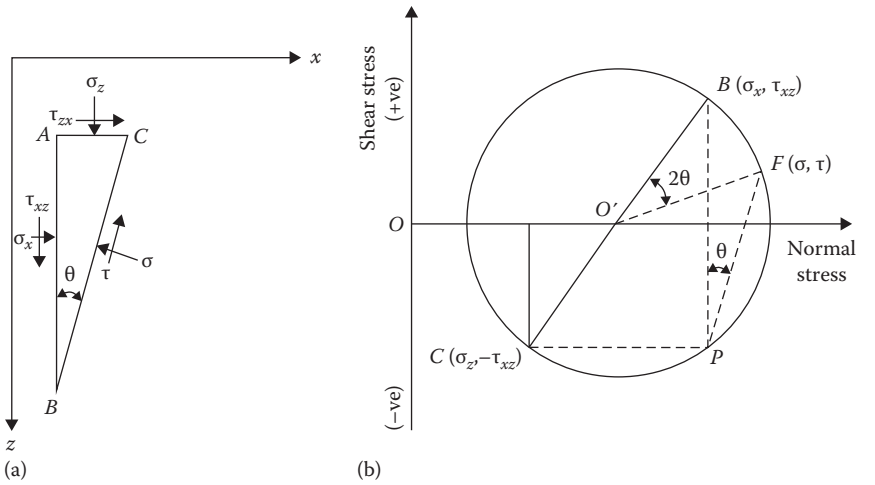

Figure 2.16 Pole method of finding stresses on an inclined plane: (a) stress element; (b) corresponding Mohr's circle.

pole for Mohr's circle. We could also have found pole *P* by drawing a line through *C* parallel to plane *AC*. To find the stresses on plane *BC*, we draw a line through *P* parallel to *BC*. It will intersect Mohr's circle at *F*, and the coordinates of point *F* will give the normal and shear stresses on plane *AB*.

Example 2.2

The stresses at a point in a soil mass are shown in Figure 2.17 (plane strain case). Determine the principal stresses and show their directions. Use $\nu = 0.35$.

Solution

Based on the sign conventions explained in Section 2.2,

$$\sigma_z = +100 \text{ kN/m}^2, \quad \sigma_x = +50 \text{ kN/m}^2, \quad \text{and} \quad \tau_{xz} = -25 \text{ kN/m}^2$$

$$\sigma_p = \frac{\sigma_x + \sigma_z}{2} \pm \sqrt{\left(\frac{\sigma_x - \sigma_z}{2}\right)^2 + \tau_{xz}^2}$$

$$= \frac{50 + 100}{2} \pm \sqrt{\left(\frac{50 - 100}{2}\right)^2 + (-25)^2} = (75 \pm 35.36) \text{ kN/m}^2$$

$$\sigma_{p(1)} = 110.36 \text{ kN/m}^2 \quad \sigma_{p(3)} = 39.64 \text{ kN/m}^2$$

$$\sigma_{p(2)} = \nu[\sigma_{p(1)} + \sigma_{p(3)}] = (0.35)(110.36 + 39.34) = 52.5 \text{ kN/m}^2$$

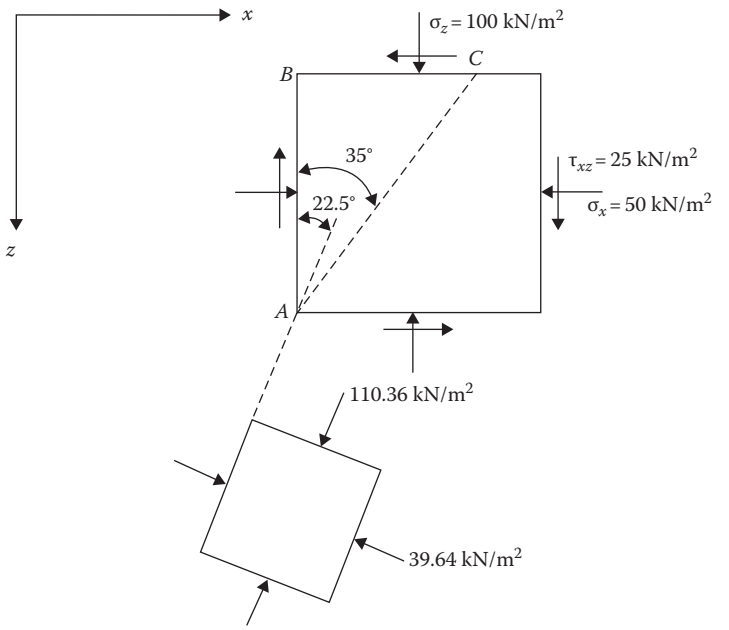

Figure 2.17 Determination of principal stresses at a point.

From Equation 2.78

$$\tan 2\theta = \frac{2\tau_{xz}}{\sigma_x - \sigma_z} = \frac{(2)(-25)}{(50-100)} = 1$$

$$2\theta = \tan^{-1}(1) = 45° \text{ and } 225° \text{ so } \theta = 22.5° \text{ and } 112.5°$$

Parameter $\sigma_{p(2)}$ is acting on the *xz* plane. The directions of $\sigma_{p(1)}$ and $\sigma_{p(3)}$ are shown in Figure 2.17.

Example 2.3

Refer to Example 2.2.

a. Determine the magnitudes of $\sigma_{p(1)}$ and $\sigma_{p(3)}$ by using Mohr's circle.
b. Determine the magnitudes of the normal and shear stresses on plane *AC* shown in Figure 2.17.

Solution

Part a: For Mohr's circle, on plane *AB*, $\sigma_x = 50$ kN/m^2 and $\tau_{xz} = -25$ kN/m^2. On plane *BC*, σ_z = +100 and τ_{xz} +25 kN/m^2. For the stresses, Mohr's circle is plotted in Figure 2.18. The radius of the circle is

$$OH = \sqrt{(OI)^2 + (HI)^2} = \sqrt{25^2 + 25^2} = 35.36 \text{ kN/m}^2$$

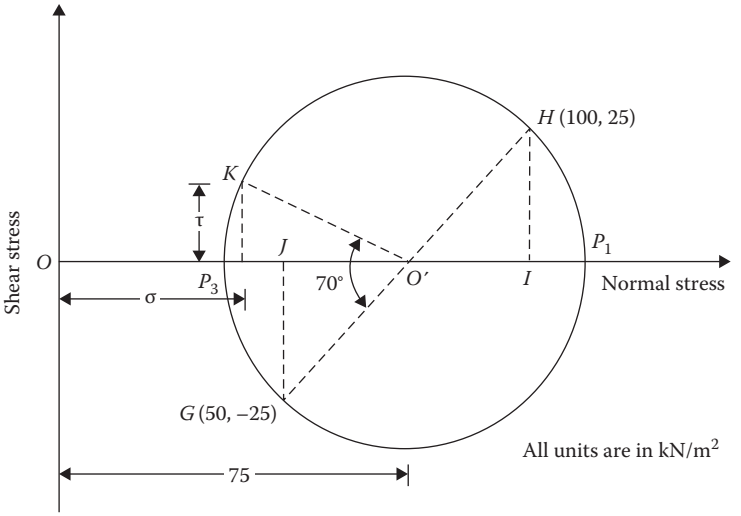

Figure 2.18 Mohr's circle for stress determination.

$$\sigma_{p(1)} = OO' + O'P_1 = 75 + 35.36 = 110.36 \text{ kN/m}^2$$

$$\sigma_{p(3)} = OO' + O'P_1 = 75 - 35.36 = 39.64 \text{ kN/m}^2$$

The angle $GO'P_3 = 2\theta = \tan^{-1}(JG/O'J) = \tan^{-1}(25/25) = 45°$. So, we move an angle $\theta = 22.5°$ clockwise from plane *AB* to reach the minor principal plane, and an angle $\theta = 22.5 + 90 = 112.5°$ clockwise from plane *AB* to reach the major principal plane. The orientation of the major and minor principal stresses is shown in Figure 2.17.

Part b: Plane *AC* makes an angle 35°, measured clockwise, with plane *AB*. If we move through an angle of (2)(35°) = 70° from the radial line *O′G* (Figure 2.18), we reach the radial line *O′K*. The coordinates of *K* will give the normal and shear stresses on plane *AC*. So

$$\tau = O'K \sin 25° = 35.36 \sin 25° = 14.94 \text{ kN/m}^2$$

$$\sigma = OO' - O'K \cos 25° = 75 - 35.36 \cos 25° = 42.95 \text{ kN/m}^2$$

Note: This could also be solved using Equations 2.73 and 2.74:

$$\tau = \tau_{xz} \cos 2\theta - \frac{\sigma_x - \sigma_z}{2} \sin 2\theta$$

where

$\tau_{xz} = -25$ kN/m²
$\theta = 35°$
$\sigma_x = +50$ kN/m²
$\sigma_z = +100$ kN/m² (watch the sign conventions)

So

$$\tau = -25\cos 70 - \frac{50-100}{2}\sin 70 = -8.55 - (-23.49)$$

$$= 14.94 \text{ kN/m}^2$$

$$\sigma = \frac{\sigma_x + \sigma_z}{2} + \frac{\sigma_x - \sigma_z}{2}\cos 2\theta + \tau_{xz}\sin 2\theta$$

$$= \frac{50+100}{2} + \frac{50-100}{2}\cos 70 + (-25)\sin 70$$

$$= 75 - 8.55 - 23.49 = 42.96 \text{ kN/m}^2$$

2.9 STRAINS ON AN INCLINED PLANE AND PRINCIPAL STRAIN FOR PLANE STRAIN PROBLEMS

Consider an elemental soil prism $ABDC$ of unit length along the y direction (Figure 2.19). The lengths of the prism along the x and z directions are $AB = dx$ and $AC = dz$, respectively. When subjected to stresses, the soil prism is deformed and displaced. The length in the y direction still remains unity. $A'B''D''C''$ is the deformed shape of the prism in the displaced position.

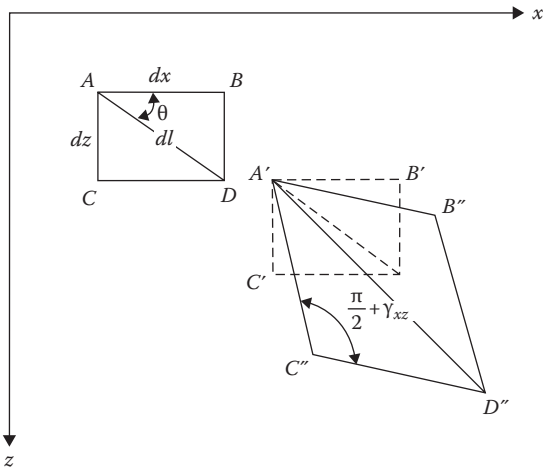

Figure 2.19 Normal and shear strains on an inclined plane (plane strain case).

If the normal strain on an inclined plane AD making an angle θ with the x axis is equal to ∈,

$$A'D' = AD(1 + \varepsilon) = dl(1 + \varepsilon) \tag{2.84}$$

where $AD = dl$.

Note that the angle $B''A'C''$ is equal to $(\pi/2 - \gamma_{xz})$. So the angle $A'C''D''$ is equal to $+(\pi/2 + \gamma_{xz})$. Now

$$(A'D')^2 = (A'C')^2 + (C'D')^2 - 2(A'C')(C'D')\cos(\pi/2 + \gamma_{xz}) \tag{2.85}$$

$$A'C' = AC(1 + \varepsilon_z) = dz(1 + \varepsilon_z) = dl(\sin\theta)(1 + \varepsilon_z) \tag{2.86}$$

$$C'D' = A'B' = dx(1 + \varepsilon_x) = dl(\cos\theta)(1 + \varepsilon_x) \tag{2.87}$$

Substitution of Equations 2.84, 2.86, and 2.87 into Equation 2.85 gives

$$\begin{aligned}(1 + \varepsilon)^2(dl)^2 &= [dl(\sin\theta)(1 + \varepsilon_z)]^2 + [dl(\cos\theta)(1 + \varepsilon_x)]^2 \\ &\quad + 2(dl)^2(\sin\theta)(\cos\theta)(1 + \varepsilon_x)(1 + \varepsilon_z)\sin\gamma_{xz}\end{aligned} \tag{2.88}$$

Taking $\sin\gamma_{xz} \approx \gamma_{xz}$ and neglecting the higher order terms of strain such as $\varepsilon^2, \varepsilon_x^2, \varepsilon_z^2, \varepsilon_x\gamma_{xz}, \varepsilon_z\gamma_{xz}, \varepsilon_x\varepsilon_z\gamma_{xz}$, Equation 2.88 can be simplified to

$$1 + 2\varepsilon = (1 + 2\varepsilon_z)\sin^2\theta + (1 + 2\varepsilon_x)\cos^2\theta + 2\gamma_{xz}\sin\theta\cos\theta$$

$$\varepsilon = \varepsilon_x\cos^2\theta + \varepsilon_z\sin^2\theta + \frac{\gamma_{xz}}{2}\sin 2\theta \tag{2.89}$$

or

$$\varepsilon = \frac{\varepsilon_x + \varepsilon_z}{2} + \frac{\varepsilon_x - \varepsilon_z}{2}\cos 2\theta + \frac{\gamma_{xz}}{2}\sin 2\theta \tag{2.90}$$

Similarly, the shear strain on plane AD can be derived as

$$\gamma = \gamma_{xz}\cos 2\theta - (\varepsilon_x - \varepsilon_z)\sin 2\theta \tag{2.91}$$

Comparing Equations 2.90 and 2.91 with Equations 2.73 and 2.74, it appears that they are similar except for a factor of 1/2 in the last terms of the equations.

The principal strains can be derived by substituting zero for shear strain in Equation 2.91. Thus

$$\tan 2\theta = \frac{\gamma_{xz}}{\varepsilon_x - \varepsilon_y} \tag{2.92}$$

There are two values of θ that will satisfy the aforementioned relation. Thus, from Equations 2.90 and 2.92, we obtain

$$\varepsilon_p = \frac{\varepsilon_x + \varepsilon_z}{2} \pm \sqrt{\left(\frac{\varepsilon_x - \varepsilon_z}{2}\right)^2 + \left(\frac{\gamma_{xz}}{2}\right)^2} \tag{2.93}$$

where $\in_p$ = principal strain. Also note that Equation 2.93 is similar to Equations 2.79 and 2.80.

2.10 STRESS COMPONENTS ON AN INCLINED PLANE, PRINCIPAL STRESS, AND OCTAHEDRAL STRESSES: THREE-DIMENSIONAL CASE

2.10.1 Stress on an inclined plane

Figure 2.20 shows a tetrahedron *AOBC*. The face *AOB* is on the *xy* plane with stresses σ_z, τ_{zy}, and τ_{zx} acting on it. The face *AOC* is on the *yz* plane subjected to stresses σ_x, τ_{xy}, and τ_{xz}. Similarly, the face *BOC* is on the *xz*

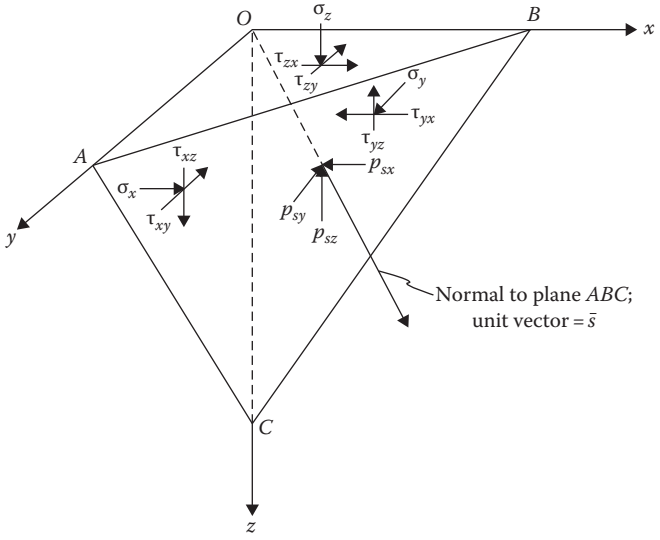

Figure 2.20 Stresses on an inclined plane—three-dimensional case.

plane with stresses σ_y, τ_{yx}, and τ_{yz}. Let it be required to find the x, y, and z components of the stresses acting on the inclined plane ABC.

Let **i**, **j**, and **k** be the unit vectors in the x, y, and z directions, and let s be the unit vector in the direction perpendicular to the inclined plane ABC:

$$s = \cos(s,x)\mathbf{i} + \cos(s,y)\mathbf{j} + \cos(s,z)\mathbf{k} \tag{2.94}$$

If the area of ABC is dA, then the area of AOC can be given as $dA(s \cdot i) = dA\cos(s, x)$. Similarly, the area of $BOC = dA(\mathbf{s} \cdot \mathbf{j}) = dA\cos(\mathbf{s}, \mathbf{y})$, and the area of $AOB = dA(\mathrm{s} \cdot \mathrm{k}) = dA\cos(\mathbf{s}, \mathbf{z})$.

For equilibrium, summing the forces in the x direction, $\sum F_x = 0$:

$$p_{sx}\,dA = [\sigma_x \cos(s, x) + \tau_{yx}\cos(s, y) + \tau_{zx}\cos(s, z)]dA$$

or

$$p_{sx} = \mathtt{s}_x \cos(s,x) + \mathtt{t}_{yx}\cos(s,y) + \mathtt{t}_{zx}\cos(s,z) \tag{2.95}$$

where p_{sx} is the stress component on plane ABC in the x direction.

Similarly, summing the forces in the y and z directions

$$p_{sy} = \mathtt{t}_{xy}\cos(s,x) + \mathtt{s}_y \cos(s,y) + \mathtt{t}_{zy}\cos(s,z) \tag{2.96}$$

$$p_{sz} = \mathtt{t}_{xz}\cos(s,x) + \mathtt{t}_{yz}\cos(s,y) + \mathtt{s}_z \cos(s,z) \tag{2.97}$$

where p_{sy} and p_{sz} are the stress components on plane ABC in the y and z directions, respectively. Equations 2.95 through 2.97 can be expressed in matrix form as

$$\begin{vmatrix} p_{sx} \\ p_{sy} \\ p_{sz} \end{vmatrix} = \begin{vmatrix} \mathtt{s}_x & \mathtt{t}_{yx} & \mathtt{t}_{xz} \\ \mathtt{t}_{xy} & \mathtt{s}_y & \mathtt{t}_{zy} \\ \mathtt{t}_{xz} & \mathtt{t}_{yz} & \mathtt{s}_z \end{vmatrix} \begin{vmatrix} \cos(s,x) \\ \cos(s,y) \\ \cos(s,z) \end{vmatrix} \tag{2.98}$$

The normal stress on plane ABC can now be determined as

$$\begin{aligned} \mathtt{s} &= p_{sx}\cos(s,x) + p_{sy}\cos(s,y) + p_{sz}\cos(s,z) \\ &= \mathtt{s}_x \cos^2(s,x) + \mathtt{s}_y \cos^2(s,y) + \mathtt{s}_z \cos^2(s,z) + 2\mathtt{t}_{xy}\cos(s,x)\cos(s,y) \\ &\quad + 2\mathtt{t}_{yz}\cos(s,y)\cos(s,z) + 2\mathtt{t}_{zx}\cos(s,x)\cos(s,z) \end{aligned} \tag{2.99}$$

The shear stress τ on the plane can be given as

$$\tau = \sqrt{\left(p_{sx}^2 + p_{sy}^2 + p_{sz}^2\right) - \sigma^2} \tag{2.100}$$

2.10.2 Transformation of axes

Let the stresses in a soil mass in the Cartesian coordinate system be given. If the stress components in a new set of orthogonal axes (x_1, y_1, z_1) as shown in Figure 2.21 are required, they can be determined in the following manner. The direction cosines of the x_1, y_1, and z_1 axes with respect to the x, y, and z axes are shown:

	x	y	z
x_1	l_1	m_1	n_1
y_1	l_2	m_2	n_2
z_1	l_3	m_3	n_3

Following the procedure adopted to obtain Equation 2.98, we can write

$$\begin{vmatrix} p_{x_1x} \\ p_{x_1y} \\ p_{x_1z} \end{vmatrix} = \begin{vmatrix} \sigma_x & \tau_{yx} & \tau_{zx} \\ \tau_{xy} & \sigma_y & \tau_{zy} \\ \tau_{xz} & \tau_{yz} & \sigma_z \end{vmatrix} \begin{vmatrix} l_1 \\ m_1 \\ n_1 \end{vmatrix} \tag{2.101}$$

where p_{x_1x}, p_{x_1y}, and p_{x_1z} are stresses parallel to the x, y, and z axes and are acting on the plane perpendicular to the x_1 axis (i.e., y_1z_1 plane).

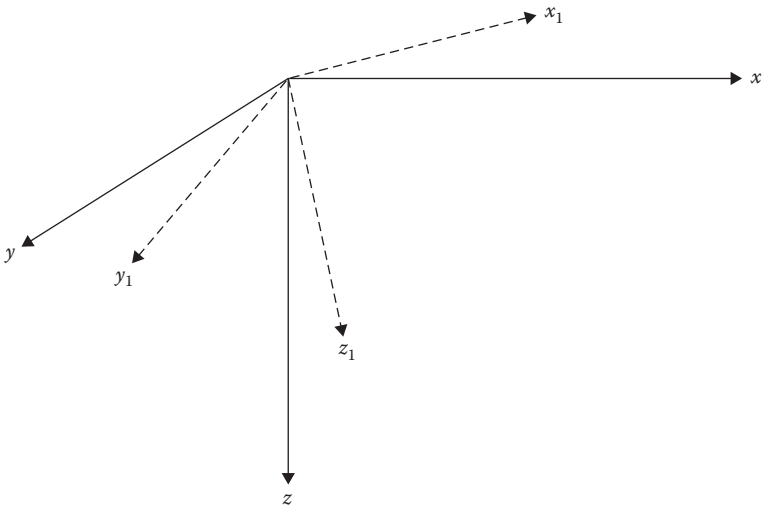

Figure 2.21 Transformation of stresses to a new set of orthogonal axes.

We can now take the components of p_{x_1x}, p_{x_1y}, and p_{x_1z} to determine the normal and shear stresses on the y_1z_1 plane, or

$$\mathbf{s}_{x_1} = l_1 p_{x_1x} + m_1 p_{x_1y} + n_1 p_{x_1z}$$

$$\mathbf{t}_{x_1y_1} = l_2 p_{x_1x} + m_2 p_{x_1y} + n_2 p_{x_1z}$$

$$\mathbf{t}_{x_1z_1} = l_3 p_{x_1x} + m_3 p_{x_1y} + n_3 p_{x_1z}$$

In a matrix form, the previous three equations may be expressed as

$$\begin{vmatrix} \mathbf{s}_{x_1} \\ \mathbf{t}_{x_1y_1} \\ \mathbf{t}_{x_1z_1} \end{vmatrix} = \begin{vmatrix} l_1 & m_1 & n_1 \\ l_2 & m_2 & n_2 \\ l_3 & m_3 & n_3 \end{vmatrix} \begin{vmatrix} p_{x_1x} \\ p_{x_1y} \\ p_{x_1z} \end{vmatrix} \tag{2.102}$$

In a similar manner, the normal and shear stresses on the x_1z_1 plane (i.e., $\mathbf{s}_{y_1}, \mathbf{t}_{y_1x_1}$, and $\mathbf{t}_{y_1z_1}$) and on the x_1y_1 plane (i.e., $\mathbf{s}_{z_1}, \mathbf{t}_{z_1x_1}$, and $\mathbf{t}_{z_1y_1}$) can be determined. Combining these terms, we can express the stresses in the new set of orthogonal axes in a matrix form. Thus

$$\begin{vmatrix} \mathbf{s}_{x_1} & \mathbf{t}_{y_1x_1} & \mathbf{t}_{z_1x_1} \\ \mathbf{t}_{x_1y_1} & \mathbf{s}_{y_1} & \mathbf{t}_{z_1y_1} \\ \mathbf{t}_{x_1z_1} & \mathbf{t}_{y_1z_1} & \mathbf{s}_{z_1} \end{vmatrix} = \begin{vmatrix} l_1 & m_1 & n_1 \\ l_2 & m_2 & n_2 \\ l_3 & m_2 & n_2 \end{vmatrix} \begin{vmatrix} \mathbf{s}_x & \mathbf{t}_{yx} & \mathbf{t}_{zx} \\ \mathbf{t}_{xy} & \mathbf{s}_y & \mathbf{t}_{zy} \\ \mathbf{t}_{xz} & \mathbf{t}_{yz} & \mathbf{s}_z \end{vmatrix} \begin{vmatrix} l_1 & l_2 & l_3 \\ m_1 & m_2 & m_3 \\ n_1 & n_2 & n_3 \end{vmatrix} \tag{2.103}$$

Note: $\tau_{xy} = \tau_{yx}$, $\tau_{zy} = \tau_{yz}$, and $\tau_{zx} = \tau_{xz}$.

Solution of Equation 2.103 gives the following relations:

$$\mathbf{s}_{x_1} = l_1^2 \mathbf{s}_x + m_1^2 \mathbf{s}_y + n_1^2 \mathbf{s}_z + 2m_1 n_1 \mathbf{t}_{yz} + 2n_1 l_1 \mathbf{t}_{zx} + 2l_1 m_1 \mathbf{t}_{xy} \tag{2.104}$$

$$\mathbf{s}_{y_1} = l_2^2 \mathbf{s}_x + m_2^2 \mathbf{s}_y + n_2^2 \mathbf{s}_z + 2m_2 n_2 \mathbf{t}_{yz} + 2n_2 l_2 \mathbf{t}_{zx} + 2l_2 m_2 \mathbf{t}_{xy} \tag{2.105}$$

$$\mathbf{s}_{z_1} = l_3^2 \mathbf{s}_x + m_3^2 \mathbf{s}_y + n_3^2 \mathbf{s}_z + 2m_3 n_3 \mathbf{t}_{yz} + 2n_3 l_3 \mathbf{t}_{zx} + 2l_3 m_3 \mathbf{t}_{xy} \tag{2.106}$$

$$\begin{aligned} \mathbf{t}_{x_1y_1} = \mathbf{t}_{y_1x_1} &= l_1 l_2 \mathbf{s}_x + m_1 m_2 \mathbf{s}_y + n_1 n_2 \mathbf{s}_z + (m_1 n_2 + m_2 n_1) \mathbf{t}_{yz} \\ &\quad + (n_1 l_2 + n_2 l_1) \mathbf{t}_{zx} + (l_1 m_2 + l_2 m_1) \mathbf{t}_{xy} \end{aligned} \tag{2.107}$$

$$\tau_{x_1z_1} = \tau_{z_1x_1} = l_1l_3\sigma_x + m_1m_3\sigma_y + n_1n_3\sigma_z + (m_1n_3 + m_3n_1)\tau_{yz} + (n_1l_3 + n_3l_1)\tau_{zx} + (l_1m_3 + l_3m_1)\tau_{xy} \quad (2.108)$$

$$\tau_{y_1z_1} = \tau_{z_1y_1} = l_2l_3\sigma_x + m_2m_3\sigma_y + n_2n_3\sigma_z + (m_2n_3 + m_3n_2)\tau_{yz} + (n_2l_3 + n_3l_2)\tau_{zx} + (l_2m_3 + l_3m_2)\tau_{xy} \quad (2.109)$$

2.10.3 Principal stresses

The preceding procedure allows the determination of the stresses on any plane from the known stresses based on a set of orthogonal axes. As discussed earlier, a plane is defined as a principal plane if the shear stresses acting on it are zero, which means that the only stress acting on it is a normal stress. This normal stress on a principal plane is referred to as a *principal stress*. In order to determine the principal stresses, refer to Figure 2.20, in which x, y, and z are a set of orthogonal axes. Let the stresses on planes OAC, BOC, and AOB be known, and let ABC be a principal plane. The direction cosines of the normal drawn to this plane are l, m, and n with respect to the x, y, and z axes, respectively. Note that

$$l^2 + m^2 + n^2 = 1 \quad (2.110)$$

If ABC is a principal plane, then the only stress acting on it will be a normal stress σ_p. The x, y, and z components of σ_p are $\sigma_p l$, $\sigma_p m$, and $\sigma_p n$. Referring to Equations 2.95 through 2.97, we can write

$$\sigma_p l = \sigma_x l + \tau_{yx} m + \tau_{zx} n$$

or

$$(\sigma_x - \sigma_p)l + \tau_{yx}m + \tau_{zx}n = 0 \quad (2.111)$$

Similarly

$$\tau_{xy}l + (\sigma_y - \sigma_p)m + \tau_{zy}n = 0 \quad (2.112)$$

$$\tau_{xz}l + \tau_{yz}m + (\sigma_z - \sigma_p)n = 0 \quad (2.113)$$

From Equations 2.110 through 2.113, we note that l, m, and n cannot all be equal to zero at the same time. So

$$\begin{vmatrix} (\sigma_x - \sigma_p) & \tau_{yx} & \tau_{zx} \\ \tau_{xy} & (\sigma_y - \sigma_p) & \tau_{zy} \\ \tau_{xz} & \tau_{yz} & (\sigma_z - \sigma_p) \end{vmatrix} = 0 \tag{2.114}$$

or

$$\sigma_p^3 - I_1\sigma_p^2 + I_2\sigma_p - I_3 = 0 \tag{2.115}$$

where

$$I_1 = \sigma_x + \sigma_y + \sigma_z \tag{2.116}$$

$$I_2 = \sigma_x\sigma_y + \sigma_y\sigma_z + \sigma_x\sigma_z - \tau_{xy}^2 - \tau_{yz}^2 - \tau_{xz}^2 \tag{2.117}$$

$$I_3 = \sigma_x\sigma_y\sigma_z + 2\tau_{xy}\tau_{yz}\tau_{xz} - \sigma_x\tau_{yz}^2 - \sigma_y\tau_{xz}^2 - \sigma_z\tau_{xy}^2 \tag{2.118}$$

I_1, I_2, and I_3 defined in Equations 2.116 through 2.118 are independent of direction cosines and hence independent of the choice of axes. So, they are referred to as stress invariants.

Solution of Equation 2.115 gives three real values of σ_p. So there are three principal planes and they are mutually perpendicular to each other. The directions of these planes can be determined by substituting each σ_p in Equations 2.111 through 2.113 and solving for l, m, and n, and observing the direction cosine condition for $l^2 + m^2 + n^2 = 1$. Note that these values for l, m, and n are the direction cosines for the normal drawn to the plane on which σ_p is acting. The maximum, intermediate, and minimum values of $\sigma_{p(i)}$ are referred to as the major principal stress, intermediate principal stress, and minor principal stress, respectively.

2.10.4 Octahedral stresses

The octahedral stresses at a point are the normal and shear stresses acting on the planes of an imaginary octahedron surrounding that point. The normals to these planes have direction cosines of $\pm 1\sqrt{3}$ with respect to the direction of the principal stresses (Figure 2.22). The axes marked 1, 2, and 3 are the directions of the principal stresses $\sigma_{p(1)}$, $\sigma_{p(2)}$, and $\sigma_{p(3)}$. The expressions for the octahedral normal stress σ_{oct} can be obtained using

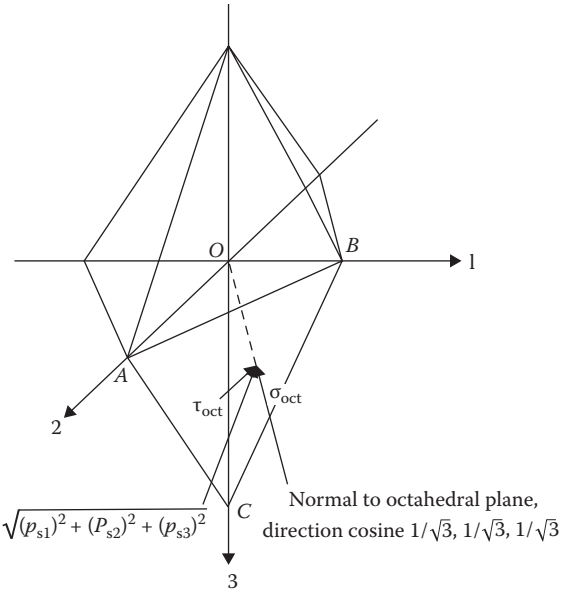

Figure 2.22 Octahedral stress.

Equations 2.95 through 2.97 and 2.99. Now, compare planes *ABC* in Figures 2.20 and 2.22. For the octahedral plane *ABC* in Figure 2.22

$$p_{s1} = \mathbf{s}_{p(1)} l \tag{2.119}$$

$$p_{s2} = \mathbf{s}_{p(2)} m \tag{2.120}$$

$$p_{s3} = \mathbf{s}_{p(3)} n \tag{2.121}$$

where p_{s1}, p_{s2}, and p_{s3} are stresses acting on plane *ABC* parallel to the principal stress axes 1, 2, and 3, respectively. Parameters l, m, and n are the direction cosines of the normal drawn to the octahedral plane and are all equal to $1/\sqrt{3}$. Thus, from Equation 2.99

$$\begin{aligned}\mathbf{s}_{oct} &= l_1^2 \mathbf{s}_{p(1)} + m_1^2 \mathbf{s}_{p(2)} + n_1^2 \mathbf{s}_{p(3)} \\ &= \frac{1}{3}[\mathbf{s}_{p(1)} + \mathbf{s}_{p(2)} + \mathbf{s}_{p(3)}]\end{aligned} \tag{2.122}$$

The shear stress on the octahedral plane is

$$\tau_{oct} = \sqrt{[(p_{s1})^2 + (p_{s2})^2 + (p_{s3})^2] - \sigma_{oct}^2} \tag{2.123}$$

where τ_{oct} is the octahedral shear stress, or

$$\tau_{oct} = \frac{1}{3}\sqrt{[\sigma_{p(1)} - \sigma_{p(2)}]^2 + [\sigma_{p(2)} - \sigma_{p(3)}]^2 + [\sigma_{p(3)} - \sigma_{p(1)}]^2} \tag{2.124}$$

The octahedral normal and shear stress expressions can also be derived as a function of the stress components for any set of orthogonal axes x, y, z. From Equation 2.116

$$I_1 = \text{const} = \sigma_x + \sigma_y + \sigma_z = \sigma_{p(1)} + \sigma_{p(2)} + \sigma_{p(3)} \tag{2.125}$$

So

$$\sigma_{oct} = \frac{1}{3}[\sigma_{p(1)} + \sigma_{p(2)} + \sigma_{p(3)}] = \frac{1}{3}(\sigma_x + \sigma_y + \sigma_z) \tag{2.126}$$

Similarly, from Equation 2.117

$$\begin{aligned} I_2 &= \text{const} = (\sigma_x\sigma_y + \sigma_y\sigma_z + \sigma_z\sigma_x) - \tau_{xy}^2 - \tau_{yz}^2 - \tau_{xz}^2 \\ &= \sigma_{p(1)}\sigma_{p(2)} + \sigma_{p(2)}\sigma_{p(3)} + \sigma_{p(3)}\sigma_{p(1)} \end{aligned} \tag{2.127}$$

Combining Equations 2.124, 2.125, and 2.127 gives

$$\tau_{oct} = \frac{1}{3}\sqrt{(\sigma_x - \sigma_y)^2 + (\sigma_y - \sigma_z)^2 + (\sigma_z - \sigma_x)^2 + 6\tau_{xy}^2 + 6\tau_{yz}^2 + 6\tau_{xz}^2} \tag{2.128}$$

Example 2.4

The stresses at a point in a soil mass are as follows:

$\sigma_x = 50$ kN/m^2 $\quad \tau_{xy} = 30$ kN/m^2
$\sigma_y = 40$ kN/m^2 $\quad \tau_{yz} = 25$ kN/m^2
$\sigma_z = 80$ kN/m^2 $\quad \tau_{xz} = 25$ kN/m^2

Determine the normal and shear stresses on a plane with direction cosines $l = 2/3$, $m = 2/3$, and $n = 1/3$.

Solution

From Equation 2.98

$$\begin{vmatrix} p_{sx} \\ p_{sy} \\ p_{sz} \end{vmatrix} = \begin{vmatrix} s_x & t_{xy} & t_{xz} \\ t_{xy} & s_y & t_{yz} \\ t_{xz} & t_{yz} & s_z \end{vmatrix} \begin{vmatrix} l \\ m \\ n \end{vmatrix}$$

The normal stress on the inclined plane (Equation 2.99) is

$$\begin{aligned} \sigma &= p_{sx}l + p_{sy}m + p_{sz}n \\ &= \sigma_x l^2 + \sigma_y m^2 + \sigma_z n^2 + 2\tau_{xy}lm + 2\tau_{yz}mn + 2\tau_{xz}ln \\ &= 50(2/3)^2 + 40(2/3)^2 + 80(1/3)^2 + 2(30)(2/3)(2/3) \\ &\quad + 2(25)(2/3)(1/3) + 2(25)(2/3)(1/3) = 97.78 \text{ kN/m}^2 \end{aligned}$$

$$\begin{aligned} p_{sx} &= \sigma_x l + \tau_{xy}m + \tau_{xz}n = 50(2/3) + 30(2/3) + 25(1/3) \\ &= 33.33 + 20 + 8.33 = 61.66 \text{ kN/m}^2 \end{aligned}$$

$$\begin{aligned} p_{sy} &= \tau_{xy}l + \sigma_y m + \tau_{yz}n = 30(2/3) + 40(2/3) + 25(1/3) \\ &= 20 + 26.67 + 8.33 = 55 \text{ kN/m}^2 \end{aligned}$$

$$\begin{aligned} p_{sz} &= \tau_{xz}l + \tau_{yz}m + \sigma_z n = 25(2/3) + 25(2/3) + 80(1/3) \\ &= 16.67 + 16.67 + 26.67 = 60.01 \text{ kN/m}^2 \end{aligned}$$

The resultant stress is

$$p = \sqrt{p_{sx}^2 + p_{sy}^2 + p_{sz}^2} = \sqrt{61.66^2 + 55^2 + 60.01^2} = 102.2 \text{ kN/m}^2$$

The shear stress on the plane is

$$t = \sqrt{p^2 - s^2} = \sqrt{102.2^2 - 97.78^2} = 29.73 \text{ kN/m}^2$$

Example 2.5

At a point in a soil mass, the stresses are as follows:

$\sigma_x = 25$ kN/m^2 $\quad \tau_{xy} = 30$ kN/m^2
$\sigma_y = 40$ kN/m^2 $\quad \tau_{yz} = -6$ kN/m^2
$\sigma_z = 17$ kN/m^2 $\quad \tau_{xz} = -10$ kN/m^2

Determine the principal stresses and also the octahedral normal and shear stresses.

Solution

From Equation 2.114

$$\begin{vmatrix} (\sigma_x - \sigma_p) & \tau_{yx} & \tau_{zx} \\ \tau_{xy} & (\sigma_y - \sigma_p) & \tau_{zy} \\ \tau_{xz} & \tau_{yz} & (\sigma_z - \sigma_p) \end{vmatrix} = 0$$

$$\begin{vmatrix} (25 - \sigma_p) & 30 & -10 \\ 30 & (40 - \sigma_p) & -6 \\ -10 & -6 & (17 - \sigma_p) \end{vmatrix} = \sigma_p^3 - 82\sigma_p^2 + 1069\sigma_p - 800 = 0$$

The three roots of the equation are

$$\sigma_{p(1)} = 65.9 \text{ kN/m}^2$$

$$\sigma_{p(2)} = 15.7 \text{ kN/m}^2$$

$$\sigma_{p(3)} = 0.4 \text{ kN/m}^2$$

$$\sigma_{oct} = \frac{1}{3}[\sigma_{p(1)} + \sigma_{p(2)} + \sigma_{p(3)}]$$

$$= \frac{1}{3}(65.9 + 15.7 + 0.4) = 27.33 \text{ kN/m}^2$$

$$\tau_{oct} = \frac{1}{3}\sqrt{[\sigma_{p(1)} - \sigma_{p(2)}]^2 + [\sigma_{p(2)} - \sigma_{p(3)}]^2 + [\sigma_{p(3)} - \sigma_{p(1)}]^2}$$

$$= \frac{1}{3}\sqrt{(65.9 - 15.7)^2 + (15.7 - 0.4)^2 + (0.4 - 65.9)^2} = 27.97 \text{ kN/m}^2$$

2.11 STRAIN COMPONENTS ON AN INCLINED PLANE, PRINCIPAL STRAIN, AND OCTAHEDRAL STRAIN: THREE-DIMENSIONAL CASE

We have seen the analogy between the stress and strain equations derived in Sections 2.7 and 2.8 for the plane strain case. Referring to Figure 2.20, let the strain components at a point in a soil mass be represented by ϵ_x, ϵ_y, ϵ_z, γ_{xy}, γ_{yz}, and γ_{zx}. The normal strain on plane ABC (the normal to plane ABC has direction cosines of l, m, and n) can be given by

$$\epsilon = l^2\epsilon_x + m^2\epsilon_y + n^2\epsilon_z + lm\gamma_{xy} + mn\gamma_{yz} + ln\gamma_{zx} \tag{2.129}$$

This equation is similar in form to Equation 2.99 derived for normal stress. When we replace ϵ_x, ϵ_y, ϵ_z, $\gamma_{xy}/2$, $\gamma_{yz}/2$, and $\gamma_{zx}/2$, respectively, for σ_x, σ_y, σ_z, τ_{xy}, τ_{yz}, and τ_{zx} in Equation 2.99, Equation 2.129 is obtained.

If the strain components at a point in the Cartesian coordinate system (Figure 2.21) are known, the components in a new set of orthogonal axes can be given by (similar to Equation 2.103)

$$\begin{vmatrix} \epsilon_{x1} & \frac{1}{2}\gamma_{x_1y_1} & \frac{1}{2}\gamma_{x_1z_1} \\ \frac{1}{2}\gamma_{x_1y_1} & \epsilon_{y_1} & \frac{1}{2}\gamma_{y_1z_1} \\ \frac{1}{2}\gamma_{x_1z_1} & \frac{1}{2}\gamma_{y_1z_1} & \epsilon_{z_1} \end{vmatrix}$$

$$= \begin{vmatrix} l_1 & m_1 & n_1 \\ l_2 & m_2 & n_2 \\ l_3 & m_3 & n_3 \end{vmatrix} \begin{vmatrix} \epsilon_x & \frac{1}{2}\gamma_{xy} & \frac{1}{2}\gamma_{xz} \\ \frac{1}{2}\gamma_{xy} & \epsilon_y & \frac{1}{2}\gamma_{yz} \\ \frac{1}{2}\gamma_{xz} & \frac{1}{2}\gamma_{yz} & \epsilon_z \end{vmatrix} \begin{vmatrix} l_1 & l_2 & l_3 \\ m_1 & m_2 & m_3 \\ n_1 & m_2 & n_3 \end{vmatrix} \tag{2.130}$$

The equations for principal strains at a point can also be written in a form similar to that given for stress (Equation 2.115) as

$$\epsilon_p^3 - J_1\epsilon_p^2 + J_2\epsilon_p - J_3 = 0 \tag{2.131}$$

where ϵ_p is the principal strain

$$J_1 = \epsilon_x + \epsilon_y + \epsilon_z \tag{2.132}$$

$$J_2 = \epsilon_x\epsilon_y + \epsilon_y\epsilon_z + \epsilon_z\epsilon_x - \left(\frac{\gamma_{xy}}{2}\right)^2 - \left(\frac{\gamma_{yz}}{2}\right)^2 - \left(\frac{\gamma_{xz}}{2}\right)^2 \tag{2.133}$$

$$J_3 = \epsilon_x\epsilon_y\epsilon_z + \frac{\gamma_{xy}\gamma_{yz}\gamma_{zx}}{4} - \epsilon_x\left(\frac{\gamma_{yz}}{2}\right)^2 - \epsilon_y\left(\frac{\gamma_{xz}}{2}\right)^2 - \epsilon_z\left(\frac{\gamma_{xy}}{2}\right)^2 \tag{2.134}$$

J_1, J_2, and J_3 are the strain invariants and are not functions of the direction cosines.

The normal and shear strain relations for the octahedral planes are

$$\epsilon_{oct} = \frac{1}{3}[\epsilon_{p(1)} + \epsilon_{p(2)} + \epsilon_{p(3)}] \tag{2.135}$$

$$\gamma_{oct} = \frac{2}{3}\sqrt{[\epsilon_{p(1)} - \epsilon_{p(2)}]^2 + [\epsilon_{p(2)} - \epsilon_{p(3)}]^2 + [\epsilon_{p(3)} - \epsilon_{p(1)}]^2} \tag{2.136}$$

where

ϵ_{oct} is the octahedral normal strain
γ_{oct} is the octahedral shear strain
$\epsilon_{p(1)}$, $\epsilon_{p(2)}$, $\epsilon_{p(3)}$ are the major, intermediate, and minor principal strains, respectively

Equations 2.135 and 2.136 are similar to the octahedral normal and shear stress relations given by Equations 2.126 and 2.128.

Chapter 3

Stresses and displacements in a soil mass

Two-dimensional problems

3.1 INTRODUCTION

Estimating the increase in stress at various points and the associated displacement caused in a soil mass due to external loading using the theory of elasticity is an important component in the safe design of the foundations of structures. The ideal assumption of the theory of elasticity, namely that the medium is homogeneous, elastic, and isotropic, is not quite true for most natural soil profiles. It does, however, provide a close estimation of geotechnical engineers and, using proper safety factors, safe designs can be developed.

This chapter deals with two-dimensional problems (plane strain cases) involving stresses and displacements induced by various types of loading. The expressions for stresses and displacements are obtained on the assumption that soil is a perfectly elastic material. Problems relating to plastic equilibrium are not treated in this chapter.

Stresses and displacements related to three-dimensional problems are treated in Chapter 4.

3.2 VERTICAL LINE LOAD ON THE SURFACE

Figure 3.1 shows the case where a line load of q per unit length is applied at the surface of a homogeneous, elastic, and isotropic soil mass. The stresses at a point P defined by r and θ can be determined by using the stress function

$$f = \frac{q}{p} r\theta \sin\theta \tag{3.1}$$

In the polar coordinate system, the expressions for the stresses are as follows:

$$\sigma_r = \frac{1}{r}\frac{\partial f}{\partial r} + \frac{1}{r^2}\frac{\partial^2 f}{\partial \theta^2} \tag{2.57}$$

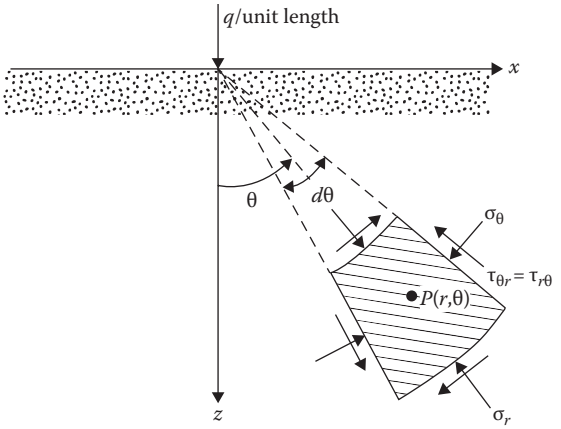

Figure 3.1 Vertical line load on the surface of a semi-infinite mass.

$$\sigma_r = \frac{\partial^2 \phi}{\partial r^2} \tag{2.58}$$

and

$$\tau_{r\theta} = -\frac{\partial}{\partial r}\left(\frac{1}{r}\frac{\partial \phi}{\partial \theta}\right) \tag{2.59}$$

Substituting the values of ϕ in the previous equations, we get

$$\sigma_r = \frac{1}{r}\left(\frac{q}{\pi}\right)\theta \sin\theta + \frac{1}{r^2}\left(\frac{q}{\pi}\right) r\cos\theta + \frac{q}{\pi}\cos\theta - \frac{q}{\pi} r\theta \sin\theta$$

$$= \frac{2q}{\pi r}\cos\theta \tag{3.2}$$

Similarly

$$\sigma_\theta = 0 \tag{3.3}$$

and

$$\tau_{r\theta} = 0 \tag{3.4}$$

The stress function assumed in Equation 3.1 will satisfy the *compatibility equation*:

$$\left(\frac{\partial^2}{\partial r^2}+\frac{1}{r}\frac{\partial}{\partial r}+\frac{1}{r^2}\frac{\partial^2}{\partial \theta^2}\right)\left(\frac{\partial^2 f}{\partial r^2}+\frac{1}{r}\frac{\partial f}{\partial r}+\frac{1}{r^2}\frac{\partial^2 f}{\partial \theta^2}\right)=0 \tag{2.60}$$

Also, it can be seen that the stresses obtained in Equations 3.2 through 3.4 satisfy the boundary conditions. For $\theta = 90°$, $r > 0$, $\sigma_r = 0$, and at $r = 0$, σ_r is theoretically equal to infinity, which signifies that plastic flow will occur locally. Note that σ_r and σ_θ are the major and minor principal stresses at point *P*.

Using the earlier expressions for σ_r, σ_θ, and $\tau_{r\theta}$, we can derive the stresses in the rectangular coordinate system (Figure 3.2):

$$\sigma_z = \sigma_r \cos^2\theta + \sigma_\theta \sin^2\theta - 2\tau_{r\theta}\sin\theta\cos\theta \tag{2.77}$$

or,

$$\sigma_z = \frac{2q}{\pi r}\cos^3\theta = \frac{2q}{\pi\sqrt{x^2+z^2}}\left(\frac{z}{\sqrt{x^2+z^2}}\right)^3 = \frac{2qz^3}{\pi(x^2+z^2)^2} \tag{3.5}$$

Similarly

$$\sigma_x = \sigma_r \sin^2\theta + \sigma_\theta \cos^2\theta + 2\tau_{r\theta}\sin\theta\cos\theta \tag{2.75}$$

or,

$$\sigma_x = \frac{2qx^2z}{\pi(x^2+z^2)^2} \tag{3.6}$$

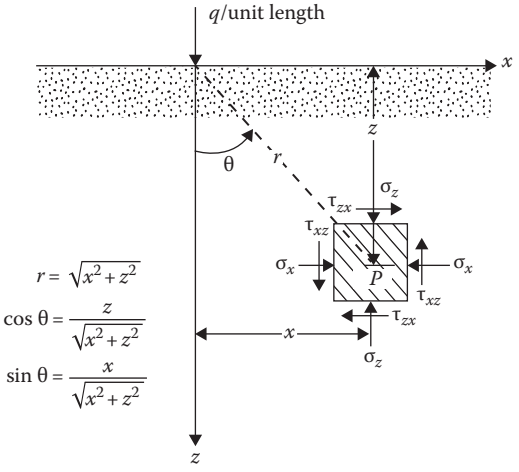

Figure 3.2 Stresses due to a vertical line load in rectangular coordinates.

Table 3.1 Values of $\sigma_z/(q/z)$, $\sigma_x/(q/z)$, and $\tau_{xz}/(q/z)$ (Equations 3.5 through 3.7)

x/z	$\sigma_z/(q/z)$	$\sigma_x/(q/z)$	$\tau_{xz}/(q/z)$
0	0.637	0	0
0.1	0.624	0.006	0.062
0.2	0.589	0.024	0.118
0.3	0.536	0.048	0.161
0.4	0.473	0.076	0.189
0.5	0.407	0.102	0.204
0.6	0.344	0.124	0.207
0.7	0.287	0.141	0.201
0.8	0.237	0.151	0.189
0.9	0.194	0.157	0.175
1.0	0.159	0.159	0.159
1.5	0.060	0.136	0.090
2.0	0.025	0.102	0.051
3.0	0.006	0.057	0.019

and

$$\tau_{xz} = -\sigma_q \sin\theta\cos\theta + \sigma_r \sin\theta\cos\theta + \tau_{rq}(\cos^2\theta - \sin^2\theta) \tag{2.76}$$

or,

$$\tau_{xz} = \frac{2qxz^2}{\pi(x^2 + z^2)^2} \tag{3.7}$$

For the plane strain case

$$\sigma_y = \nu(\sigma_x + \sigma_z) \tag{3.8}$$

The values for σ_x, σ_z, and τ_{xz} in a nondimensional form are given in Table 3.1.

3.2.1 Displacement on the surface (z = 0)

By relating displacements to stresses via strain, the vertical displacement w at the *surface* (i.e., $z = 0$) can be obtained as

$$w = \frac{2}{\pi}\frac{1-\nu^2}{E} q \ln|x| + C \tag{3.9}$$

where

E is the modulus of elasticity
ν is Poisson's ratio
C is a constant

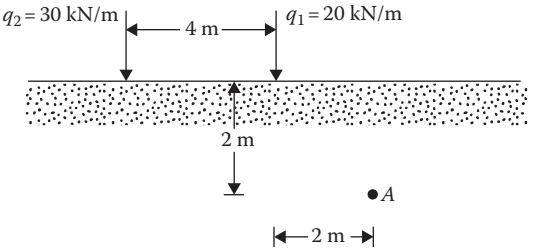

Figure 3.3 Two line loads acting on the surface.

The magnitude of the constant can be determined if the vertical displacement at a point is specified.

Example 3.1

For the point *A* in Figure 3.3, calculate the increase of vertical stress σ_z due to the two line loads.

Solution

The increase of vertical stress at *A* due to the line load q_1 = 20 kN/m:

$$\text{Given, } \frac{x}{z} = \frac{2\,\text{m}}{2\,\text{m}} = 1$$

From Table 3.1, for x/z = 1, $\sigma_z/(q/z)$ = 0.159. So

$$\Delta\sigma_{z(1)} = 0.159\left(\frac{q_1}{z}\right) = 0.159\left(\frac{20}{2}\right) = 1.59\ \text{kN/m}^2$$

The increase of vertical stress at *A* due to the line load q_2 = 30 kN/m:

$$\text{Given, } \frac{x}{z} = \frac{6\,\text{m}}{2\,\text{m}} = 3$$

From Table 3.1, for x/z = 3, $\sigma_z/(q/z)$ = 0.006. Thus

$$\Delta\sigma_{z(2)} = 0.006\left(\frac{q_2}{z}\right) = 0.006\left(\frac{30}{2}\right) = 0.09\ \text{kN/m}^2$$

So, the total increase of vertical stress is

$$\Delta\sigma_z = \Delta\sigma_{z(1)} + \Delta\sigma_{z(2)} = 1.59 + 0.09 = 1.68\ \text{kN/m}^2$$

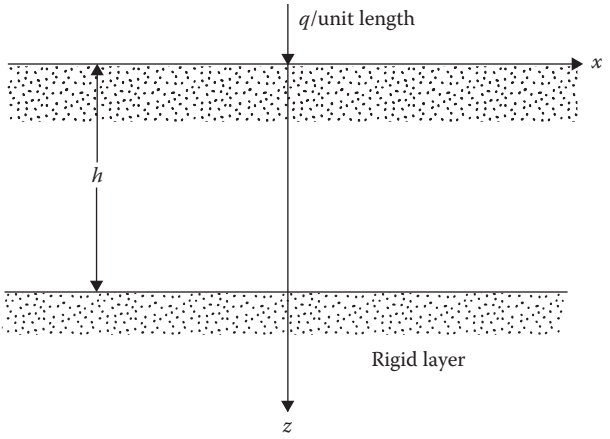

Figure 3.4 Vertical line load on a finite elastic layer.

3.3 VERTICAL LINE LOAD ON THE SURFACE OF A FINITE LAYER

Equations 3.5 through 3.7 were derived with the assumption that the homogeneous soil mass extends to a great depth. However, in many practical cases, a stiff layer such as rock or highly incompressible material may be encountered at a shallow depth (Figure 3.4). At the interface of the top soil layer and the lower incompressible layer, the shear stresses will modify the pattern of stress distribution. Poulos (1966) and Poulos and Davis (1974) expressed the vertical stress σ_z and vertical displacement at the surface (w at $z = 0$) in the forms:

$$\sigma_z = \frac{q}{\pi h} I_1 \tag{3.10}$$

$$w_{z=0} = \frac{q}{\pi E} I_2 \tag{3.11}$$

where I_1 and I_2 are influence values.

I_1 is a function of z/h, x/h, and ν. Similarly, I_2 is a function of x/h and ν. The variations of I_1 and I_2 are given in Tables 3.2 and 3.3, respectively, for $\nu = 0$.

3.4 VERTICAL LINE LOAD INSIDE A SEMI-INFINITE MASS

Equations 3.5 through 3.7 were also developed on the basis of the assumption that the line load is applied on the surface of a semi-infinite mass. However, in some cases, the line load may be embedded. Melan (1932) gave the solution of stresses at a point P due to a vertical line load of

Table 3.2 Variation of I_1 ($\nu = 0$)

	z/h				
x/h	0.2	0.4	0.6	0.8	1.0
0	9.891	5.157	3.641	2.980	2.634
0.1	5.946	4.516	3.443	2.885	2.573
0.2	2.341	3.251	2.948	2.627	2.400
0.3	0.918	2.099	2.335	2.261	2.144
0.4	0.407	1.301	1.751	1.857	1.840
0.5	0.205	0.803	1.265	1.465	1.525
0.6	0.110	0.497	0.889	1.117	1.223
0.8	0.032	0.185	0.408	0.592	0.721
1.0	0.000	0.045	0.144	0.254	0.357
1.5	−0.019	−0.035	−0.033	−0.018	0.010
2.0	−0.013	−0.025	−0.035	−0.041	−0.042
4.0	0.009	0.009	0.008	0.007	0.006
8.0	0.002	0.002	0.002	0.002	0.002

Table 3.3 Variation of I_2 ($\nu = 0$)

x/h	I_2
0.1	3.756
0.2	2.461
0.3	1.730
0.4	1.244
0.5	0.896
0.6	0.643
0.7	0.453
0.8	0.313
1.0	0.126
1.5	−0.012
2.0	−0.017
4.0	−0.002
8.0	0

q per unit length applied inside a semi-infinite mass (at point A, Figure 3.5). The final equations are given as follows:

$$\sigma_z = \frac{q}{2\pi(1-\nu)}\left[\frac{(z-d)^3}{r_1^4} + \frac{(z+d)[(z+d)^2+2dz]}{r_2^4} - \frac{8dz(d+z)x^2}{r_2^6}\right.$$

$$\left. + \frac{1-2\nu}{4(1-\nu)}\left(\frac{z-d}{r_1^2} + \frac{3z+d}{r_2^4} - \frac{4zx^2}{r_2^4}\right)\right] \tag{3.12}$$

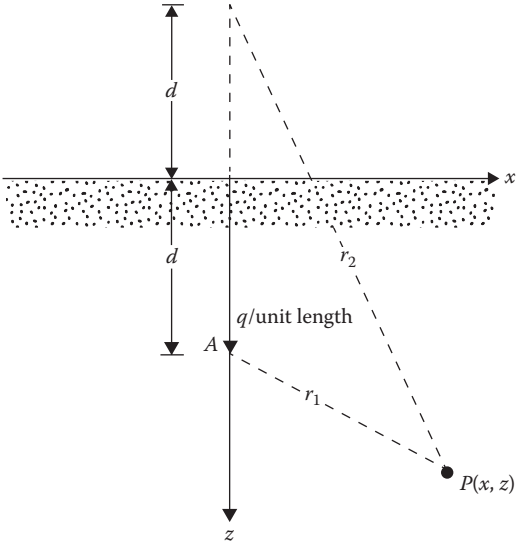

Figure 3.5 Vertical line load inside a semi-infinite mass.

$$\sigma_x = \frac{q}{\pi}\left[\frac{1}{2(1-\nu)}\left\{\frac{(z-d)x^2}{r_1^4} + \frac{(z+d)(x^2+2d^2)-2dx^2}{r_2^4} + \frac{8dz(d+z)x^2}{r_2^6}\right\}\right.$$

$$\left. + \frac{1-2\nu}{4(1-\nu)}\left\{\frac{d-z}{r_1^2} + \frac{z+3d}{r_2^2} + \frac{4zx^2}{r_2^4}\right\}\right] \tag{3.13}$$

$$\tau_{xz} = \frac{qx}{\pi}\left[\frac{1}{2(1-\nu)}\left\{\frac{(z-d)^2}{r_1^4} + \frac{z^2-2dz-d^2}{r_2^4} + \frac{8dz(d+z)^2}{r_2^6}\right\}\right.$$

$$\left. + \frac{1-2\nu}{4(1-\nu)}\left\{\frac{1}{r_1^2} - \frac{1}{r_2^2} + \frac{4z(d+z)}{r_2^4}\right\}\right] \tag{3.14}$$

Figure 3.6 shows a plot of $\sigma_z/(q/d)$ based on Equation 3.12.

3.5 HORIZONTAL LINE LOAD ON THE SURFACE

The stresses due to a horizontal line load of q per unit length (Figure 3.7) can be evaluated by a stress function of the form

$$\phi = \frac{q}{\pi} r\theta\cos\theta \tag{3.15}$$

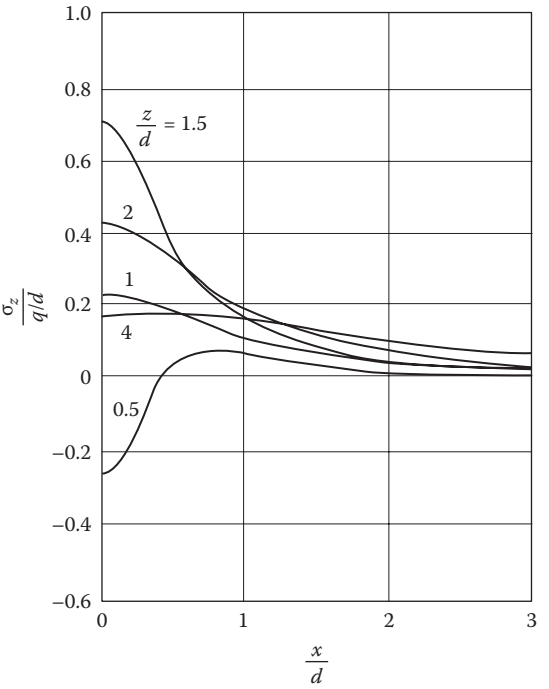

Figure 3.6 Plot of $\sigma_z/(q/d)$ versus x/d for various values of z/d (Equation 3.12).

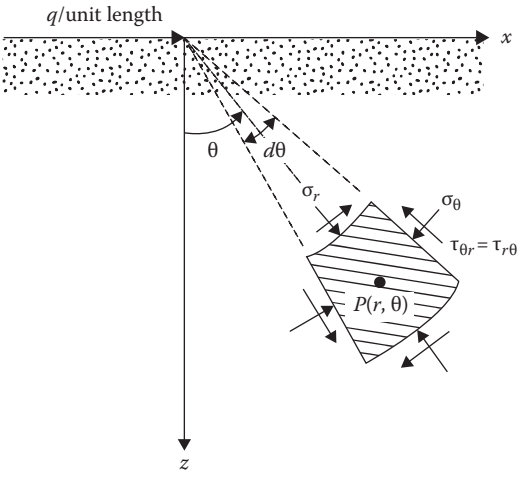

Figure 3.7 Horizontal line load on the surface of a semi-infinite mass.